

Dissertation on
A Study on Deterministic Methods and Factors Influencing Soil Liquefaction
Submitted in partial fulfilment of the requirements for the award of the degree of
MASTER OF TECHNOLOGY
in CIVIL ENGINEERING
(With specialization in Geotechnical Engineering)
Under ASSAM SCIENCE AND TECHNOLOGY UNIVERSITY
SESSION: 2022-2024



Submitted by:

SWAPNALI PEGU

M.TECH 4th Semester Roll No: PG/CE/20

ASTU Registration No: 004006222 of 2022



Under the guidance of:

DR.(MRS.) MALAYA CHETIA

Professor, Assam Engineering College

Department of Civil Engineering

ASSAM ENGINEERING COLLEGE

JALUKBARI, GUWAHATI-13, ASSAM

ACKNOWLEDGEMENT

I would like to express my sincere appreciation to my supervisor Dr. (Mrs.) Malaya Chetia, Professor, Department of Civil Engineering of Assam Engineering College for her extensive support and encouragement throughout the project work. I am highly indebted for her guidance and constant supervision as well as for providing necessary information regarding the project work. Working under her has indeed been a great experience and inspiration for me. This project would not have been possible without the help of several individuals who in one way or another contributed and extended their valuable assistance in the preparation and completion of this study. I express my gratitude to Dr. Jayanta Pathak, Professor and Head of Department of Civil Engineering of Assam Engineering College and also towards the entire fraternity of the Department of Civil Engineering of Assam Engineering College. I cannot help myself without thanking Assam Engineering College, which provided us the required infrastructure and comforts all throughout this course and my project in particular.

Date:

Swapnali Pegu

Place:

M.Tech, 4th Semester
Geotechnical Engineering
Department of Civil Engineering
Assam Engineering College
Jalukbari, Guwahati-13.

CERTIFICATE OF SUPERVISION

This is to certify that the work presented in this report entitled “**A Study on Deterministic Methods and Factors Influencing Soil Liquefaction**” is carried out by Swapnali Pegu, Roll No:PG/CE/20, a student of M.Tech 4th semester, Department of Civil Engineering, Assam Engineering College, under my guidance and supervision and submitted in the partial fulfilment of the requirement for the award of the Degree of Master of Technology in Civil Engineering with specialization in Geotechnical Engineering under Assam Science and Technology University.

Date:

DR. (MRS.) MALAYA CHETIA

Place:

Professor, Department of Civil Engineering
Assam Engineering College
Jalukbari, Guwahati-781013

Certificate from the Head of the Department

This is to certify that the following student of M.Tech 4th semester of Civil Engineering Department (Geotechnical Engineering), Assam Engineering College, has submitted her project on “**A Study on Deterministic Methods and Factors Influencing Soil Liquefaction**” in partial fulfilment of the requirement for the award of the Degree of Master of Technology in Civil Engineering with specialization in Geotechnical Engineering under Assam Science and Technology University.

Name: SWAPNALI PEGU

College Roll No: PG/CE/20

ASTU Roll No: 220620062019

ASTU Registration No: 004006222 of 2022

Date:

Place:

DR. JAYANTA PATHAK

Professor & Head of the Department
Department of Civil Engineering
Assam Engineering College
Jalukbari, Guwahati- 781013

LIST OF TABLES

Table No.	Table name	Page No.
3.1	Field case histories indicating higher liquefaction resistance in aged soils.	13
5.1	(N ₁) ₆₀ values	39
5.2	Correction Factors for Non-Standard SPT Procedures and Equipment	41
5.3	Magnitude scaling factors	42
6.1	Iwasaki et al.(1986) hazard level	48
6.2	Soil parameters at various depths for BH1	48
6.3	Total and effective stresses at various depths	49
6.4	(N ₁) ₆₀ (N ₁) _{60CS} and r _d at various depths for BH1	50
6.5	Calculation of CSR, CRR and F.O.S for other depths	52
6.6	Calculation of LPI for BH1	53
6.7	Soil parameters at various depths for BH2	54
6.8	Total and effective stresses at various depths	55
6.9	(N ₁) ₆₀ , (N ₁) _{60CS} and r _d at various depths for BH4	56
6.10	Calculations of CSR, CRR and F.O.S for other depths	58
6.11	Calculations of LPI for all depths for BH2	59
6.12	Soil parameters at various depths for BH3	60
6.13	Total and effective stresses at various depths	61
6.14	(N ₁) ₆₀ , (N ₁) _{60CS} and r _d at various depths	62
6.15	Calculations of CSR, CRR and F.O.S for other depths	64
6.16	Calculations of LPI for all depths for BH3	65
6.17	Soil parameters at various depths for BH4	66
6.18	Total and effective stresses at various depths	67
6.19	(N ₁) ₆₀ , (N ₁) _{60CS} and r _d at various depths	68

6.20	Calculations of CSR, CRR and F.O.S for other depths	71
6.21	Calculations of LPI for all depths for BH4	72
6.22	Calculation of Vertical Settlement for all the depths for BH1	73
6.23	Calculation of Vertical Settlement for all depths for BH2	73
6.24	Calculation of Vertical Settlement for all depths for BH3	74
6.25	Calculation of Vertical Settlement for all depths for BH4	75
6.26	Calculation of CSR, CRR and F.O.S for all depths using V_s data	77
7.1	Calculations for $\Delta\tau_{rz}$, $\Delta\sigma_z$, CSR and F.O.S for all depths for BH1	82
7.2	Calculations for $\Delta\tau_{rz}$, $\Delta\sigma_z$, CSR and F.O.S for BH2	83
7.3	Calculations for $\Delta\tau_{rz}$, $\Delta\sigma_z$, CSR and F.O.S for BH3	84
7.4	Calculations for $\Delta\tau_{rz}$, $\Delta\sigma_z$, CSR and F.O.S for BH4	85
7.5	Calculations for $\Delta\tau_{rz}$, $\Delta\sigma_z$, CSR and F.O.S for all depths using V_s data	86
9.1	Advantages and disadvantages of SPT and V_s methods	96

LIST OF FIGURES

Figure No.	Description	Page No.
3.1	Figure for a Stable soil and a Liquefied soil	11
3.2	Picture of Bhuj earthquake, Gujarat in 2001	12
3.3	Picture of Chile earthquake in Hawaii, Japan in 1960	12
3.4	Variation of liquefaction resistance ratio with (a) B-value; (b) suction; and (c) degree of saturation for specimens at DR \approx 49%–54%.	17
3.5	Cyclic resistance curves for SAS: saturated and unsaturated tests with (a) $S_r = 55\%$ and (b) $S_r = 87\%$	18
3.6	Liquefaction resistance ratio LRR plotted against degree of saturation S_r	19
3.7	Photographic images of granular materials used a glass beads, b river sand, c manufactured sand	24
3.8	Microscopic images of typical particles a glass beads, b river sand, c manufactured sand	24
3.9	Effect of grain size on the liquefaction potential of granular assemblies	25
3.10	Grain size effects on densification and liquefaction	26
3.11	Effect of size of grain shape on the liquefaction potential of granular assemblies	27
3.12	Grain shape effects on interlocking and liquefaction	27
4.1	Particle Size Distribution for liquefiable soils (Tsuchida H-1970)	29
4.2	Photograph of Standard Penetration Test conducted at site	29
4.3	Cross-section and Sub-soil profile of BH1	30
4.4	Cross-section and Sub-soil profile of BH2	31
5.1	Conditions assumed for the derivation of the earthquake equation	35
5.2	Reduction factor r_d versus depth below level or gently sloping ground surfaces	36

5.3	r_d versus depth curves (Seed and Idriss, 1971)	37
5.4	Plot used to determine the cyclic resistance ratio for clean and silty sands for $M= 7.5$ earthquakes.	40
5.5	Magnitude scaling factors derived by various investigators	43
5.6	Relation between CRR and V_{s1} for M_w 7.5 earthquakes	44
5.7	Plot for Shear wave velocity, V_s against Depth	45
6.1	Plot for Factor of Safety against Liquefaction for BH1	51
6.2	Plot for Factor of Safety against Liquefaction for BH2	57
6.3	Plot for Factor of Safety against Liquefaction for BH3	65
6.4	Plot for Factor of Safety against Liquefaction for BH4	70
6.5	Charts of Volumetric Strain in % versus Factor of Safety against Cyclic Instability	76
6.6	Plot for Factor of Safety against Depth using V_s data	78
7.1	Charts for Shear Stresses due to circular loading of Foster and Ahlvin, 1954	80
7.2	Charts for Vertical Stresses due to circular loading of Foster and Ahlvin, 1954	81
8.1	Spreadsheet for the Analysis of Liquefaction Potential with SPT data	89-91
8.2	Spreadsheet for the Analysis of Liquefaction Potential with V_s data	92,93

ABSTRACT

Liquefaction, a phenomenon where soil loses its strength and behaves like a liquid during an earthquake, is a crucial factor in assessing earthquake risk. Earthquakes are powerful natural disasters triggering liquefaction when certain conditions meet that can cause widespread destruction to both structures and people in a short span of time. People were hardly aware of the word “Liquefaction” until the Earth was shaken by the devastating earthquakes that occurred in various places namely Alaska; U.S.A; Niigata, Japan in the year 1964. In the year 2001, India was shaken by the Bhuj earthquake, Gujarat only after which liquefaction study became priority by various research workers. The simplified procedure introduced by Seed and Idriss (1971) is widely used to assess liquefaction potential of soil. This involves calculating the seismic stress demand on a soil layer, expressed in terms of cyclic stress ratio (CSR) and capacity to resist liquefaction, expressed in terms of the cyclic resistance ratio (CRR). Field methods namely the standard penetration test (SPT) or the cone penetration test (CPT) or the shear wave velocity (V_s) are preferred for CRR estimation. In this project work, assessment of liquefaction potential within a proposed building area in North Guwahati of Kamrup district, Assam which falls in the high seismic zone-V was carried out by obtaining SPT borehole data and measured V_s . SPT based evaluation of liquefaction potential of a soil beneath a structure is normally conducted by considering the soil as if it is in the free field, away from the structure. It has been found from the studies available in the literature that the excess pore pressure distribution near a structure can significantly differ from that in the free field. It indicates that the presence of structure at ground surface has significant effect on liquefaction potential in terms of vertical stress and horizontal shear stresses induced by the structure. The researchers have found from their analysis that under the static structural load, the soil layers are expected to settle and become stronger. Thus, the presence of the initial static shear stress induced by the structures has significant effect on the liquefaction resistance of soils, depending on the type of structures and soil density. Hence, there is a need to modify the typical procedure of evaluating the liquefaction potential by incorporating the stresses induced by a structure. In this study, the cyclic shear stress (CSR) has been determined for free field and by taking the vertical stress and shear stress into account. A water tank was considered at the site while computing the liquefaction potential index of the soil. The analysis clearly highlights that the initial static shear has significant influence on the liquefaction potential of a

soil. An attempt has been made to bring out a comparison on the results obtained from SPT bore hole data and measured V_s for site without and with structure on the ground surface.

Keywords: Liquefaction, Cyclic Resistance Ratio, Cyclic Stress Ratio, Standard Penetration Test, Shear Wave Velocity, Vertical Stress, Shear Stress, Liquefaction Potential Index

CONTENTS

	Page No.
Acknowledgement	i
Certificate	ii
Certificate	iii
List of Tables	iv
List of Figures	vi
Abstract	viii
Chapters	
1. Introduction	1
1.1 Background	1
1.2 Study Area	2
1.3 Motivation of the Study	2
2. Literature Review	3
2.1 Introduction	3
2.2 Literature Survey	3
3. Liquefaction	11
3.1 Introduction	11
3.2 Factors influencing liquefaction of soil	13
1. Effect of Aging or Diagenesis on liquefaction	13
2. Effect of Degree of Saturation on liquefaction	15
3. Effect of Drainage condition on liquefaction	20
4. Combined effect of buoyancy and excess pore pressure on liquefaction	21
5. Effect of Grain Shape on liquefaction	22
4. Identification of Liquefiable Soil	28
4.1 Introduction	28
4.2 Identification of liquefiable soil	28
5. Liquefaction Analysis by Simplified Procedure	32
5.1 Introduction	32
5.2 Determination of Liquefaction Potential	32
5.3 Cyclic Stress Ratio (CSR) Caused by the Earthquake	33
5.4 Evaluation of Cyclic Resistance Ratio (CRR)	38
5.5 Correction for K_{σ}	42

5.6 Correction for other magnitude earthquakes	42
5.7 Factor of Safety against Liquefaction	44
6. Evaluation of Liquefaction Potential without any Surcharge	47
6.1 Introduction	47
6.2 Evaluation of Liquefaction Potential using SPT values	48
6.2.1 Evaluation of Liquefaction Potential for BH1	48
6.2.1.1 Calculation of LPI for BH1	53
6.2.2 Evaluation of Liquefaction Potential for BH2	53
6.2.2.1 Calculation of LPI for BH2	59
6.2.3 Evaluation of Liquefaction Potential for BH3	59
6.2.3.1 Calculation of LPI for BH3	65
6.2.4 Evaluation of Liquefaction Potential for BH4	66
6.2.4.1 Calculation of LPI for BH4	72
6.3 Calculation of Vertical Settlement (Δv) due to liquefaction	73
6.3.1 Vertical Settlement for BH1	73
6.3.2 Vertical Settlement for BH2	73
6.3.3 Vertical Settlement for BH3	74
6.3.4 Vertical Settlement for BH4	75
6.4 Evaluation of Liquefaction Potential using measured Shear Wave Velocity	76
7. Evaluation of Liquefaction Potential with Surcharge	79
7.1 Introduction	79
7.2 Calculation of Vertical Stress Increment, $\Delta\sigma_z$ and Horizontal Shear Stress increment, $\Delta\tau_{zh}$ due to a circular loading with SPT data	79
7.2.1 Vertical Stress Increment and Horizontal Shear Stress increment for BH1	79
7.3 Calculation of Vertical Stress Increment, $\Delta\sigma_z$ and Horizontal Shear Stress increment, $\Delta\tau_{zh}$ due to a circular loading with measured V_S data	86
8. Results and Discussions	88
8.1 Introduction	88
8.2 Results	94
8.2.1 The results obtained from the assessment of liquefaction potential of soil with SPT data	94
8.2.2 The results obtained from the assessment of liquefaction potential of soil with measured V_S data	94

8.3 Discussions	95
9. Advantages and Disadvantages of SPT and Shear Wave Velocity	96
9.1 Introduction	96
9.2 The advantages and disadvantages of SPT and V_s tests	96
10. Conclusion and Future Scope	97
10.1 Conclusion	97
10.2 Future Scope	98
References	

Chapter 1

Introduction

1.1 Background

Earthquakes are powerful natural disasters that can cause widespread destruction to both structures and people in a short span of time (Kramer,1986.). The Great Chile Earthquake of May 22, 1960, which had a magnitude of 9.5, caused significant loss of life in Hawaii, Japan, and the Philippines. Liquefaction is a phenomenon where soil loses its strength or stiffness due to escalation of excess pore water pressure during an earthquake, resulting to significant vertical settlement or deformation and nearly zero effective stress and ultimately behaves like a liquid. It is a crucial factor in assessing earthquake risk.

Liquefaction is generally observed in loose saturated sandy soils (Chillarige et al.; Grozic et.al; Hsu et al.). This is due to the reason that loose sand has a tendency to compress under application of load whereas dense sand in contrary has a tendency to dilate or expand in volume. However, there are studies that show liquefaction could also occur in unsaturated soils. There are field evidences of liquefaction occurring in case of unsaturated soils. Thus, it is very important to study liquefaction in unsaturated soils also. There are various other factors such as aging effect, drainage condition, combined effect of buoyancy and excess pore pressure, grain shape etc influencing soil liquefaction which needs to be addressed.

People were hardly aware of the word “Liquefaction” until the Earth was shaken by the devastating earthquakes that occurred in various places namely Alaska; U.S.A; Niigata, Japan in the year 1964. In the year 2001, India was shaken by the Gujarat earthquake, also known as the Bhuj earthquake only after which the liquefaction study became priority by the engineers, scientists and research workers.

The simplified procedure introduced by Seed and Idriss in the year 1971 is widely used to assess liquefaction potential of soil. The procedure involves determining of seismic stress demand on a soil layer, expressed in terms of cyclic stress ratio (CSR) and capacity to resist liquefaction, expressed in terms of the cyclic resistance ratio (CRR). Field methods namely standard penetration test (SPT) or cone penetration test (CPT) or shear wave velocity (V_s) are preferred for CRR estimation due to challenges related with undisturbed sampling and laboratory testing.

The present study is carried out to investigate methods and appropriate field tests for obtaining the requisite data for evaluating liquefaction potential for sites with structure and observe the effect of vertical stress and horizontal shear stress induced by the structure.

1.2 Study area

For the study purpose, data of two boreholes namely BH1, BH2 were taken by conducting Standard penetration test within the proposed building area of North Guwahati in the Kamrup district, Guwahati, Assam to evaluate liquefaction potential of soil. The study area falls in the high seismic zone-V for which the study on liquefaction potential for site becomes very necessary to find out if the soil is susceptible to liquefaction or not. Accordingly, mitigation techniques can be adopted for the site, if the soil is found liquefiable. Data of two more boreholes namely BH3 and BH4 were also collected from earlier project work for carrying out the analysis. One seismic cross hole test was also conducted at the study area for the evaluation of liquefaction potential. A surcharge load (Here a circular water tank of uniform surcharge) at ground surface of the study area was also considered to observe the effect of initial shear stress induced by the structure on liquefaction potential of soil. From this study, a comparison on the results obtained from the liquefaction analysis for sites under two scenarios i) in absence of structure and ii) in presence of structure can be obtained.

1.3 Motivation of the study

Evaluation of liquefaction potential of a soil beneath a structure is normally conducted by considering the soil as if it is in the free field, away from the structure. But it is learnt from literatures that distribution of excess pore water pressure in soil in a free field condition differs significantly from the soil near a structure. It indicates that the presence of structure at ground surface has significant effect on liquefaction potential in terms of vertical stress and horizontal shear stresses which are induced by the structure. Researchers have found from their analysis that under the static structural load, the soil layers are expected to settle and become stronger. This means that the presence of the initial static shear stress induced by the structures has significant effect on the liquefaction resistance of soils, depending on the type of structures and soil density. Numerous works have been carried out on the liquefaction potential for site by considering the soil as if it is in the free field, away from the structure; but there are insufficient studies on liquefaction potential of soil by considering a structure on ground surface. So there is a need of comparison on the results obtained from the liquefaction analysis for sites without and with structure.

Chapter 2

Literature Review

2.1 Introduction

The comprehensive review of literatures presented in this chapter incorporates factors influencing soil liquefaction and methods adopted by research workers for the assessment of liquefaction potential of soil with a purpose to find the effect of initial static shear stress induced by the structure on liquefaction potential of soil.

2.2 Literature survey

Bwambale (2018) in his study investigated the uncertainties linked with the assessment of diagenesis or aging effects on liquefaction of soil. Soil liquefaction triggered by earthquake may cause significant ground failure and is generally evaluated based on field case histories, where liquefaction is found to occur in soil deposits that are less than a few thousand years old. The evaluation procedures without taking diagenesis into account can give inordinately conservative predictions leading to unnecessary and expensive ground improvements in natural and aged man-made soils. The assessment includes a thorough review of several field case histories showing that aged soils are more resistant to liquefaction compared to young uncemented soils during earthquakes, discussions on mechanisms that increases resistance to liquefaction with time, evaluates proposed methods for quantifying the impact of aging effect on liquefaction resistance (K_{DR}) and also evaluates proposed predictor variables for K_{DR} . The published literature shows that in case of sand deposits where sufficient cements agents are absent then the physical diagenetic processes likely to control the interactions at the grain -to - grain contacts and on the contrary in presence of cementing agents, chemical processes likely to control. The proposed variables for predicting aging effect (K_{DR}) contains-Time since deposition or last major disturbance, ratio of measured to estimated small-strain shear wave velocity (MEVR), ratio of small-strain shear modulus to cone tip resistance (G_{max}/q_c), adjusted G_{max}/q_c (KG) and ratio of measured to estimated adjusted G_{max}/q_c (MEKG). The proposed variable MEVR seems to be a more reliable predictor of aging effect (K_{DR}) than the other variables. The predictor variable time should only be used at sites where correct age deposit can be determined. In this study, it is found that diagenesis or the aging effect plays a significant role in evaluation of liquefaction potential. So, without correction for aging effect, the liquefaction potential is over estimated.

Liu and Xu (2003) studied that soil liquefaction is one of the most hazardous phenomenon leading to destruction and disruption to the civil infrastructure systems. It

generally occurs in loose saturated sand or low plasticity silts. A series of strain-controlled cyclic loading tests conducted on both saturated and unsaturated sand revealed that not only saturated sand undergoes liquefaction but unsaturated sand too undergoes liquefaction under certain conditions. In this laboratory study, soil specimens under different initial conditions such as relative density (30 and 70%), effective confining stress (50 and 200kPa) and degree of saturation (90, 95 and 100%) are tested. All specimens, except the one with D_r 70%, confining stress of 200kPa and S_r 90% attained liquefaction by the end of the tests. Even though it is well established that resistance to liquefaction escalates with relative density and confining stress and decreases with the S_r , this study provides quantitative guidance for assessing soil liquefaction in unsaturated sand.

Debnath et al (2021) in their study focuses on small strain dynamic properties of soil such as the small strain shear modulus (G_s or G_{max}) and damping ratio (ξ) by the bender element tests on subsoil samples obtained from a railway construction site at Agartala, India alongwith evaluation of liquefaction potential on sandy soil. The purpose of this study is to generate a database and empirical relationship on dynamic properties of soil of Agartala which will help in carrying out seismic hazard studies at sites of the city. In this study, both undisturbed and disturbed soil samples were obtained from twelve boreholes near to study area which features of mainly soft marshy ground and localised peat deposit, similar to soils found in various parts of Agartala basin and other regions of India. Experimental results show that V_s , G_{max} and ξ differ widely based on soil type. A closed form empirical equation are proposed to determine G_{max} for different soils which can be used for evaluating dynamic properties for similar type of soil present across various sites in India.

Das et al. (2023) in their paper includes bearing capacity and liquefaction potential analysis of shallow foundations in soil densified with vibro-stone columns, as per Indian Standard (IS) codes and finite element methods. The effectiveness of stone columns was shown through a real field project in Vallur oil terminal, Chennai, India. The site mainly had non-plastic silty liquefiable soil with a very soft clay layer in the top 2m to 3m. The analysis using IS codes revealed a liquefiable layer at a depth of 3m to 5m. However, the ultimate bearing capacity escalated by 3 to 4.5 times and settlement decreased to 84-92% after the installation of vibro-stone columns. The numerical analyses were performed with the finite element based computer program PLAXIS 2D. This analyses displayed that with vibro-stone columns, the bearing capacity enhanced by 43% and settlement decreased by 2 times. It was also seen with introduction of vibro-stone columns, the excess pore water

pressure substantially reduced. Comparisons of the values of bearing capacity and settlement acquired from both numerical and codal analyses were done and found matching. The calculated settlements were within limited range and the estimated bearing capacity values were found to exceed the allowable load intensity. Therefore, introduction of vibro-stone columns is an effective means of enhancing the strength of liquefiable soil.

Latha and Lakkimsetti (2022) in their paper highlights that inspite of the qualitative effects of grain size and grain shape on the resistance of sand to liquefaction being well established but it is difficult to find the quantitative correlations between them. Most of the studies in this area used traditional methods such as sieve analysis and visual observations for quantification of grain shape and size. This study mainly focuses on image based characterizations to evaluate the grain shape and size and relates them to the liquefaction of the sand quantified in laboratory cyclic simple shear tests. Microscopic images of sand particles photographed were analysed with MATLAB codes to determine the mean particle size, sphericity, roundness and surface roughness of the sand particles. The laboratory cyclic simple shear tests were conducted on sands and sand like glass beads with varying sizes and sands with both rounded and angular grains. Results reveal that smaller grain size of regular shape with high sphericity and roundness has more tendency to liquify. In the laboratory test conducted in the study shows that spherical particles liquified in 8 cycles, followed by river sand with sub-rounded particles liquified in 13 cycles and manufactured sand with relatively elongated particles liquified in 16 cycles, all with similar particle sizes.

Lentini and Castelli (2018) have studied liquefaction in sandy soil has been observed from recent earthquakes. In this case, the prime challenge is the selection of the appropriate residual strength of liquefied materials to evaluate the post-liquefaction stability of embankments and soil structures. Cyclic triaxial tests have been conducted in coarse grained soils for the evaluation of liquefaction potential of soil. The design for the seismic retrofitting of “Viadotto Ritiro” foundations along the A20 motorway linking Messina and Palermo incorporatess a soil liquefaction study where a thorough geotechnical characterisation has been conducted. This paper mainly highlights the results of laboratory tests conducted out on soil specimens in sandy soil to evaluate liquefaction potential.

Chanda et al. (2003) in their study focusses on the evaluation of liquefaction potential of soil using the technique Liquefaction Potential Index (LPI). In the study, they employed the hydraulic fill method for dredging the soil to the reclaimed ground site of Jaigarh Port in Maharashtra. As a result, loose clean non-plastic fines under saturated condition are liable to be liquefied during earthquake. The engineering essence is not just

bounded to identify this sudden loss of strength of liquefied soil, but to assess the severity of the phenomenon. Hence, a method is required for assessing the severity based on field results like Standard Penetration Test (SPT) or other available methods. They employed LPI technique which quantifies and forecasts some of ground's failure potential. This procedure is a well established numerical technique to calculate LPI.

In past, many researches in this area have been evolved and enhanced. This study highlights various techniques to evaluate liquefaction potential of soil with practical examples and field study.

Pokhrel et al. (2022) have studied an evaluation of liquefaction potential for the Kathmandu Valley based on seasonal variation of ground water. To gain insights, seven historical liquefaction records situated near to borehole datapoints were taken to compare two methods for the computation of liquefaction potential. The new liquefaction potential maps were created with the SPT blow count data obtained from 75 boreholes. Various scenarios including seasonal variation of ground water table and peak ground acceleration were modelled. Maps at urban scale were prepared with ordinary kriging in ArcGIS. The evaluation of liquefaction potential from the approach of Sonmez (2003) provided a good match with the records of historical liquefaction records in the region. It is found that the seasonal variation has a significant effect on the spatial distribution of calculated liquefaction potential across the valley, which reveals the lower than expected liquefaction from the Gorkha earthquake.

Banerjee et al. (2022) in their study mentioned that liquefaction of soil has mainly been linked to saturated soils. But it may also occur in unsaturated soil under seismic activity. Hence, neglecting non-saturated soil that are close to saturation which is the primary rule for evaluation of liquefaction can be dangerous and hazardous. For this study, a cyclic double-walled triaxial device was modified to conduct cyclic triaxial tests on suction-equilibrated specimen at low suction rates. The existence of highly compressible air voids within an unsaturated soil sample prevents the effective confining pressure from reaching zero, which is a mark of initial liquefaction. Therefore, in this study, liquefaction was assumed to happen when the soil specimen reached a 5% double-amplitude strain. The cyclic triaxial tests performed on unsaturated soil were analysed to study and confirms the possibility of liquefaction in unsaturated soil. Additional suction-controlled monotonic triaxial tests were performed to compare the stress paths derived from cyclic triaxial tests to evaluate if the technique Induced Partial Saturation can mitigate liquefaction. It was seen that unsaturated soil may undergo liquefaction with relative density 50% and a degree of

saturation exceeding 70%. However with desaturation the resistance to soil liquefaction increased rapidly. This shows the potential of the technique IPS can mitigate liquefaction in moderately compacted soils whose degree of saturation is decreased to below 70%.

Mele et al. (2022) in their study have mentioned that liquefaction in saturated soil is well-identified as per stress or strain criteria. On the other hand, the attainment of liquefaction in non-saturated soil is still a matter of discussion among the researchers community. Even though the resistance to liquefaction is higher in case of non-saturated soil than that of saturated soil, non-saturated soil may liquefy as well. The interest for the technique Induced Partial Saturation (IPS) mitigating soil liquefaction in non-saturated soil has been increasing. Therefore, it is crucial to accurately define the attainment of liquefaction as this determines the estimation of resistance to liquefaction. It has already been demonstrated the importance of apparent viscosity as the parameter in accurate identification of the liquefaction triggering for fully saturated soil. The viscous triggering approach to non-saturated soil has been used for processing some cyclic triaxial tests being conducted on variety of sandy soil. The results confirm the solidity of the apparent viscosity as a liquefaction triggering parameter that exhibits a strong correlation with the strain liquefaction triggering criterion in non-saturated sandy soil.

Ben-Zeev et al. (2023) have studied that earthquake induced soil liquefaction is a disastrous phenomenon linked with loss of soil strength due to earthquake, leading to catastrophic liquidlike soil deformation. Conventionally, liquefaction was sighted as an effectively undrained process. Undrained liquefaction initiates only under high energy density but it is found many earthquakes initiate at low energy density that is initiating far from the earthquake epicentre, which remains unexplained. In this study, they have highlighted that liquefaction can happen under drained process too at remarkably low energy density offering a general explanation for earthquake initiating far from earthquake epicentre. Drained conditions stimulate interstitial fluid flow across the soil during earthquake shaking creating differences in excess pore pressure and loss of soil strength. Their findings emphasized on the importance of considering soil liquefaction under drained conditions in assessing liquefaction potential and related hazards.

Ben Zeev et al. (2017) have studied that soil liquefaction is a disastrous phenomenon caused due to earthquake shaking which may lead to tilting, sinking and floating of infrastructure. Liquefaction generally occurs in loose soil under undrained conditions, which upon shear experiences excess pore pressure and ultimately leading to zero effective stress. But some field and experimental observations do not fit this statement.

These incorporates liquefaction of pre-densified soils, liquefaction under drained conditions, repeated liquefaction events. Their study reflects a new mechanism for soil liquefaction which arises only from buoyancy effects of fluids and grain accelerations. Here, the term Liquefaction is defined as a macroscopic transition from a rigid to a fluid like behaviour. They extended their study and sought a unifying mechanism for field observed liquefaction by considering both the effect of buoyancy and high pore pressure, without insisting on lithostatic values. To obtain this goal, they used a coupled fluid flow and granular dynamics numerical model to examine the effect of pore pressure on the sinking of a large object (Intruder) into a drained densely packed granular system undergoing cyclic shearing. The findings show that despite drained conditions, pore pressure rises during shaking. Pore pressures being below lithostatic values, still the soil liquefies which can be identified from intruder sinking to its isostatic position. Simulations with the effect of buoyancy alone can show liquefaction leading to intruder sinking under certain scenarios. The inclusion of pore pressure effect to the buoyancy effect can enhance liquefaction which promotes intruder sinking.

Satyam and Rao (2014) have studied that the cyclic behaviour of a saturated soil rely on the potential for remarkable strain or loss of strength that may lead to deformation of ground at the time of earthquake. Large earthquakes that created world history describes that liquefaction related ground deformation leads to large-scale damage to structure and lifeline in urban areas. Thorough assessment of liquefaction hazard is crucial for evaluating and minimizing the risk through effective mitigation techniques. Liquefaction of soil generally occurs in areas with low density and saturated granular sediments that results to ground failure, sand boiling and the structure subsided unevenly causing tilting, cracking or even collapse. Following the devastating 2001 Gujarat earthquake, the government of India paid strict attention to carry out thorough site characterization and ground response studies which are very important in seismic microzonation and serves as a guiding tool in land use planning and safe construction practices to mitigate future earthquake losses. This research paper focuses on two urban centres namely Delhi and Vijayawada falling in seismic zones IV and III for liquefaction hazard assessment. The assessment for both the cities are conducted with measured shear wave velocity and SPT borehole data. From the thorough investigation, it is found that severe liquefaction potential in the north and north eastern side of Delhi and less likelihood in the western part of the city. The occurrence of liquefaction potential is likely at multiple locations of Vijayawada city.

2.3 Summary and critical appraisal of literature review

The literature reviews signify that numerous research and study have been conducted on factors influencing soil liquefaction and methods adopted by research workers for the assessment of liquefaction potential of soil. It is observed from literature reviews that soil liquefaction occurs not only in saturated soil but it may also occur in case of unsaturated soil when certain conditions meet. So, the implications of neglecting unsaturated soil that are near to saturation as the foremost rule for evaluating of liquefaction can be hazardous and catastrophic. Apart from the factors influencing soil liquefaction such as earthquake intensity and duration, groundwater table, soil type, placement conditions or depositional environment, confining pressures, building load etc, there are other lesser-known factors such as aging or diagenesis effect; drainage condition; combined effect of buoyancy and excess pore pressure; grain shape etc that contribute to soil liquefaction. The approach adopted by the research workers for the evaluation of liquefaction potential of soil was the “Simplified procedure” introduced by Seed and Idriss (1971) with data obtained from Standard penetration test (SPT) or Cone penetration test (CPT) or Shear wave velocity (V_s). It is found from literatures that there are extensive studies on evaluation of liquefaction potential with SPT data. However, there are limited studies on liquefaction potential with data obtained from CPT and V_s . As observed from literatures that the presence of structure at site has significant effect on liquefaction potential in terms of vertical stress and horizontal shear stress induced by the structure.

So, there is a need to study soil liquefaction by considering a surcharge at site and bring out a comparison on the results obtained from the liquefaction potential for sites under two scenarios i) in absence of structure and ii) in presence of structure.

2.4 Objective and scope of the work

The main objective of this dissertation is to investigate methods for evaluating liquefaction potential of soil. The scope of this dissertation includes the following-

1. Various factors influencing soil liquefaction.
2. Liquefaction Analysis for sites under two scenarios-i) in absence of structure and ii) in presence of structure with data obtained from SPT blow count and measured Shear wave velocity.
3. To calculate Liquefaction Potential Index to check the severity of earthquake.
4. To calculate deformation or vertical settlement of the soil due to liquefaction.

5. To determine vertical stress and horizontal shear stresses induced by a structure.
6. To Design a Spread Sheet in Microsoft excel for the Liquefaction Analysis as per IS Code Method.
7. To bring out a comparison on the results obtained from Liquefaction Analysis for sites without and with structure.

Chapter 3

Liquefaction

3.1 Introduction

The term “liquefaction” refers a condition where a soil will undergo continued deformation at a constant low residual stress or with no residual resistance due to the build-up and maintenance of high pore water pressure which reduces the effective confining pressure to a very low value(Saran, 1999). Pore pressure build-up leading to true liquefaction of this type may be either due to static or cyclic stress applications. The strength of sand is primarily due to internal friction between the soil particles which is lost due to build up of pore water pressure during earthquake shaking, resulting in liquefaction of the soil and hence the strength of the soil decreases. An important feature of the phenomenon of liquefaction is the fact that its onset in one zone of deposit may lead to liquefaction of other zones, which would have remained stable otherwise. The liquefaction phenomenon is shown in fig.3.1 below. Pictures of Bhuj earthquake, Gujarat and Chile earthquake, Japan are shown below in fig 3.1a and 3.1b.

Liquefaction of soil is often linked to saturated soils in undrained condition. Even unsaturated soils can be susceptible to liquefaction under seismic loading. There are limited studies on cyclic loading of unsaturated soils that have indicated that even without reaching complete saturation, soils are susceptible to liquefaction thereby losing shear strength of soil without reaching a zero effective stress condition. Therefore, the implications of ignoring unsaturated soils that are near to saturation as the foremost rule for evaluating of liquefaction can be hazardous and catastrophic.

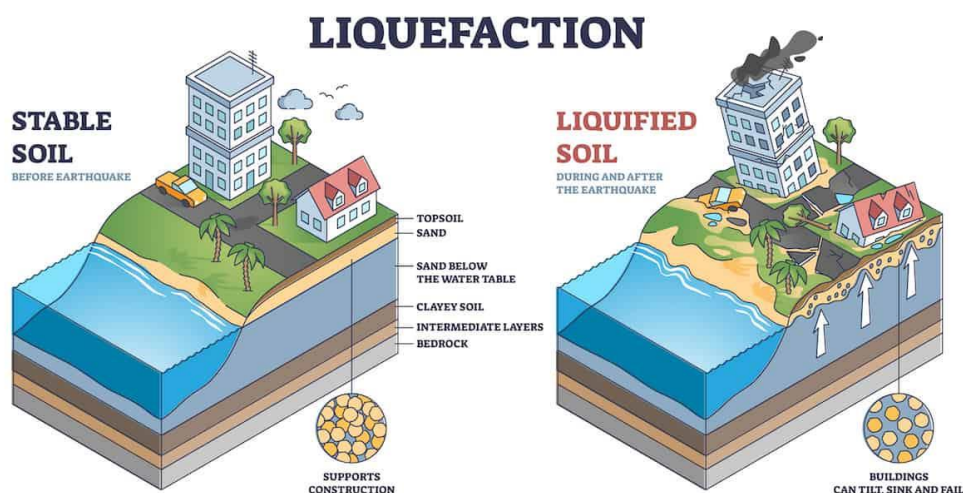


Fig. 3.1 Figure for a Stable soil and a Liquefied soil (Source- vectormine.com)



Fig. 3.2 Picture of Bhuj earthquake, Gujarat in 2001 (Source-pinterest.com)



Fig. 3.3 Picture of Chile earthquake in Hawaii, Japan in 1960 (Source-reddit.com)

3.2 Factors influencing liquefaction of soil

There are several factors influencing liquefaction of soil such as earthquake intensity and duration, groundwater table, soil type, placement conditions or depositional environment, confining pressures, building load etc. In addition to these factors, researchers are also studying other lesser-known factors that contribute to liquefaction. Following are these factors in details studied by them.

1. Effect of Aging or Diagenesis on liquefaction- (Bwambale, 2018) studied the effect of aging and had mentioned in his paper that the strength of granular soil increases with its age, thereby increasing resistance to soil liquefaction. Several field cases were studied where it was observed that the ground behaviour following earthquakes indicate greater liquefaction resistance in case of older soils than in younger soils, which is presented below in tabular format. The Table 3.1 below provides a summary of various case histories of earthquakes and its consequences and the need to consider the effects of aging. He noted that for some of the field cases that measured penetration resistance or small-strain shear wave velocity were similar in both older and younger soil deposits.

Table 3.1 Field case histories indicating higher liquefaction resistance in aged soils

Reference	Area	Age (years)	Earthquake and Observation
Youd and Hoose (1977); Youd and Perkins (1978)	Worldwide	Holocene, Pleistocene and older	Pleistocene and pre-Pleistocene deposits reveal lower susceptibility to liquefaction than Holocene and recent deposits. Even within the Holocene, susceptibility to liquefaction decreased with age.
Balon and Andrus (2006); Hayati and Andrus (2008); Heidari and Andrus (2010, 2012)	Charleston, SC	70,000 - 130,000	August 31, 1886 Charleston earthquake: Moderate to severe surface manifestations of liquefaction occurred in the fills and Silver Bluff sand deposits on the peninsula of Charleston, but none occurred in the older Wando Formation sand deposits with similar penetration resistance.
Seed et al. (1991)	San Francisco Bay Area, CA	> 120	October 17, 1989 Loma Prieta earthquake: Moderate to severe surface manifestations of liquefaction occurred in the loosely dumped sandy fills and uncompacted hydraulic sand fills placed during the period from 1870 to 1912, whereas no surface manifestations of

			liquefaction occurred in natural alluvial deposits.
Arango et al. (2000)	Gillibrand Quarry, Tapo Canyon, CA	1,000,000	January 17, 1994 Northridge earthquake: Failure occurred at a water-retaining dam located in the quarry, yet no surface manifestations of liquefaction were observed in the natural sand deposit.
Hamada et al. (1996); Wakamatsu and Numata (2004)	Kobe, Ashiya and Nishinomiya, Japan	Not available	January 17, 1995 Hyogoken-Nabu (Kobe) earthquake: Substantial sand boils and liquefaction-induced ground failures were prevalent in unimproved reclaimed areas, and few ground failures occurred in the northern section of the old coastline. Natural soils of the inland region did not exhibit any sand boils.
Longwei et al. (2009); Liu-Zeng et al. (2017)	Western Sichuan Basin, China	Pleistocene and older	May 12, 2008 Wechuan earthquake: Substantial sand boils, ejected gravel, and water ejection features occurred in the Holocene alluvium, but only a few sand boils occurred in the surrounding Pleistocene and older deposits.
Dobry et al. (2015); El-Sekelly et al. (2017); Dobry and Abdoun (2017)	Wildlife (and other sites), Imperial Valley, CA	103	April 4, 2010 El Mayor-Cucupah earthquake: Only small pore pressure was generated in a geologically young, natural silty sand at Wildlife. Estimated liquefaction resistance of natural silty sand is double that of recent uncompacted clean and silty sand fills with similar shear wave velocity.
Cubrinovski et al. (2012); Bwambale and Andrus (2017)	Port Hills, New Zealand	10,000 - 200,000	February 22, 2011 Christchurch earthquake: Substantial sand boils were seen in alluvial/marine deposits, but none occurred in adjacent loess and loess-colluvium deposits with low penetration resistance
Kokusho et al. (2012); Tohwata et al. (2014, 2017)	Tokyo Bay, Japan	50-13,000	March 11, 2011 Tohoku earthquake: Liquefaction occurred in manmade lands constructed after 1960s, but no liquefaction was observed in adjacent older fills and natural alluvial deposits with comparable penetration resistance.

The capacity of the soil to resist liquefaction caused due to earthquake is often expressed by the cyclic resistance ratio (CRR). CRR can be assessed from semi-empirical charts based on field tests such as standard penetration test (SPT), cone penetration test

(CPT) or shear wave velocity (V_s). For determination of CRR, these fields tests are mostly conducted for shallow, level ground, saturated, uncemented, young soil deposits with an initial overburden stress of 1 atmosphere (~ 100 kPa) and an earthquake of moment magnitude (M_w) of 7.5. Hence, correction factors are necessary to apply the CRR curves to different conditions. The corrected CRR ($CRR_{corrected}$) is expressed as given below:

$$CRR_{corrected} = K_{\sigma} K_{\alpha} K_S K_{DR} CRR$$

where K_{σ} is the correction factor for effective overburden stress; K_{α} is the correction factor for sloping ground or initial static shear stress; K_S is the correction factor for unsaturated conditions below the groundwater table; and K_{DR} is the correction factor for the effect of aging or diagenesis. Bwambale (2018) dealt with quantifying and predicting K_{DR} . He stated the three approaches such as Laboratory test results; Laboratory and field test results; and Field test results and ground behaviour observations for quantifying the effect of aging on liquefaction resistance.

2. Effect of Degree of Saturation on liquefaction-

Banerjee et al. (2022) studied the effect of degree of saturation on liquefaction and stated his findings in his paper that liquefaction of soil is often linked to saturated soils. Even unsaturated soils can be susceptible to liquefaction under seismic loading. There are limited studies on cyclic loading of unsaturated soils that have indicated that even without reaching complete saturation, soils are susceptible to liquefaction thereby losing shear strength of soil without reaching a zero effective stress condition (Unno, 2022; Okamura, 2009; Eseller-Bayat, 2013.; Banerjee, 2017; Mele et al. 2019). He observed that unsaturated soils above the ground water table had experienced liquefaction, such as those during the 2003 earthquake in Miyagi, Japan, and at other places. Therefore, the implications of ignoring unsaturated soils that are near to saturation as the foremost rule for evaluating of liquefaction can be hazardous and catastrophic. The liquefaction in unsaturated soils may not happen due to flow liquefaction, but happens due to cyclic mobility resulting in limited yet significant deformations and cause gradual failure of structure. It is mentioned that desaturation process increases the resistance to liquefaction. A new technique known as induced partial saturation has been developed and it is found to be effective in reducing seismic liquefaction. This technique aids in mitigating the potential for liquefaction by introduction of air into soil mass or by desaturating the soils. There were limited studies

conducted on the increase of liquefaction resistance in unsaturated soils. The initial studies on unsaturated soil which involved cyclic triaxial testing is dependent on the value of Skempton's pore pressure parameter B for identifying the effect of desaturation on potential for liquefaction of sandy soils. A few studies were carried out on such soils by conducting cyclic triaxial tests of suction-equilibrated specimens in undrained conditions. Therefore, an experimental program was set up performing cyclic triaxial tests on suction-equilibrated soil specimens using the axis translation technique to find the liquefaction resistance ratio caused due to IPS. The investigations were carried out on a mixed soil, a silty sandy soil. The LRR for a particular suction level is determined as the ratio between the cyclic resistance ratio (CRR) at that suction level (CRR_{unsat}) to the cyclic resistance ratio in a saturated specimen (CRR_{sat}) at the same number of loading cycles as provided below. To ensure the uniformity in the comparative analysis in saturated and unsaturated soil specimens, a criteria for soil liquefaction to occur when the double amplitude axial strain reached 5% was considered. Okamura and Soga (2006) suggested the number of loading cycles was predetermined to be 20 cycles for the calculation of LRR.

$$LRR = \frac{CRR_{unsat, N=20}}{CRR_{sat, N=20}}$$

Employing the LRR equation, the plots generated from the values of LRR plotted against the variation of B-value, matric suction and degree of saturation are depicted in Fig. 3.4(a-c) respectively. It was noticed that the LRR increased exponentially with desaturation. For example it increased from 1.18 at $S_r=98\%$ to 1.61 at $S_r=70\%$ whereas liquefaction was not possible for S_r below 65%. Thus, the incorporation of air voids or induced partial saturation has a significant influence on the mitigation of liquefaction in mixed cohesionless soils. Furthermore, it reiterates the susceptibility of liquefaction at elevated degrees of saturation, particularly above 70%, which should not be neglected in the design and evaluation of liquefaction.

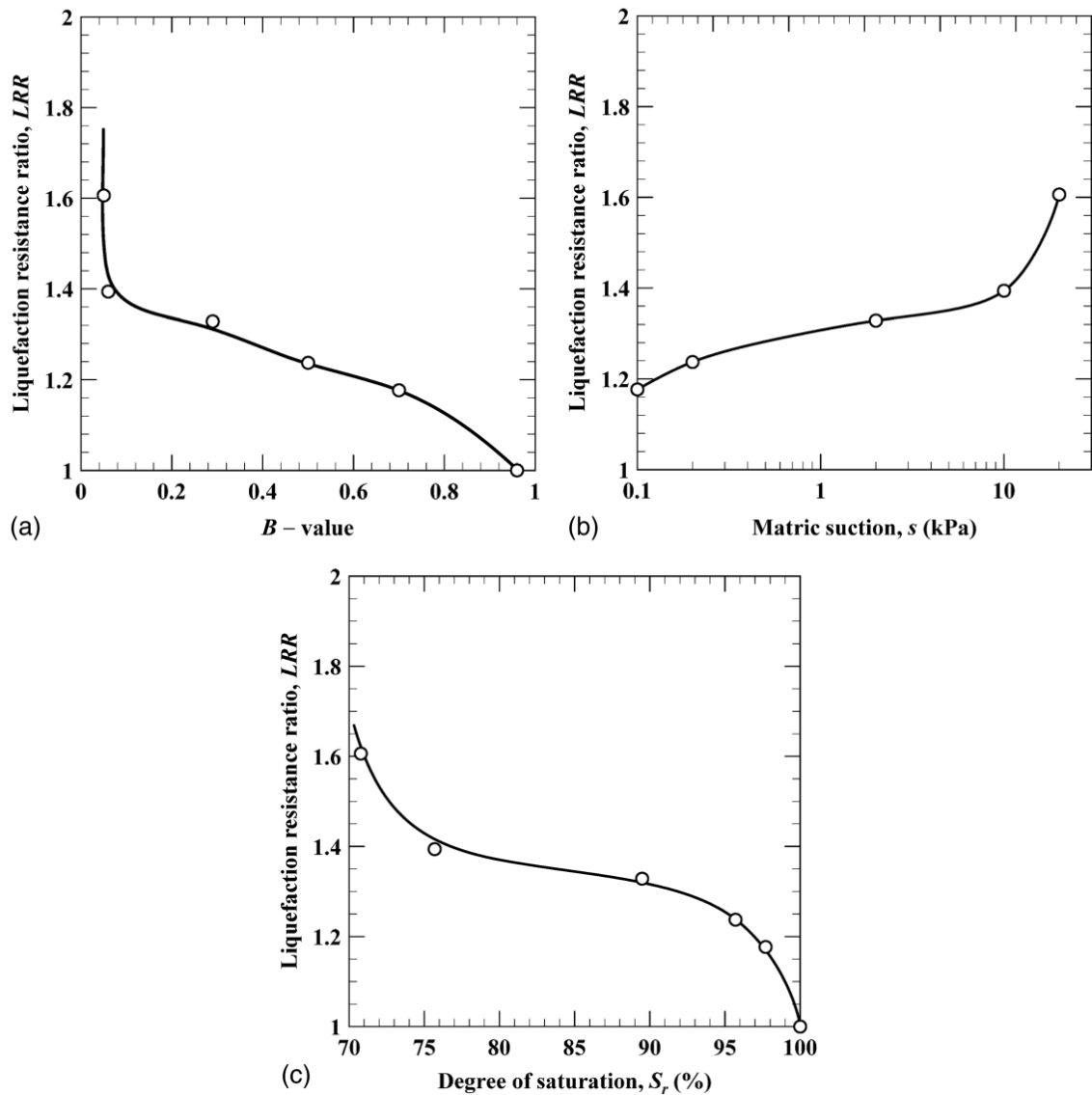


Fig.3.4 Variation of liquefaction resistance ratio with (a) B -value; (b) suction; and (c) degree of saturation for specimens at $DR \approx 49\%–54\%$.

Mele et al. (2019) also studied the effect of degree of saturation and stated the effectiveness of induced partial saturation, IPS on liquefaction resistance that has been experimentally verified by means of cyclic triaxial tests. Starting from the experimental observations by Okamura & Soga (2006), finally, an energetic approach is proposed to quantify the resistance to liquefaction of unsaturated soils. In their research work, seven undrained cyclic triaxial tests using SAS (Sant'Agostino sand) were performed in a stress control mode, on fully saturated specimens, in a Bishop and Wesley triaxial cell; the specimens were 38 mm dia. and 76 mm high. At the laboratory of the University of Tokyo, undrained cyclic triaxial

tests were carried out on saturated and unsaturated specimens of bauxite, Inagi sand and SAS with the linkage double cell system. The tests were performed on reconstituted specimens with 50 mm dia. and 100 mm high. The attainment of liquefaction can be conventionally defined either in terms of measured pore pressure increments Δu (typically assuming that the soil liquefies when the pore pressure ratio $R_u \geq 0.9$, where $R_u = \Delta u / \sigma'_c$), or in terms of axial strain (typically assuming that the soil liquefies when $\epsilon_{DA} = 5\%$, where ϵ_{DA} is the double-amplitude axial strain). The liquefaction resistance curves ($CRR-N_{liq}$) obtained on SAS specimens are plotted in Figs 3.5(a) and 3.5(b), for the two mean values of the initial relative density D_r ($D_r = 50-60\%$) and two mean value of S_r (55 and 87%). The figure clearly shows the relevant role played by the degree of saturation S_r : for each relative density, the liquefaction resistance curve of the unsaturated specimens ($55\% < S_r < 87\%$) is much higher than that obtained on saturated specimens. The ratio between the CRR of nonsaturated soil (CRR_{unsat}) and the CRR of the saturated soil (CRR_{sat}) at the same D_r and at the same number of cycles ($LRR = CRR_{unsat} / CRR_{sat}$) is termed as the liquefaction resistance ratio. This parameter highlights the beneficial effect of desaturation on liquefaction resistance. In this paper, LRR was computed for the value $N_{cyc} = 15$. Its values are plotted against the degree of saturation S_{r0} in Fig.3.6. Consistently with the results previously reported, LRR_{15} increases as the degree of saturation decreases. Interestingly, the rate of increase is extremely high for the highest degrees of saturation, reducing towards the lower values. This means that, for a sand having a high initial degree of saturation, a very small reduction of S_r is able to induce a significant increase of LRR, which is very interesting from an engineering point of view.

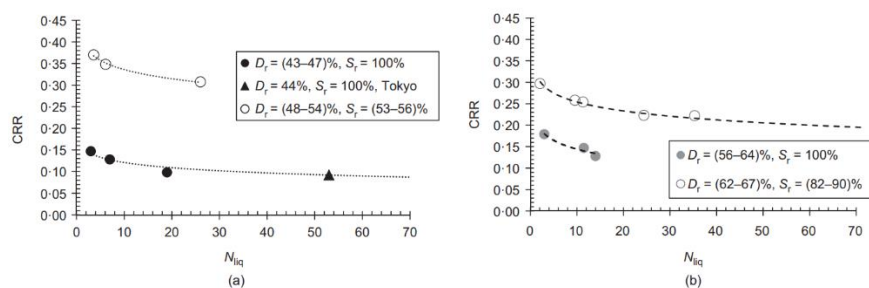


Fig. 3.5 Cyclic resistance curves for SAS: saturated and unsaturated tests with (a) $S_r = 55\%$ and (b) $S_r = 87\%$

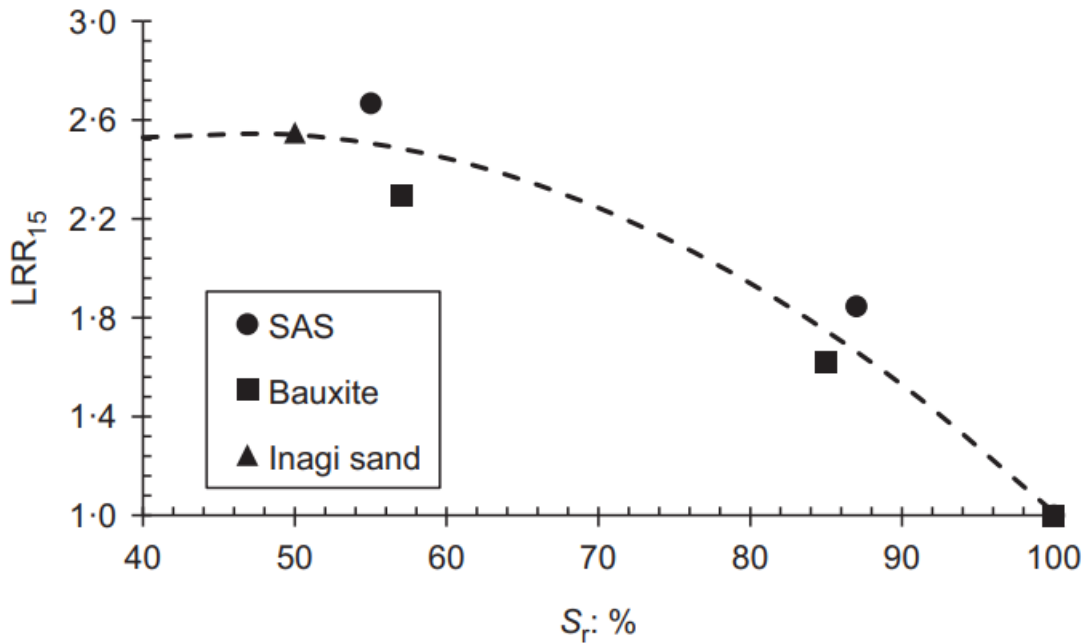


Fig. 3.6 Liquefaction resistance ratio LRR plotted against degree of saturation S_r

Mele et al. (2023) also studied the effects of degree of saturation on liquefaction and he stated in his paper that apparent viscosity, η a physically based parameter able to capture the state change from solid to liquid occurring when liquefaction is reached. Through the processing of some cyclic triaxial tests conducted on three different unsaturated sandy soils, the study highlighted the attainment of liquefaction phenomenon.

Liu et.al also studied the effects of degree of saturation and he devised and executed a comprehensive laboratory test plan to study the effects of the initial conditions such as degree of saturation, relative density, and effective confining stress on liquefaction of unsaturated sand to enhance the current understanding on mechanical behaviour of unsaturated sand liquefaction. In attain this objective, a sequence of undrained cyclic loading triaxial tests was implemented, systematically scrutinizing and drawing comparisons between the mechanical responses of both saturated and unsaturated sand. This study aims to (1) showcase that unsaturated soils can undergo liquefaction when specific initial and loading conditions are met (2) assess performance disparities between saturated and unsaturated soils, considering factors like degree of saturation, relative density, and confining stress and (3) offer some guidance for evaluating site conditions in scenarios involving unsaturated soils. In the course of this laboratory investigation, a set of triaxial tests were carried out on Nevada sand specimens featuring different relative densities, effective confining stresses and degrees of saturations. All tests were conducted as undrained strain-controlled cyclic loading tests. He concluded from his study that it may be

safe to conclude that a soil will not undergo liquefaction only under the condition its relative density is higher than a certain value, its confining stress is high enough and at the same time, its degree of saturation is lower than a certain value. The findings from this laboratory study provide a basis to transform current practices in the assessment of geohazard and geotechnical design when dealing with unsaturated soils. It is important to understand that a sandy soil in unsaturated state does not necessarily mean that liquefaction is not a concern. At times, despite soil being in an unsaturated state with high degree of saturation, a thorough assessment of potential liquefaction becomes imperative by considering other factors such as relative density, confining stress and loading information.

3. Effect of Drainage condition on liquefaction-

Ben-Zeev et al. (2023) studied the effects of drainage condition on liquefaction and stated his findings that traditionally, soil liquefaction is associated with undrained condition under the impact of high energy density. Most earthquake liquefaction events remain unexplained due to its initiation far from the earthquake epicenter under the impact of low energy density. In this paper, Shahar Ben-Zeev et.al had carried out studies related to soil liquefaction that can occur under drained conditions at remarkably low seismic energy density which provides a general explanation for earthquake far-field liquefaction. Drained conditions assist interstitial fluid flow within the soil during ground shaking, leading to excess pore water pressure gradients and loss of soil strength. Their research findings emphasize the significance of considering soil liquefaction across varying drainage conditions, with critical implications for assessing liquefaction potential and associated hazards. Soil liquefaction due to seismic events is a natural hazard occurs during earthquake. When liquefaction occurs, soil initially with elasto-plastic rheology characteristics, able to bear infrastructure loads, undergoes a loss of strength and stiffness due to earthquake shaking, transforming into a fluid-like rheology. Soil liquefaction due to induced earthquake leads to sinking of buildings and infra-structures, floating and tilting, ground lateral spreading, settlement and land sliding. Devastation caused due to liquefaction often leads to widespread human casualties, destruction of lifelines and economic losses, that may result in complete abandonment of once-inhabited areas, presenting a significant challenge to community resilience. The conventional explanation for seismically induced soil liquefaction views the soil as an effectively undrained medium. An initially loosely packed soil on subjection to cyclic shear has the tendency to decrease its pore volume, as readily documented under dry and drained conditions. In cases where the pore fluid flow rate is slower than the rate of porosity reduction, as is expected in an undrained soil response, the

fluid becomes confined within the contracting pores, leading to an increase in pressure. When the pore pressure escalates to match the overburden stress, often reaching lithostatic values, the effective stress reduces to zero. At this point, the soil undergoes a loss of shear strength and stiffness, entering a liquefied state. In laboratory experiments under undrained conditions reveal that during continuous shaking and depending on the initial soil density and the applied shear stress, the pore pressure builds up gradually and eventually reaches lithostatic values after several to tens of shear cycles. In spite of overall positive result of the undrained perspective in explaining the conditions leading to rise of pore pressure and losing of soil strength and stiffness during earthquakes, it fails to explain soil liquefaction beyond near-field i.e far from the earthquake epicenter where the intensity of seismic energy is small. Seismic energy density of minimum 30 J m^{-3} is empirically inferred to induce soil liquefaction by undrained consolidation. Nevertheless, the compilation of the majority of the seismic events leading to soil liquefaction were triggered beyond the earthquake near field, where the seismic earthquake density is below the threshold value 30 J m^{-3} and as low as 0.1 J m^{-3} .

4. Combined Effect of Buoyancy and Excess Pore Pressure on liquefaction-

Zeev et.al (2017) studied the Combined Effect of Buoyancy and Excess Pore Pressure on liquefaction and stated that a recent study proposes an innovative mechanism for soil liquefaction which emerges only from buoyancy effects of fluids plus grain accelerations, defining the term “liquefaction” as a macroscopic transition from solid to fluid like behaviour. They expanded this study with an objective to establish a unified mechanism for field observed liquefaction by considering both the buoyancy effect and elevated pore pressure, without adhering to lithostatic values. To attain this goal, they used a coupled fluid flow and granular dynamics numerical model to examine the effect of pore pressure on the sinking of a large object(Intruder) into a drained densely packed granular system, experiencing cyclic shearing. Outcomes reveal that even in the drained condition, there is rise in pore pressure during shaking. Even though rise of pore pressure remains below lithostatic values, the soil undergoes liquefaction which is identified macroscopically by intruder sinking to its isostatic position. Even simulations with effects of buoyancy alone shows liquefaction, facilitating intruder sinking under certain conditions. But adding the pore pressure effect to the buoyancy effect enhances liquefaction and promote sinking of intruder. Employing a modified DEM (Discrete Element Method) that accounts only buoyancy effects of the fluid and not including pore pressure, Clément, 2017 simulated the reaction of a tightly packed saturated granular media to earthquake shaking. In their

simulations, they pin pointed the beginning of liquefaction both via micromechanics and via the sinking of an intruder lying on top of a saturated granular layer, which undergoes horizontal cyclic shaking. Liquefaction through simulations was specified by following the intruder sinking pattern in the same manner to phenomenological field observations of liquefaction during and following earthquakes. The outcomes of simulations show that dynamic response of the grains and the intruder are dependent on the horizontal acceleration. Both the grains and intruder move together with almost no sliding along granular contacts during low acceleration, resulting to no sinking of the intruder. At higher horizontal acceleration, grains show increased relative velocity, except in the intruder's vicinity where they move synchronously. The result of this dynamics shows the intruder sinks towards its isostatic position. The sinking of intruder is facilitated by the sliding of grain to grain contact, allowing for rearrangements of the medium surrounding the intruder. Granular sliding becomes easier with the buoyancy effect as the normal force between grains is reduced with respect to a dry layer. As the intruder is only partially immersed, there is less sliding in the intruder's vicinity and the buoyancy force acting to reduce the normal contact forces between the intruder and its neighbouring grains is smaller. Since these simulations do not account pore pressure, their results show that liquefaction with sinking structures can happen without increased pore pressure rise beyond hydrostatic values. The liquefaction of pre-compacted soil under drained conditions and repeated liquefaction events may be elaborated by this mechanism of buoyancy dependent liquefaction. It also predicts liquefaction with minimal energy and minimal earthquake-induced peak ground accelerations, presenting an elaboration for far-field liquefaction events with relatively small seismic energy input.

5. Effect of Grain Shape and Size on liquefaction-

Latha et al. (2022) studied the effect of grain shape on liquefaction and stated in his paper that as natural sand with regular shapes undergoes liquefaction easily, scientists came to conclusion that structures such as slopes and retaining walls can be built with natural sand of irregular manufactured sand to improve the stability and sustainability. Although the qualitative impacts of grain shape and size on the sand's resistance to liquefaction are well established, quantitative correlations between them remains challenging. Previous studies in this area have primarily relied on traditional methods such as sieve analysis and visual observations to quantify the grain size and shape. In a breakthrough investigation, scientists at the Indian Institute of Science (IISc) employed digital image analysis for grain shape characterizations and their associations with liquefaction potential of the sands. They found

a strong connection between the two. This is due to the reason that shear force needed to break the inter-locking between the soil particles is higher in case of sands with irregular shapes. Microscopic images of sand particles were analysed using computational algorithms developed in MATLAB (Matrix Laboratory), a powerful computing platform. This high-performance tool was employed to determine the shape parameters of the sand particles accurately. In cyclic simple shear tests, the sand samples are subjected to simulated earthquake conditions of alternate cycles of tension and compression. These tests were conducted to assess the sand's susceptibility to liquefaction under specific seismic scenarios. The researchers have found that glass beads having regular shape with higher roundness and sphericity undergoes liquefaction first in the cyclic shear test, while river sand having roundness and sphericity fall in between glass beads and manufactured sand liquifies next, followed by manufactured sand whose shape is comparatively irregular. These tests clearly indicates that grain shape plays an important role in influencing liquefaction resistance to soil. As the shape of sand grains is more irregular, deviating from their regular shape and their corners being sharper, they gets interconnected tightly during shearing. The inter-locking offers additional resistance to shear and hence the tendency to get separated from each other to float in the fluid becomes lesser for particles with irregular shapes. Moreover, tortuosity increases with sand particles having irregular shapes. Greater the tortuosity, water flow through the pores decreases and hence the chance for water to separate the particles decreases.

Latha and Lakkimsetti, (2022) also studied the effect of grain shape on liquefaction which are based on image based shape characterizations and laboratory liquefaction experiments. Microscopic images of sand particles were analysed using computational algorithms developed in MATLAB to determine their shape parameters. Performing cyclic simple shear tests on sand samples helps in assessing their potential to liquefy under cyclic loading conditions. Shape parameters of sands are associated to the liquefaction response of sands to unveil the basic mechanisms involved in the particle flow during liquefaction and the impacts of microscopic grain size and shape on the microscopic grain flow during liquefaction. Granular materials used in experiments are two different sands of same grain size with different grain shapes and glass beads of two different sizes. Samples of sands are extracted from sands originating from two different sources to maintain the difference in their grain shape. One of them is a natural river sand with subrounded particles and the other is a manufactured one with angular particles. Comparing the responses of spherical glass beads, subrounded river sand and the

manufactured angular sand will clearly unveil the effects of grain shape on the liquefaction response. Figure 3.7 illustrates the photograph of the granular materials used in this study.

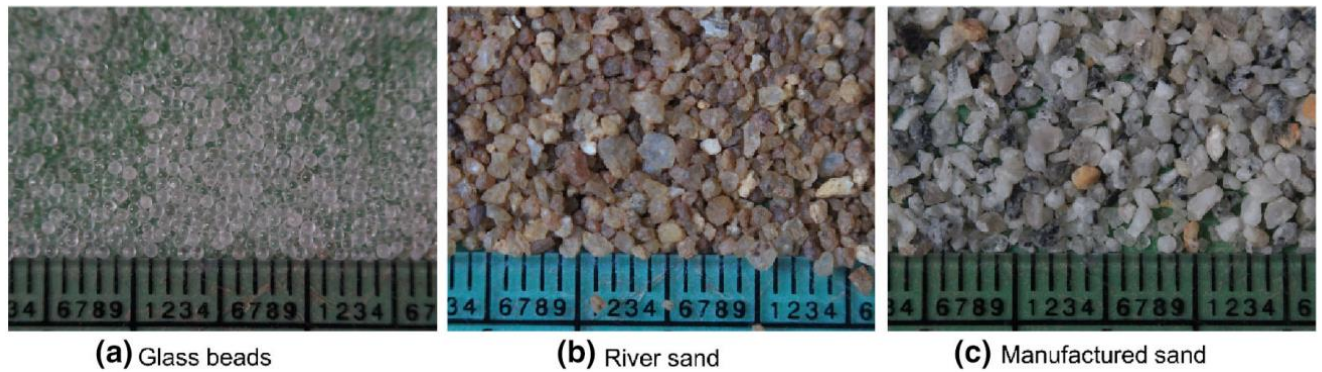


Fig.3.7 Photographic images of granular materials used a glass beads, b river sand, c manufactured sand

An advanced digital optical microscope is employed for capturing the microscopic images of representative grains taken from the granular assemblies. The shape computation is done in three steps such as preprocessing, image segmentation and shape analysis. During preprocessing, microscopic images are transformed into grayscale images to clearly distinguish the outline of the particle. Image segmentation technique available in MATLAB toolbox is used to transform the grayscale image to a binary image. Geometric computations are conducted on the binary image employing special algorithms developed in MATLAB to obtain the shape parameters. Figure 3.8 illustrates the microscopic images of representative particles from glass beads, river sand, and manufactured sand.

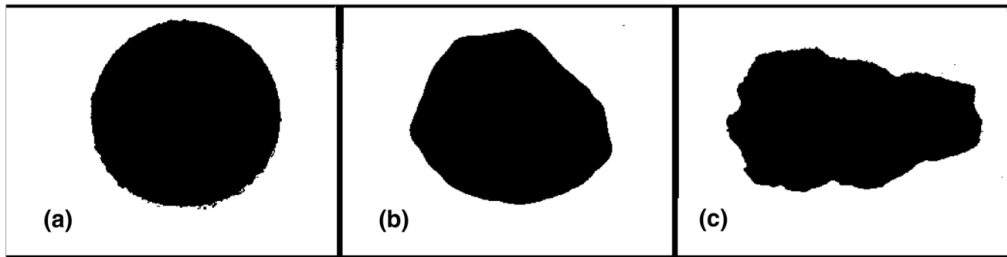


Fig.3.8 Microscopic images of typical particles a glass beads, b river sand, c manufactured sand

In the present study, A cyclic simple shear test setup (GCTS USA make) is employed for conducting cyclic simple tests. Figure 3.9 illustrates the response of glass beads of two varied grain sizes of 0.7 mm and 1.4 mm to the cyclic shear. The specimen with smaller glass beads will liquefy first in the 8th cycle, as compared to specimen with bigger glass beads which will be liquified in the 32nd cycle. These tests clearly unveils that the liquefaction potential of specimen decreases with increasing grain size.

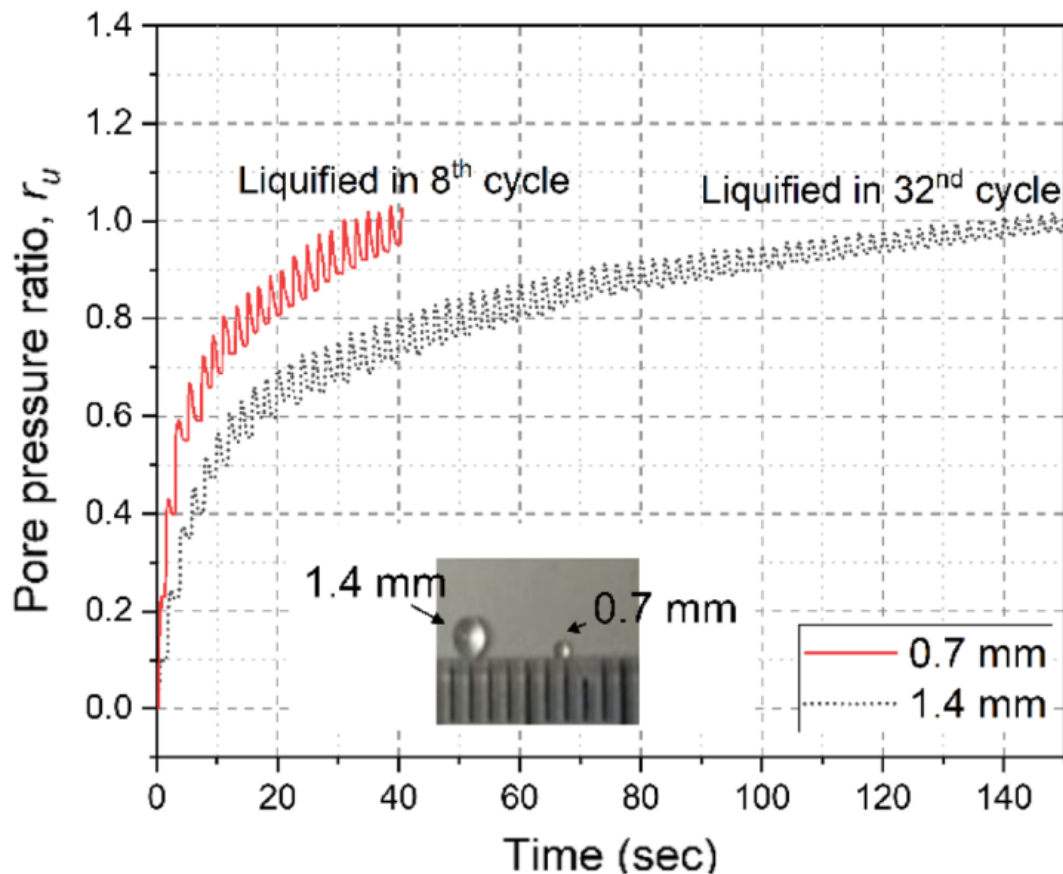


Fig.3.9 Effect of grain size (glass beads) on the liquefaction potential of granular assemblies

The reason behind quicker liquefaction in specimen with smaller grains is depicted in Fig.3.10. In the undrained tests carried out in this study, the propensity for densification is manifested through a notable rise in porewater pressure. Since small sized specimens have smaller pores, the pore water pressure developed is higher in these specimens as compared to large sized specimens, where pore sizes are bigger and the pore water pressure developed is smaller. Hence, the pore water pressure rises intensely in small sized specimens with progressive shearing, which implies that small sized particles undergoes liquefaction quickly as compared to large sized particles. To explore the impacts of grain shape, consolidated undrained cyclic simple shear tests were conducted on specimens made of the same sized glass beads, river sand and manufactured sand. Examining Fig. 3.10 reveals that in the cyclic shear tests, glass beads, characterized by a regular shape with higher roundness and sphericity, experienced liquefaction first. Subsequently, river sand, with intermediate roundness and sphericity between glass beads and manufactured sand, underwent

liquefaction, followed by manufactured sand, exhibiting a relatively irregular shape. Glass beads, river sand, and manufactured sand required 8, 13, and 16 cycles, respectively, to attain a porewater pressure ratio of 1.0.

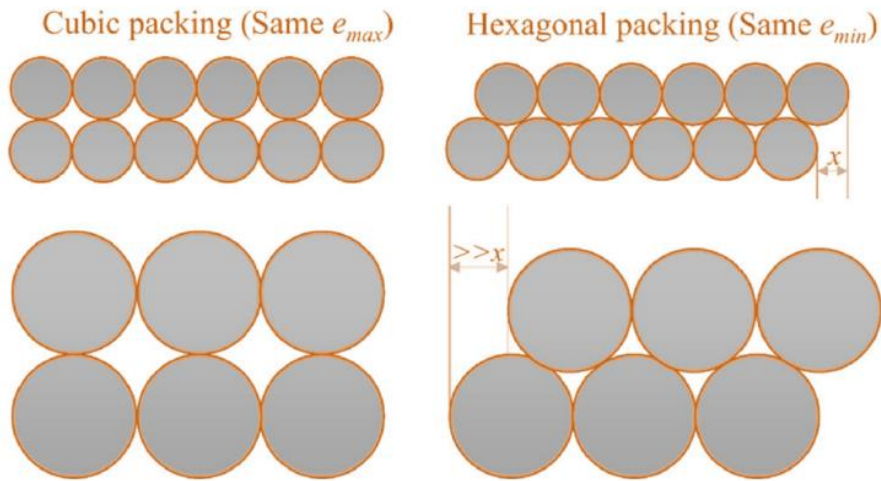


Fig.3.10 Grain size effects on densification and liquefaction

These tests reveal the significant impacts of grain shape on the liquefaction potential of granular materials which can be explained through fig.3.11. Examining Fig.3.12 reveals that particles with higher roundness and sphericity exhibit rolling behaviour during shearing. In contrast, particles with irregular shape deviate from a spherical form and corners become more and more sharper gets interlocked with each other during shearing. This interlocking imparts extra resistance to shear and hence the tendency to get disconnected from each other to float in the fluid becomes lesser for irregular shaped particles. The prolonged liquefaction time observed in manufactured sand specimens is due to the shear force needed to disrupt the interparticle locking is more because of their relatively irregular shape, as indicated by the lowest sphericity and roundness values.

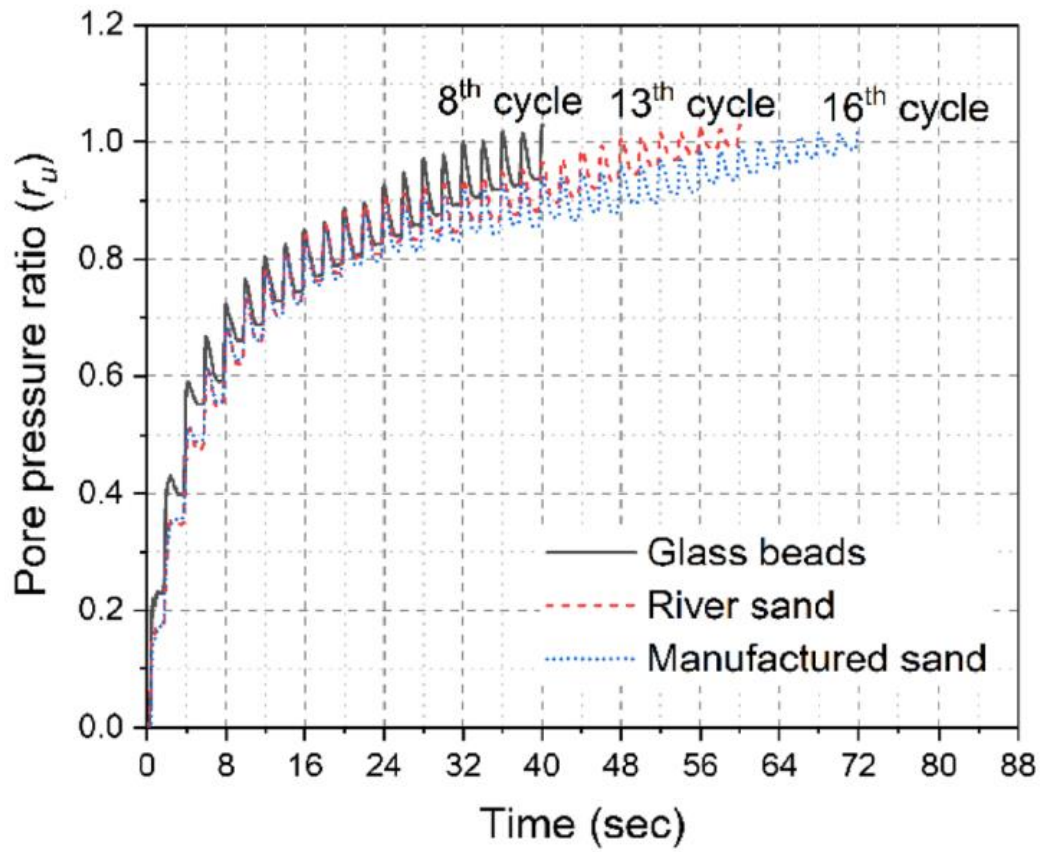


Fig. 3.11 Effect of size of grain shape on the liquefaction potential of granular assemblies

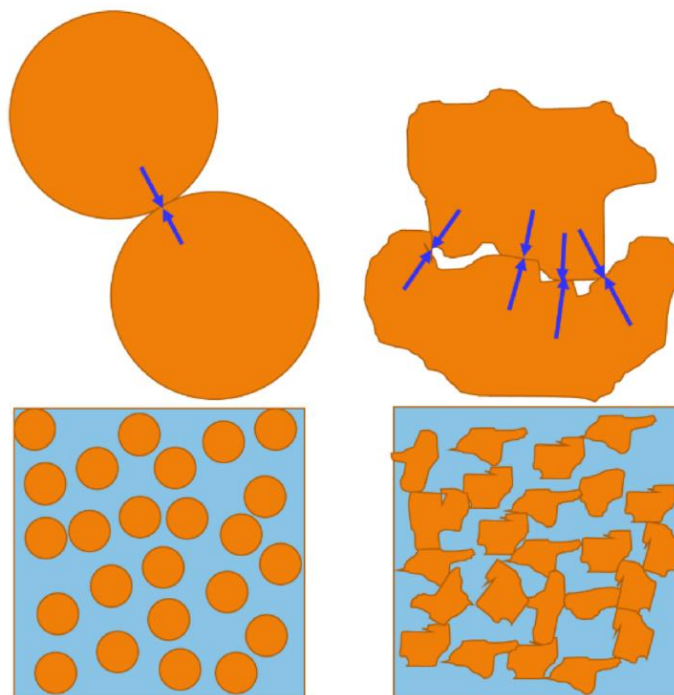


Fig.3.12 Grain shape effects on interlocking and liquefaction

Chapter 4

Identification of Liquefiable Soil

4.1 Introduction

Liquefiable soil is that soil which undergoes liquefaction resulting to loss of shear strength or stiffness due to rise of pore water pressure during an earthquake. There is significant vertical settlement or deformation and nearly zero effective stress in liquefied soil (EN 1998-5: Eurocode 8:2004). As we are aware of the aftermath of soil liquefaction, so it is crucial to evaluate liquefaction potential of soil to counteract its effect and ensure structural safety. So, before proceeding to its assessment, it is essential to identify liquefiable soil.

4.2 Identification of liquefiable soil

Liquefaction generally occurs in case of saturated fine sand and silt. Tsuchida H pioneered the identification of liquefaction susceptibility with the use of grain size distribution curves for silt and sand (Debnath R et al., 2021). Fig.4.1 depicts the ranges of particle sizes of silt and sand which are falling under liquefiable zone and highly liquefiable zone respectively. Generally, soils with a significant plasticity do not undergo soil liquefaction but some clayey soils in China have been observed to undergo liquefaction in past earthquakes. Based on the Chinese findings, Seed and Idriss (1981,1982; Seed et al. 1983) suggested that soils with significant plastic fines should be assessed for possible liquefaction based on the Atterberg limits. The identification of liquefaction in case of cohesive soil is based on the following four criteria originally stated by Seed and Idriss (1982) and subsequently confirmed by Youd and Gilstrap (1999)-

1. The soil must contain less than 15 percent of the particles, based on dry weight which are finer than 0.005 mm (i.e., percent finer at 0.005 mm < 15 percent).
2. The liquid limit (LL) of the soil must be less than 35 (that is, $LL < 35$).
3. The water content w of the soil must exceed 90% of the liquid limit [i.e., $w > 0.9 LL$].
4. The liquidity index must be less than 0.75.

Although a soil fulfils all the above criteria, it still may or may not undergo liquefaction as liquefaction is also influenced by factors such as density and initial stress conditions. As the development of excess pore water pressure during an earthquake is firmly influenced by both density and initial stress conditions, liquefaction depends on the initial state of the soil.

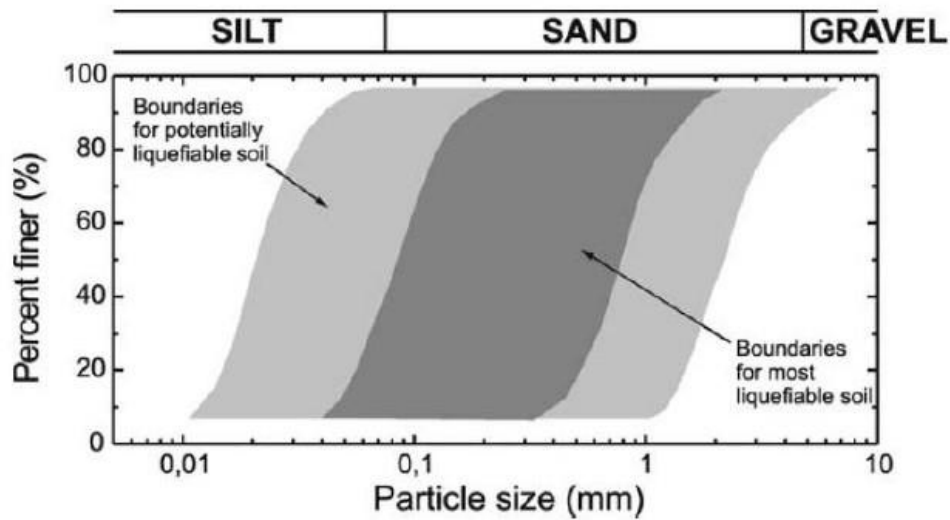


Fig. 4.1 Particle Size Distribution for liquefiable soils (Tsuchida H-1970)

Identification of soil susceptibility to liquefaction provides a preliminary idea of soil resistance to liquefaction. Once the liquefiable soil has been identified, one can proceed to evaluate the liquefaction potential of soil as per methods mentioned in previous chapter. Standard penetration test was conducted at two borehole points namely BH1 and BH2 for carrying out detailed assessment on liquefaction potential of soil. Photograph of Standard Penetration Test conducted at site is shown in Fig.4.2.



Fig.4.2 Photograph of Standard Penetration Test conducted at site

Data of two more borehole points namely BH3 and BH4 from earlier project work were taken for the assessment (Barbhuiya B S F et al. 2020). One seismic cross hole test

was conducted at one location in the study area. The cross-section and sub-soil profile of BH1 and BH2 are illustrated in Fig. 4.3 and 4.4 respectively. The subsoil profile of BH1 comprises of reddish, brown clay with silt upto a depth of 14.00m, followed by grayish medium sand upto 35.00m. The reddish, brown clay with silt layer was suspected as a liquefiable layer. Similarly, the identification of liquefiable soil based on particle sizes or as per criteria laid by Chinese criteria can be carried out for other boreholes. Thereafter, detailed assessment of liquefaction potential for the boreholes BH1, BH2, BH3 and BH4 were carried out following the “Simplified Procedure” which was introduced by Seed and Idriss, 1971(IS 1893(Part 1):2016).

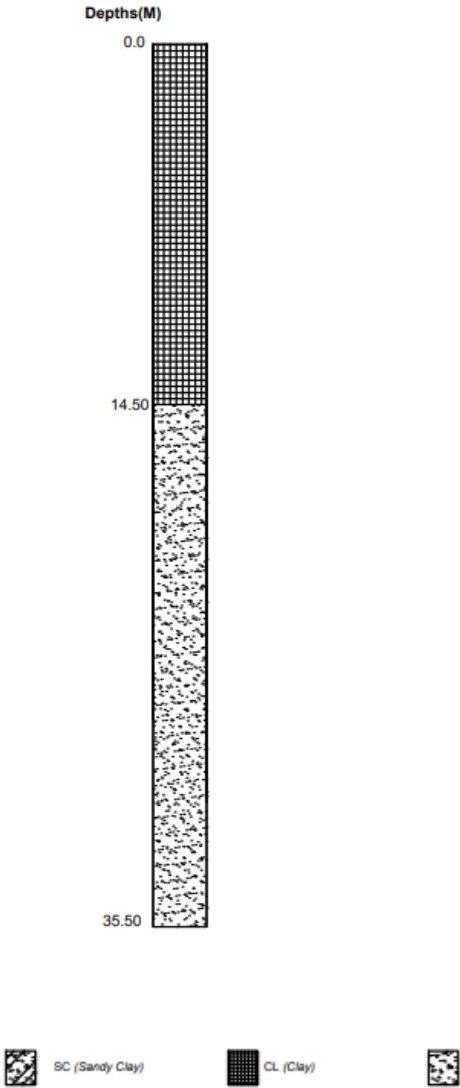


Fig.4.3 Cross-section and subsoil profile for BH1(Source-Reliant Foundations)

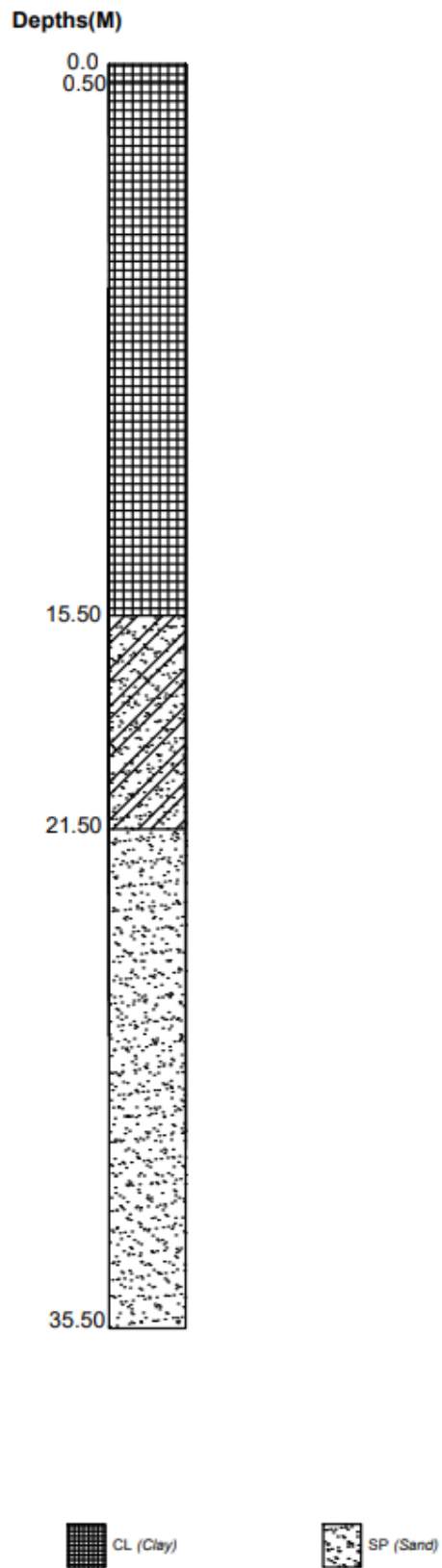


Fig.4.4 Cross-section and subsoil profile for BH2(Source-Reliant Foundations)

Chapter 5

Liquefaction Analysis by Simplified Procedure

5.1 Introduction

The first step in engineering assessment of the potential of initiation of soil liquefaction is the determination of whether the soils present at the site are potentially liquefiable or not. It is generally adopted that loose, saturated, cohesionless soils are susceptible to liquefaction while dense cohesionless soils are considered to be non liquefiable because they tend to dilate during shearing. Cohesive soils are to be considered susceptible to liquefaction when they fulfil all the three criteria listed below, originally stated by Seed and Idriss (1982) and subsequently confirmed by Youd and Gilstrap (1999):

1. The soil must contain less than 15 percent of the particles, based on dry weight which are finer than 0.005 mm (i.e., percent finer at 0.005 mm < 15 percent).
2. The liquid limit (LL) of the soil must be less than 35 (that is, LL < 35).
3. The water content w of the soil must exceed 90% of the liquid limit [i.e., $w > 0.9$ LL].
4. The liquidity index must be less than 0.75.

If the cohesive soil does not fulfil all the three criteria, then it is generally considered to be not susceptible to liquefaction. Although the cohesive soil may not liquefy, but there could still be a significant undrained shear strength loss due to the seismic shaking.

5.2 Determination of Liquefaction Potential

The most common type of analysis for determining the liquefaction potential is the use of standard penetration test (Seed et al, 1985; Stark and Olson, 1995). The analysis is based on a method often termed as the Simplified Procedure proposed by Seed and Idriss (1971). This is the most commonly used and the oldest method to evaluate the liquefaction potential of a site. This procedure can also be used with Cone Penetration Test (CPT) tip resistance or Shear Wave Velocity V_s . This approach, which is mainly empirical in nature, has developed into the standard method for assessing soil liquefaction resistance over time. It has been updated and refined, particularly through key papers by Seed in 1979, Seed and Idriss in 1982, and Seed et al. in 1985. In 1966, Professors T.L. Youd and I.M. Idriss alongwith 20 experts organized a workshop sponsored by the National Centre for Earthquake Engineering Research (NCEER) to gather insights and enhancements for the simplified procedure. This paper outlines the suggestions from the NCEER 1996 workshop.

The steps involved in the are as follows:

1. Appropriate soil type: As discussed above, the first step is to determine if the soil has the ability to liquefy during an earthquake. The soil must meet the requirements listed above.

2. Groundwater table: The soil must be below the groundwater table. However, the liquefaction analysis could also be performed if it is anticipated that the groundwater table will rise in the future, and thus the soil will eventually be below the groundwater table.

3. CSR induced by earthquake: If the soil meets the above two requirements, then the simplified procedure can be performed. The first step in the simplified procedure is to determine the cyclic stress ratio (CSR) that will be induced by the earthquake. A major unknown in the calculation of the CSR induced by the earthquake is the peak horizontal ground acceleration a_{max} that should be used in the analysis. A liquefaction analysis would typically not have required for sites having a peak ground acceleration a_{max} less than 0.10g or a local magnitude M_L less than 5.

4. CRR from standard penetration test: By using the standard penetration test, the cyclic resistance ratio (CRR) of the in situ soil is then determined. If the CSR induced by the earthquake is greater than the CRR determined from the standard penetration test, then liquefaction may occur during the earthquake, and vice versa.

5. Factor of safety (FS): The final step is to determine the factor of safety against liquefaction which is defined as below.

$$FS = CRR/CSR$$

5.3 Cyclic Stress Ratio (CSR) Caused by the Earthquake

If it is found by analysis that the soil has the potential to liquefy during an earthquake and the soil is below or will be below the groundwater table, then the liquefaction analysis is performed. As per Seed and Idriss (1971), the first step in the simplified procedure is to calculate the C.S.R) which is caused by the earthquake.

To develop the equation for CSR, it is assumed that there is a level ground surface and a soil column of unit width and length, and that the soil column will move horizontally as a rigid body in response to the maximum horizontal acceleration, a_{max} exerted by the earthquake at ground surface. Figure 5.1 shows a diagram of these assumed conditions. Given these assumptions, the weight W of the soil column is equal to $\gamma_t z$, where γ_t = total unit weight of the soil and z = depth below ground surface. The horizontal earthquake force, F acting on the soil column with a unit width and length is-

$$F = ma = \left(\frac{W}{g}\right) a = (\gamma_t z/g) a_{\max} = \sigma_{vo} (a_{\max}/g) \quad (5.1)$$

where,

F- horizontal earthquake force acting on soil column with a unit width and length, kN

m- total mass of soil column, kg, which is equal to W/g

W- total weight of soil column, kN

γ_t - total unit weight of soil, kN/m³

z- depth below ground level of soil column

a- acceleration, which in this case is the maximum horizontal acceleration at ground surface caused due to earthquake ($a = a_{\max}$), m/s²

a_{\max} - maximum horizontal acceleration at ground surface that is induced by the earthquake, m/s². The maximum horizontal acceleration is also commonly known as the peak ground acceleration

σ_{vo} - total vertical stress at bottom of soil column, kN/m²

As shown in Fig. 5.1, taking summation of the forces in the horizontal direction, the force F acting on the rigid soil element is equal to the maximum shear force at the base on the soil element. Since the soil element is assumed to have a unit base width and length, the maximum shear force F is equal to the maximum shear stress τ_{\max} , or from Eq

$$\tau_{\max} = F = \sigma_{vo} (a_{\max}/g) \quad (5.2)$$

The above expression is divided by the vertical effective stress σ'_{vo} which gives

$$\tau_{\max}/ \sigma'_{vo} = (\sigma_{vo} / \sigma'_{vo})(a_{\max}/g) \quad (5.3)$$

Since the soil column does not act as a rigid body during the earthquake, but rather the soil is deformable, Seed and Idriss (1971) incorporated a depth reduction factor r_d into the right side of Eq. (5.3), or

$$\tau_{\max}/ \sigma'_{vo} = r_d (\sigma_{vo} / \sigma'_{vo})(a_{\max}/g) \quad (5.4)$$

For the simplified method, Seed et al. (1975) transformed the typical irregular earthquake record to an equivalent series of uniform stress cycles by assuming the following:

$$\tau_{cyc} = 0.65 \tau_{max} \quad (5.5)$$

where, τ_{cyc} - uniform cyclic shear stress amplitude of the earthquake (kN/m²)

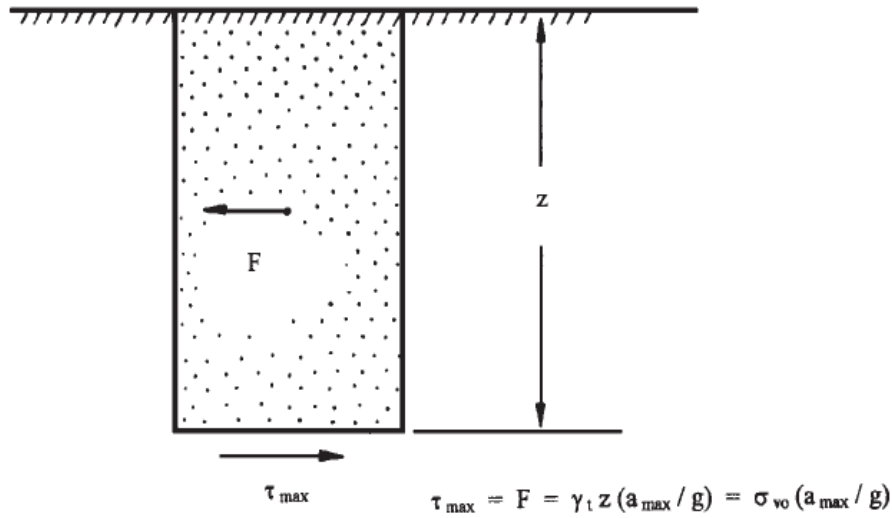


Fig 5.1: Conditions assumed for the derivation of the earthquake equation

In essence, the erratic earthquake motion was converted to an equivalent series of uniform cycles of shear stress, referred to as τ_{cyc} . By substituting Eq. (5.5) into Eq. (5.4), the earthquake-induced cyclic stress ratio is obtained.

$$CSR = \tau_{cyc} / \sigma'_{v0} = 0.65 r_d (\sigma_{v0} / \sigma'_{v0}) (a_{max} / g) \quad (5.6)$$

where

CSR- cyclic stress ratio, also known as seismic stress ratio.

a_{max} - maximum horizontal acceleration at ground surface that is induced by the earthquake, m/s², also commonly referred to as the peak ground acceleration

g- acceleration of gravity (9.81 m/s²).

σ_{v0} - total vertical stress at a particular depth where the liquefaction analysis is being performed, kN/m². To calculate total vertical stress, total unit weight γ_t of soil layer (s) must be known.

σ'_{v0} - vertical effective stress at that same depth in soil deposit where σ_{v0} was calculated, kN/m². To calculate vertical effective stress, location of groundwater table must be known

r_d - depth reduction factor, also termed as stress reduction coefficient is a dimensionless factor

As previously mentioned, the depth reduction factor was introduced to account for the fact that the soil column shown in Fig.5.1 does not behave as a rigid body during the earthquake. Fig.5.2 presents the range in values for the depth reduction factor r_d versus depth below ground surface. Point to note that with depth, the depth reduction factor decreases to account for the fact that the soil is not a rigid body, but is rather deformable. As indicated in Fig. 5.2 Idriss (1999) indicates that the values of r_d depend on the magnitude of the earthquake. As a practical matter, the r_d values are usually obtained from the curve labelled “Average values by Seed & Idriss (1971)” in Fig. 5.2.

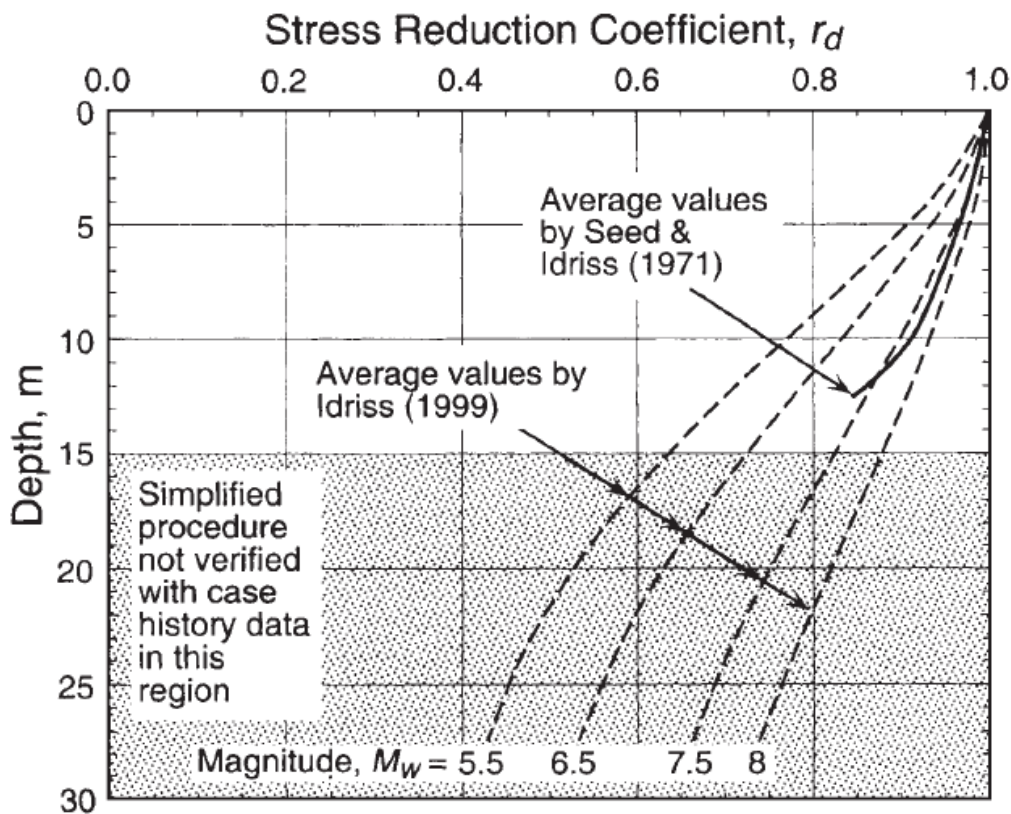


Fig. 5.2: Reduction factor r_d versus depth below level or gently sloping ground surfaces

Another alternative is to presume a linear relationship of r_d versus depth and use the following expression by Kayen et al. 1992-

$$r_d = 1 - 0.012z \quad (5.7)$$

where z = depth in meters below the ground level where the liquefaction assessment is being conducted (i.e., depth used is same to calculate σ_{v0} and σ'_{v0})

The participants from the workshop suggested minor modification to the procedure for calculation of CSR as follows-

For routine applications and less critical projects, the following equation can be utilized to estimate the average values of r_d (Liao and Whitman, 1986.).

$$r_d = 1.0 - 0.00765z \quad \text{for } 0 < z \leq 9.15 \text{ m} \quad (5.8)$$

$$r_d = 1.174 - 0.0267z \quad \text{for } 9.15 \text{ m} < z \leq 23.0 \text{ m} \quad (5.9)$$

where z is the depth in metre below the ground level

The value of r_d is obtained from the following plot for computational simplicity. T.F. Blake derived an approximation of the mean curve depicted in the above figure using the following equation.

$$r_d = (1.000 - 0.4113z^{0.5} + 0.04052z + 0.001753z^{1.5}) / (1.000 - 0.4177z^{0.5} + 0.05729z - 0.006205z^{1.5} + 0.001210z^2)$$

where z is the depth (in metre) below the ground level.

The r_d versus depth curves from Seed and Idriss, 1971 is shown below (Fig.5.3).

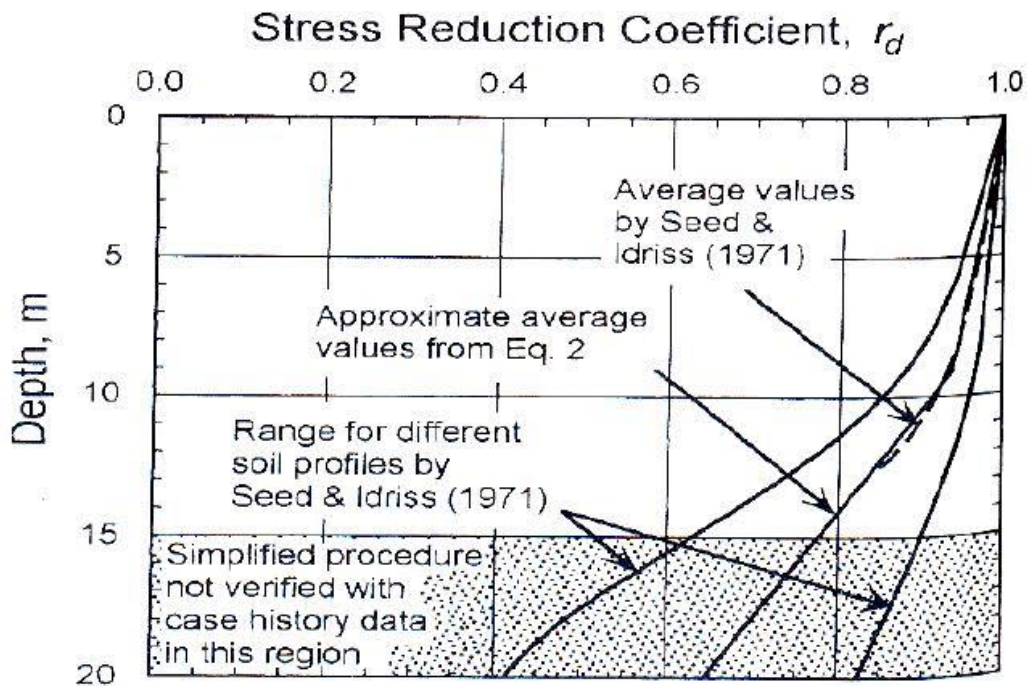


Fig. 5.3 r_d versus depth curves (Seed and Idriss, 1971)

For Eq. (5.6), the vertical total stress σ_{vo} and vertical effective stress σ'_{vo} can be readily calculated using basic geotechnical principles. Equation (5.7) or Fig.5.3 could be used to determine the depth reduction factor r_d . Thus all parameters in Eq. (5.6) can be readily calculated, except for the peak ground acceleration a_{max} .

5.4 Evaluation of Cyclic Resistance Ratio (CRR)

The second step in the simplified procedure is to determine the cyclic resistance ratio of the in situ soil. The cyclic resistance ratio represents the liquefaction resistance of the in situ soil which is given by the equation -

$$CRR = CRR_{7.5}(MSF) K_{\sigma} K_{\alpha} \quad (5.10)$$

where $CRR_{7.5}$ is standard cyclic resistance ratio for a 7.5 magnitude earthquake obtained using values of SPT or CPT or V_s .

MSF is magnitude scaling factor given by,

$$MSF = 10^{2.24} / M_w^{2.56}$$

This factor is required when magnitude is different than 7.5. K_{σ} and K_{α} are correction for high overburden stresses and correction for static shear stresses respectively. The most commonly used method for determining the liquefaction potential is to use the SPT data. The advantages of using the standard penetration test to assess the liquefaction potential are as follows:

1. Groundwater table: A boring must be excavated in order to perform the standard penetration test. The location of the groundwater table can be measured in the borehole. Another option is to install a piezometer in the borehole, which can then be used to monitor the groundwater level over time.

2. Soil type: In clean sand, the SPT sampler may not be able to retain a soil sample. But for most other types of soil, the SPT sampler will be able to retrieve a soil sample. The soil sample retrieved in the SPT sampler can be used to visually classify the soil and to estimate the percent fines in the soil. In addition, the soil specimen can be returned to the laboratory, and classification tests can be performed to further assess the liquefaction susceptibility of the soil.

3. Relationship between N value and liquefaction potential: In general, the factors that increase the liquefaction resistance of a soil will also increase the $(N_1)_{60}$ from the standard penetration test. For example, a well-graded dense soil that has been preloaded or aged will be resistant to liquefaction and will have high values of $(N_1)_{60}$. Likewise, a uniformly graded soil with a loose and segregated soil structure will be more susceptible to liquefaction and will have much lower values of $(N_1)_{60}$.

Based on the standard penetration test and field performance data, Seed et al. (1985) concluded that there are three approximate ranges for potential damage that can be identified.

Table 5.1: $(N_1)_{60}$ values

$(N_1)_{60}$	0–20	20–30	> 30
Potential damage	High	Intermediate	No significant damage

As indicated in above table 5.1, an $(N_1)_{60}$ value of 20 is the approximate boundary between the medium and dense states of the sand. Above an $(N_1)_{60}$ of 30, the sand is in either a dense or a very dense state. For this condition, initial liquefaction does not produce large deformations because of the dilation tendency of the sand upon reversal of the cyclic shear stress. This is the reason that such soils produce no significant damage, as indicated by the above table.

Determination of the cyclic resistance ratio of the in situ soil as follows:

1. With SPT values

This figure was developed from investigations of numerous sites that had liquefied or did not liquefy during earthquakes. For most of the data used in Fig. 5.4, the earthquake magnitude was close to 7.5 (Seed et al. 1985). The three lines shown in Fig. 5.4 are for soil that contains 35, 15, or 5 percent fines. The lines shown in Fig. 5.4 represent approximate dividing lines, where data to the left of each individual line indicate field liquefaction, while data to the right of the line indicate sites that generally did not liquefy during the earthquake. Use of Fig. 5.4 to determine the cyclic resistance ratio of the in situ soil is obtained from the CRR versus $(N_1)_{60}$ plot as shown. It is observed from the original development Seed et al. 1985 that CRR increases with increase in fines content. Seed et al. developed CRR curves for various fines content based on available empirical data. Workshop participants created an updated correction for fines content to better match the empirical data and facilitate computations using spreadsheets and other electronic tools.

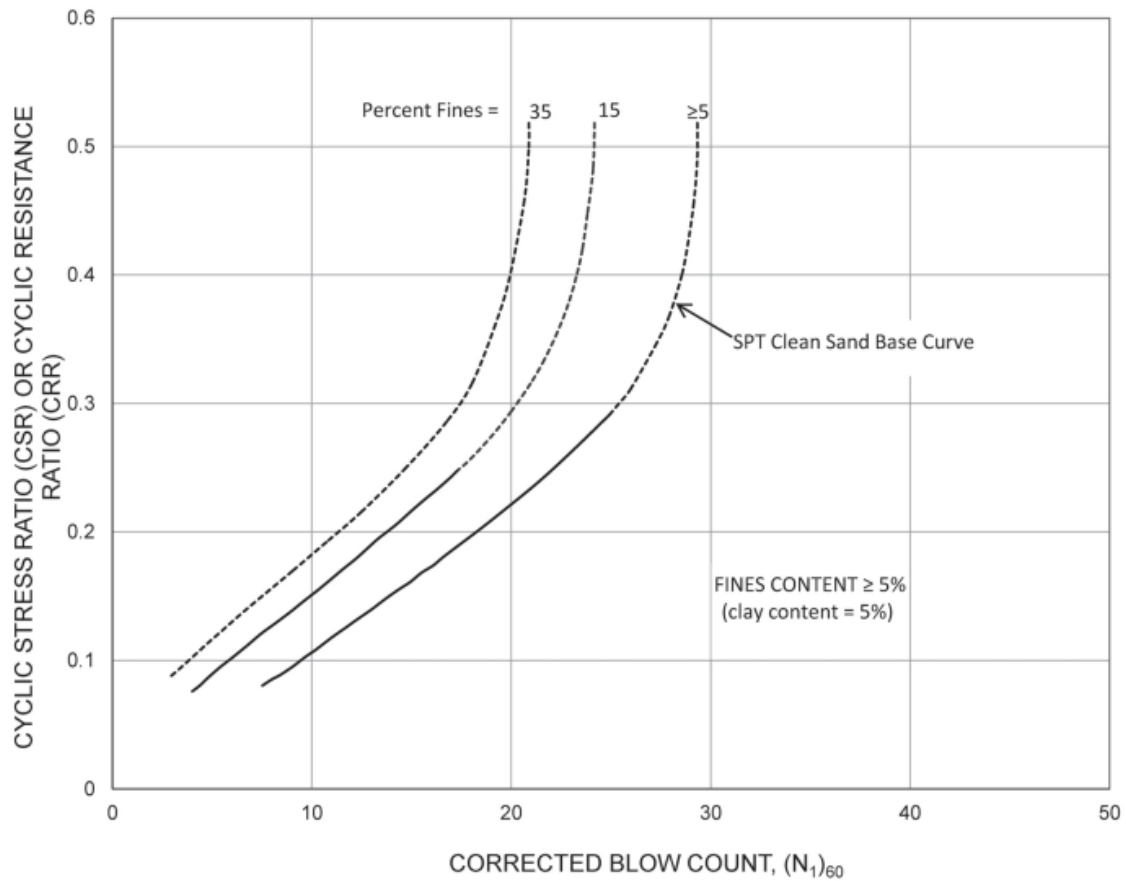


Fig. 5.4: Plot used to determine the cyclic resistance ratio for clean and silty sands for $M= 7.5$ earthquakes.(Source-IS 1893 Part 1:2016)

$(N_1)_{60}$ is the blow count normalised to an effective overburden pressure of approximately 100kPa and a hammer efficiency of 60% which is given by the following equation-

$$(N_1)_{60} = C_N N_{60}$$

where $C_N = \sqrt{(P_a / \sigma'_{vo})} \leq 1.7$ [For effective overburden pressures less than 200kPa]

$$C_N = 2.2 / (1.2 + \sigma'_{vo} / P_a) \text{ [For effective overburden pressures greater than 200kPa]}$$

The CRR for 7.5 earthquake magnitude, $CRR_{7.5}$ is estimated from Fig.5.4 using $(N_1)_{60}$ value.

The effect of fines content FC (%) can be rationally accounted by correcting $(N_1)_{60}$ and finding $(N_1)_{60CS}$ as follows-

$$(N_1)_{60CS} = \alpha + \beta(N_1)_{60}$$

where

$$\alpha = 0 \quad \beta = 1 \quad \text{for } FC \leq 5 \text{ percent}$$

$$\alpha = e^{\left[1.76 - \left(\frac{190}{FC^2}\right)\right]} \quad \beta = 0.99 + \frac{FC^{1.5}}{1000} \quad \text{for } 5 \text{ percent} < FC < 35 \text{ percent}$$

$$\alpha = 0.5 \quad \beta = 1.2 \quad \text{for } FC \geq 35 \text{ percent}$$

Instead of using fig.5.4, $CRR_{7.5}$ can be estimated using the following equation-

$$CRR_{7.5} = 1/[34 - (N_1)_{60CS}] + (N_1)_{60CS}/135 + 50/[10 * (N_1)_{60CS} + 45]^2 - 1/200$$

The corrected N value is computed as follows-

$$(N_1)_{60} = C_N N_{60} = C_N N C_{60} = N C_N C_{HT} C_{HW} C_{SS} C_{RL} C_{BD}$$

where N = measured standard penetration resistance

C_{HT} , C_{HW} , C_{SS} , C_{RL} and C_{BD} are correction factors

The various corrections are tabulated in Table 5.2 below:

Table 5.2 Correction Factors for Non-Standard SPT Procedures and Equipment

Sl No. (1)	Correction for (2)	Correction Factor (3)
i)	Non-standard hammer weight or height of fall	$C_{HT} = \begin{cases} 0.75 \text{ (for Donut hammer with rope and pulley)} \\ 1.33 \text{ (for Donut hammer with trip/auto)} \end{cases}$ and Energy ratio = 80 percent
ii)	Non-standard hammer weight or height of fall	$C_{HW} = \frac{HW}{48387}$ where H = height of fall (mm), and W = hammer weight (kg)
iii)	Non-standard sampler setup (standard samples with room for liners, but used without liners)	$C_{SS} = \begin{cases} 1.1 \text{ (for loose sand)} \\ 1.2 \text{ (for dense sand)} \end{cases}$
iv)	Non-standard sampler setup (standard samples with room for liners, but liners are used)	$C_{SS} = \begin{cases} 0.9 \text{ (for loose sand)} \\ 0.8 \text{ (for dense sand)} \end{cases}$
v)	Short rod length	$C_{RL} = \begin{cases} = 0.75 \text{ (for rod length 0-3 m)} \\ = 0.80 \text{ (for rod length 3-4 m)} \\ = 0.85 \text{ (for rod length 4-6 m)} \\ = 0.95 \text{ (for rod length 6-10 m)} \\ = 1.0 \text{ (for rod length 10-30 m)} \end{cases}$
vi)	Nonstandard borehole diameter	$C_{BD} = \begin{cases} = 1.00 \text{ (for bore hole diameter of 65-115 mm)} \\ = 1.05 \text{ (for bore hole diameter of 150 mm)} \\ = 1.15 \text{ (for bore hole diameter of 200 mm)} \end{cases}$

NOTES

1 N = Uncorrected SPT blow count.

2 $C_{60} = C_{HT} C_{HW} C_{SS} C_{RL} C_{BD}$

3 $N_{60} = N C_{60}$

4 C_N = Correction factor for overburden pressure $(N_1)_{60} = C_N C_{60} N$.

5.5 Correction for K_σ : This correction for high overburden stresses is needed when overburden pressure is high for depth more than 15 m and can be found as follows-

$$K_\sigma = (\sigma'_{vo} / P_a)^{(f-1)}$$

where σ'_{vo} is the effective overburden pressure and P_a is the atmospheric pressure both measured in the same units and f is an exponent and its value depends on the relative density D_r . For $D_r = 40\% - 60\%$, $f = 0.8-0.7$ and for $D_r = 60\% - 80\%$, $f = 0.7-0.6$.

5.6. Correction for other magnitude earthquakes: Fig.5.4 is for a projected earthquake that has a magnitude of 7.5. The final factor that must be included in the analysis is the magnitude of the earthquake. The higher the magnitude of the earthquake, the longer the duration of ground shaking. A higher magnitude will thus result in a higher number of applications of cyclic shear strain, which will decrease the liquefaction resistance of the soil. Fig.5.4 was developed for an earthquake magnitude of 7.5; and for other different magnitudes, the CRR values from Fig. 5.4 would be multiplied by the magnitude scaling factor indicated in Table 5.3. Fig.5.5 presents other suggested magnitude scaling factors.

Table 5.3: Magnitude scaling factors

Anticipated earthquake magnitude	Magnitude scaling factor
8.5	0.89
7.5	1.00
6.75	1.13
6	1.32
5.25	1.50

(Source: Seed et al. (1985))

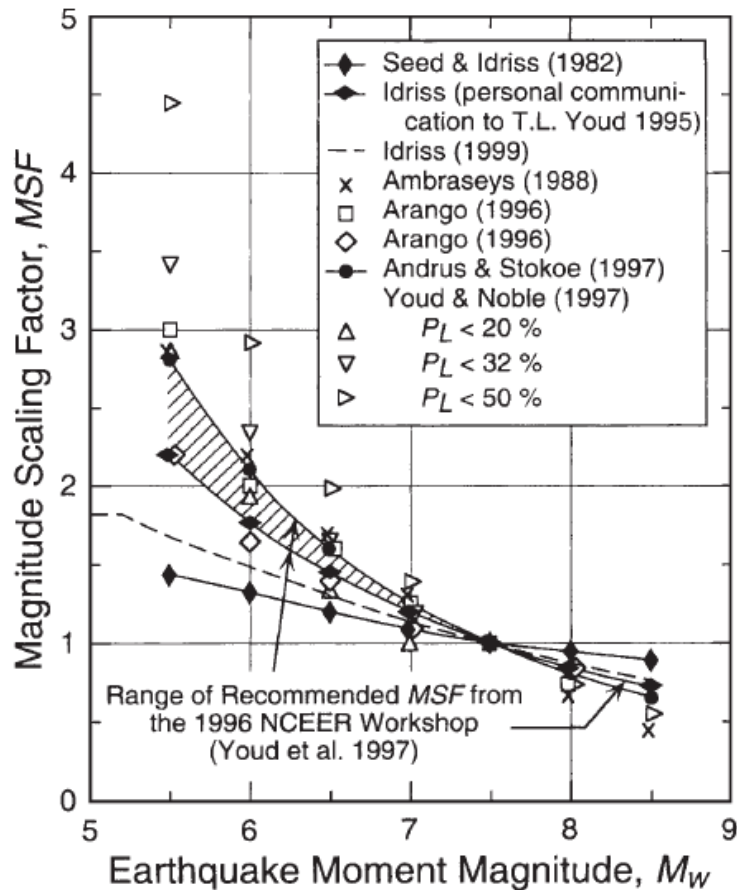


Fig.5.5: Magnitude scaling factors derived by various investigators

It could be concluded that the local magnitude M_L , the surface wave magnitude M_s , and moment magnitude M_w scales are reasonably close to one another below a value of about 7. Thus for a magnitude of 7 or below, any one of these magnitude scales can be used to determine the magnitude scaling factor. At high magnitude values, the moment magnitude M_w tends to significantly deviate from the other magnitude scales, and the moment magnitude M_w should be used to determine the magnitude scaling factor from Table 5.3 or Fig. 5.5.

Two additional correction factors may need to be included in the analysis. The first correction factor is for the liquefaction of deep soil layers (i.e., depths where $\sigma'_{vo} > 100$ kN/m², in which liquefaction has not been verified by the Seed and Idriss simplified procedure). The second correction factor is for sloping ground conditions. Both the peak ground acceleration a_{max} and the length of ground shaking increase for sites having soft, thick, and submerged soils. In a sense, the earthquake magnitude accounts for the increased shaking at a site; that is, the higher the magnitude, the longer the ground is subjected to shaking. Thus for sites having soft, thick and submerged soils, it may be prudent to increase

both the peak ground acceleration a_{max} and the earthquake magnitude to account for local site effects.

5.7 Factor of Safety against Liquefaction:

The final step in the liquefaction analysis is to calculate the factor of safety against liquefaction. If the cyclic stress ratio caused due to anticipated earthquake [Eq. (5.6)] exceeds the cyclic resistance ratio of the in situ soil, then liquefaction could occur during the earthquake, and vice versa. The factor of safety against liquefaction (FS) is defined as follows:

$$FS = CRR/CSR \quad (5.11)$$

The higher the factor of safety, the more resistant the soil is to liquefaction. However, soil that has a factor of safety slightly greater than 1.0 may still liquefy during an earthquake. For example, if a lower layer liquefies, then the upward flow of water could induce liquefaction of the layer that has a factor of safety slightly exceeding 1.0.

2. With Shear Wave Velocity, V_s

Shear wave velocity V_s for clean sands after correction for overburden stress is given by-

$$V_{s1} = \left(\frac{P_a}{\sigma'_{vd}} \right)^{0.25} V_s$$

where V_{s1} is overburden stress corrected shear wave velocity. We can obtain the value of $CRR_{7.5}$ using V_{s1} from Fig.5.6. The graphical representation between shear wave velocity and depth is shown in Fig. 5.7.

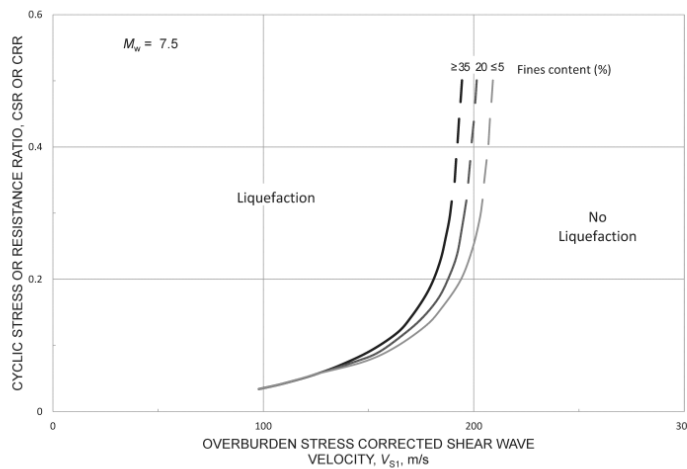


Fig. 5.6 Relation between CRR and V_{s1} for M_w 7.5 earthquakes (Source-IS 1893 Part 1:2016)

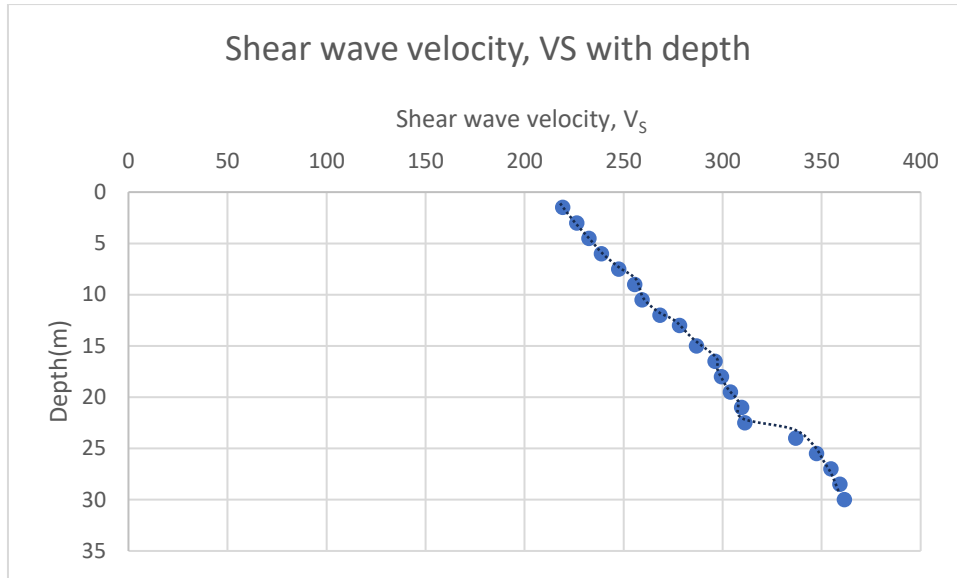


Fig.5.7 Plot for Shear wave velocity, V_s against Depth

$CRR_{7.5}$ can also be calculated from the following equation-

$$CRR_{7.5} = a \left(\frac{V_{s1}}{100} \right)^2 + b \left(\frac{1}{V_{s1}^* - V_{s1}} - \frac{1}{V_{s1}^*} \right)$$

where V_{s1}^* is limiting upper value of V_{s1} for liquefaction occurrence; a and b are curve fitting parameters. The values of a and b are 0.022 and 2.8 respectively in the above Fig.5.6. V_{s1}^* can be presumed to vary linearly from 200 m/s for soils with fines content of 35% to 215 m/s for soils with fines content with 5% or less. Andrus and Stokoe (2000) recommended the following relationship for calculating V_{s1}^* for fines content in between 5% and 35% -

$$V_{s1}^* = 215 - 0.5(FC - 5) \text{ m/s for } 5\% < FC < 35\%$$

where FC is average fines content in percent by mass. CRR yield a value of about 0.6 at V_{s1} 210 m/s. Based on penetration- V_s correlations, a V_{s1} value of 210 m/s is considered equivalent to a corrected SPT blow count of 30 in clean sands.

Then factor of safety against liquefaction using V_{s1} can be calculated by the equation-

$$FS = CRR/CSR$$

where CRR is as estimated above in step 5.10 and CSR in step 5.6. When the design ground motion is conservative, earthquake related permanent ground deformation is typically minimal, if FS greater than equal to 1.2. If FS less than 1 then the soil is assumed to liquefy.

In the above liquefaction analysis, there are many different equations and corrections that are applied to both the cyclic stress ratio induced by the anticipated earthquake and the cyclic resistance ratio of the in situ soil in order to calculate the $(N_1)_{60}$ value. All these different equations and various corrections may provide the engineer with a sense of high accuracy, when in fact the entire analysis is only a gross approximation. The analysis should be treated as such that engineering experience and judgment are essential in the final determination of whether a site has liquefaction potential.

Chapter-6

Evaluation of Liquefaction Potential without any Surcharge

6.1 Introduction

The evaluation of liquefaction potential for the boreholes were carried out by using the values obtained from Standard Penetration Test, SPT and Shear Wave Velocity, V_s . SPT (IS2131: 1981) was conducted in the study area upto a depth of 35m. Ground water table was at 0.50 m below the existing ground level for both borehole no.1 and borehole no.2. Boring method employed was wash boring. Seismic cross hole test (IS 13372 (Part 2) : 1992) was conducted for one location at the study area upto a depth of 30m to measure the V_s . One source hole and two receiver holes were used for the seismic cross hole test. The calculations for the boreholes were done by using the data of SPT and V_s to obtain the factor of safety (FOS) against liquefaction. As per the Simplified Procedure, FOS against liquefaction of soil are calculated layerwise. Hence, Iwasaki et al. 1984 came up with their approach presenting a single parameter to evaluate the liquefaction potential over different layers of soil. This is termed as the Liquefaction Potential Index (LPI) given by the following expression-

$$LPI = \int_0^{20} F \cdot w(z) dz$$

In this integral equation, “z” depicts the depth from existing ground level. The upper limit of the integral is considered upto a depth of 20m below the existing ground level. “w(z)” is weighting function which is equal to (10-0.5z). “F” is termed as the severity number given by the equation below.

$$F = 1 - F_L \quad \text{for, } F_L \leq 1.0 \\ = 0 \quad \text{for, } F_L > 1.0$$

where F_L is the factor of safety against liquefaction which is defined as CRR/CSR . (Sonmez, 2003) modified the equation for LPI developed by Iwasaki et al. (1984) by taking the ranges of $F(z)$ from 0.95 to 1.2 as below.

$$F(z) = \begin{cases} 1 - F_L & \text{for } F_L \leq 0.95 \\ 2 \cdot 10^6 \cdot e^{-18.427F_L} & \text{for } 0.95 < F_L < 1.2 \\ 0 & \text{for } F_L \geq 1.2 \end{cases}$$

Iwasaki T, 1986 has proposed the following hazard level in Table 6.1 for measuring the hazard level against LPI.

Table 6.1 Iwasaki et al.(1986) hazard level

Liquefaction potential index (LPI)	RD level, Iwasaki et al. (1986)
LPI =0	Very low
0 < LPI < 5	Low
5 < LPI < 15	High
LPI > 15	Very high

6.2 Evaluation of Liquefaction Potential using SPT data

6.2.1 Evaluation of Liquefaction Potential for BH1

$$FOS = CRR/CSR \quad (6.1)$$

Soil parameters for BH1 at various depths are shown in table 6.2.

Table 6.2 Soil parameters for BH1 at various depth

Sl No.	Depth, z (m)	Observed N-value	% Fines	Bulk density (KN/m ³)
1	2	5	100	17.76
2	5	17	100	20.50
3	8	14	100	20.01
4	11	21	100	20.80
5	14	29	100	21.39
6	17	43		21.39
7	20	61		21.68
8	23	65		22.07
9	26	86		22.37
10	29	101		22.56
11	32	109		23.05
12	35	118		23.35

1. Calculation of total stress (σ_{vo}) and effective stress (σ'_{vo})

At depth 2m

$$\sigma_{vo} = 17.76 * 2 = 35.52 \text{ KN/m}^2$$

$$\sigma'_{vo} = 35.52 - 9.81 * (2 - 0.5) = 20.81 \text{ KN/m}^2$$

At depth 5m

$$\sigma_{vo} = 35.52 + 20.50 \times 3 = 97.02 \text{ KN/m}^2$$

$$\sigma'_{vo} = 97.02 - 9.81 \times (5 - 0.5) = 52.87 \text{ KN/m}^2$$

Similarly, total and effective stresses for the other depths are calculated and shown in table 6.3.

Table 6.3 Total and effective stresses at various depths

Depth, z (m)	σ_{vo} (KN/m ²)	σ'_{vo} (KN/m ²)
2.0	35.51	20.80
5.0	97.01	52.87
8.0	157.04	83.47
11.0	219.44	116.44
14.0	283.61	151.18
17.0	347.78	185.92
20.0	412.82	221.53
23.0	479.03	258.31
26.0	546.14	295.99
29.0	613.82	334.24
32.0	682.97	373.96
35.0	753.02	414.58

2. Calculation of $(N_1)_{60}$

At depth 17m, $N = 43$

$$(N_1)_{60} = NC_N C_{60}$$

$$C_N = \sqrt{(100/185.92)} = 0.73$$

$$C_{60} = C_{HT} C_{HW} C_{SS} C_{RL} C_{BD} = 1 \times 0.984 \times 1.1 \times 1 \times 1.05 = 1.136$$

$$\therefore (N_1)_{60} = 43 \times 0.73 \times 1.14 = 35.66$$

Calculations of $(N_1)_{60}$ for other depths are done in a similar manner

3. Calculation of $(N_1)_{60CS}$

$$(N_1)_{60CS} = \alpha + \beta(N_1)_{60} = 0 + 1 \times 35.66 = 35.66 \text{ [For } FC \leq 5 \text{]}$$

Calculations of $(N_1)_{60CS}$ for other depths are done in a similar manner.

4. Calculations of r_d

$$r_d = 1.174 - 0.0267z \text{ for } 9.15 \text{ m} < z \leq 23.0 \text{ m}$$

$$= 1.174 - 0.0267 \times 17 = 0.72 \text{ (for } z = 17 \text{ m)}$$

Calculations of r_d for other depths are done in a similar manner.

The values of $(N_1)_{60}$, $(N_1)_{60CS}$ and r_d are listed in table 6.4.

Table 6.4 Calculation of $(N_1)_{60}$ $(N_1)_{60CS}$ and r_d at various depths for BH1

Depth, z(m)	Observed N-value	FC (%)	$(N_1)_{60}$	$(N_1)_{60CS}$	r_d
2	5	100	-	-	0.99
5	17	100	-	-	0.97
8	14	100	-	-	0.94
11	21	100	-	-	0.88
14	29	100	-	-	0.79
17	43	-	35.69	35.69	0.70
20	61	-	46.47	46.47	0.62
23	65	-	45.82	45.82	0.57
26	86	-	56.71	56.71	0.53
29	101	-	63.16	63.16	0.51
32	109	-	64.45	64.45	0.49
35	118	-	65.74	65.74	0.48

5. Calculation of Cyclic Stress Ratio (CSR)

$$\begin{aligned} \text{CSR} &= 0.65 \cdot (a_{\max}/g) \cdot (\sigma_{vo}/\sigma'_{vo}) \cdot r_d \\ &= 0.65 \cdot 0.36 \cdot (347.78/185.92) \cdot 0.72 = 0.32 \end{aligned}$$

Calculations of CSR for other depths are carried in a similar manner.

6. Calculations of K_σ

$$K_\sigma = 1$$

$$K_\sigma = (\sigma'_{vo}/P_a)^{(f-1)} \quad [\text{This factor is required only for depth } > 15\text{m}]$$

At depth 17m

$$\begin{aligned} K_\sigma &= (185.92/100)^{(6-1)} \\ &= 0.78 \end{aligned}$$

7. Calculations of Cyclic Resistance Ration (CRR)

$$\text{CRR} = \text{CRR}_{7.5}(\text{MSF})K_\sigma K_\alpha$$

For $(N_1)_{60CS} = 35.69$, $\text{CRR}_{7.5} = 0.6$ [From Plot used to determine the CRR and $(N_1)_{60CS}$ for sand for $M_w 7.5$ earthquakes]

$$\therefore \text{CRR} = 0.6 \cdot 0.78 \cdot 1 \cdot 1 = 0.47$$

8. Calculations of Factor of Safety against liquefaction

At depth 17m

$$\begin{aligned} \text{From eq.6.1, F.O.S} &= \text{CRR/CSR} \\ &= 0.47/0.32 \\ &= 1.47 > 1 \end{aligned}$$

Hence, the soil will not liquefy.

Calculations of CSR, CRR and F.O.S for other depths are done in a similar way and is shown in table 6.5.

The assessment for BH1 shows that the soil layers at this site will not liquefy in the magnitude 7.5 design earthquake with peak ground acceleration of 0.36g. The plot for factor of safety against liquefaction is shown in Figure 6.1.

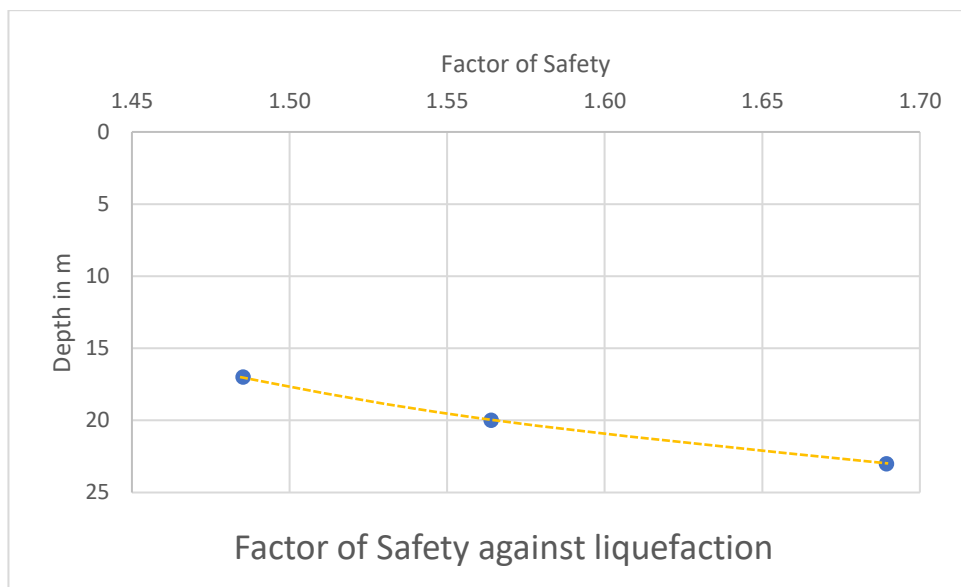


Fig 6.1 Plot for Factor of Safety against Liquefaction for BH1

Table 6.5 Calculation of CSR, CRR and F.O.S for other depths

Borehole no. 1

z(m)	N	FC (%)	σ'_{vo} (kN/m ²)	r _d	CSR	C ₆₀	$N_{60} = \frac{N_{C60}}{NC_{60}}$	$C_N = \sqrt{P_d / \sigma'_{vo}}$	C _N	(N ₁) ₆₀	α	β	$\frac{(N_1)_{60CS}}{= \alpha + \beta(N_1)_{60}}$	CRR _{7.5}	MSF	K _σ	K _α	CRR	F.O.S	
2.0	5	100	20.80																	
5.0	17	100	52.87																	
8.0	14	100	83.47																	
11.0	21	100	116.44																	
14.0	29	100	151.18																	
17.0	43		185.92	0.72	0.32	1.14	48.89	0.73	0.73	35.69	0	1	35.69	0.60	1	0.780	1	0.47	1.49	
20.0	61		221.53	0.64	0.28	1.14	69.36	0.67	0.67	46.47	0	1	46.47	0.60	1	0.727	1	0.44	1.56	
23.0	65		258.31	0.56	0.24	1.14	73.91	0.62	0.62	45.82	0	1	45.82	0.60	1	0.684	1	0.41	1.69	
26.0	86		295.99																	
29.0	101		334.24																	
32.0	109		373.96																	
35.0	118		414.58																	

6.2.1.1 Calculation of LPI for BH1

LPI is given by-

$$LPI = \int_0^{20} F \cdot w(z) dz$$

Calculations of LPI for all depths for BH1 by Iwasaki et al.(1984) and Sonmez(2003) are shown in Table 6.6

Table 6.6 Calculation of LPI for BH1

z (m)	z _i from mid-layer (m)	F _L	F(z _i) Iwasaki et al.(1984)	F(z _i) Sonmez (2003)	w(z _i)	d(z)	w(z _i)F(z _i)dz [Iwasaki et al.(1984)]	w(z _i)F(z _i)dz [Sonmez (2003)]
2	1	-	-	-	-	-	-	-
5	4	-	-	-	-	-	-	-
8	7	-	-	-	-	-	-	-
11	10	-	-	-	-	-	-	-
14	13	-	-	-	-	-	-	-
17	16	1.49	-	-	-	-	0	0
20	19	1.56	-	-	-	-	0	0
23	22	1.69	-	-	-	-	0	0
26	25	-	-	-	-	-	-	-
29	28	-	-	-	-	-	-	-
32	31	-	-	-	-	-	-	-
35	34	-	-	-	-	-	-	-

∴ For the entire soil layer, $LPI = \sum w(z_i) F(z_i) d(z) = 0$

From Iwasaki et al.(1984), $LPI > 15$ means the hazard level is very low for the site.

6.2.2 Evaluation of Liquefaction Potential for BH2

Soil parameters at various depths are shown in Table 6.7.

Table 6.7: Soil parameters at various depths for BH2

Sl No.	Depth, z (m)	Observed N-value	% Fines	Bulk density (KN/m ³)
1	2	3	100	16.58
2	5	9	100	19.13
3	8	16	100	20.50
4	11	24	100	21.09
5	14	31	100	21.58
6	17	35	15	20.80
7	20	46	10	21.68
8	23	55		21.88
9	26	64		22.07
10	29	79		22.46
11	32	90		22.76
12	35	107		23.05

1. Calculation of total stress (σ_{vo}) and effective stress(σ'_{vo})

At depth 2m

$$\sigma_{vo} = 16.58 * 2 = 33.16 \text{ KN/m}^2$$

$$\sigma'_{vo} = 33.16 - 9.81 * (2 - 0.5) = 18.45 \text{ KN/m}^2$$

At depth 5m

$$\sigma_{vo} = 33.16 + 19.13 * 3 = 90.55 \text{ KN/m}^2$$

$$\sigma'_{vo} = 90.55 - 9.81 * (5 - 0.5) = 46.41 \text{ KN/m}^2$$

Similarly, total and effective stresses for the other depths are calculated and shown in table 6.8.

Table 6.8 Total and effective stresses at various depths

Depth, z (m)	σ_{vo} (KN/m ²)	σ'_{vo} (KN/m ²)
2.0	33.16	18.44
5.0	90.55	46.40
8.0	152.06	78.48
11.0	215.33	112.32
14.0	280.08	147.64
17.0	342.47	180.60
20.0	407.51	216.21
23.0	473.14	252.41
26.0	539.35	289.20
29.0	606.75	327.16
32.0	675.03	366.01
35.0	744.19	405.74

2. Calculation of $(N_1)_{60}$

At depth 17m, $N = 35$

$$(N_1)_{60} = N C_N C_{60}$$

$$C_N = \sqrt{(100/180.60)} = 0.744$$

$$C_{60} = C_{HT} C_{HW} C_{SS} C_{RCL} C_{BD} = 1 * 0.984 * 1.1 * 1 * 1.05 = 1.136$$

$$\therefore (N_1)_{60} = 35 * 0.74 * 1.136 = 29.58$$

Calculations of $(N_1)_{60}$ for other depths are done in a similar manner.

3. Calculation of $(N_1)_{60CS}$

$$(N_1)_{60CS} = \alpha + \beta(N_1)_{60} = 2.5 + 1.05 * 29.58 = 33.42 \quad (5 < FC \leq 35)$$

Calculations of $(N_1)_{60CS}$ for other depths are done in a similar manner.

4. Calculations of r_d

$$r_d = 1 - 0.00765z \text{ for } 0 < z \leq 9.15 \text{ m}$$

$$= 1 - 0.00765*2 = 0.985$$

Calculations of r_d for other depths are done in a similar manner.

The values of $(N_1)_{60}$, $(N_1)_{60CS}$ and r_d are listed in table 6.9.

Table 6.9 $(N_1)_{60}$, $(N_1)_{60CS}$ and r_d at various depths for BH2

Depth, z(m)	Observed N-value	FC(%)	$(N_1)_{60}$	$(N_1)_{60CS}$	r_d
2.0	3	100	-	-	-
5.0	9	100	-	-	-
8.0	16	100	-	-	-
11.0	24	100	-	-	-
14.0	31	100	-	-	-
17.0	35	15	29.45	33.42	0.72
20.0	46	10	35.57	37.14	0.64
23.0	55		39.40	39.40	0.56
26.0	64		-	-	-
			-	-	-
29.0	79		-	-	-
			-	-	-
32.0	90		-	-	-
			-	-	-
35.0	107		-	-	-

5. Calculation of Cyclic Stress Ratio (CSR)

$$CSR = 0.65*(a_{max}/g)*(\sigma_{vo}/ \sigma'_{vo})*r_d$$

$$= 0.65*0.36*(342.47/180.60)*0.72 = 0.32$$

Calculations of CSR for other depths are carried in a similar manner.

6. Calculations of K_σ

$$K_\sigma = 1$$

$$K_\sigma = (\sigma'_{vo}/P_a)^{(f-1)} \text{ [This factor is required only for depth } > 15\text{m]}$$

At depth 17m

$$K_{\sigma} = (180.60/100)^{(0.6-1)}$$
$$= 0.79$$

7. Calculations of Cyclic Resistance Ration (CRR)

$$CRR = CRR_{7.5}(MSF)K_{\sigma}K_{\alpha}$$

For $(N_1)_{60CS} = 33.42$, $CRR_{7.5} = 0.60$ [From Plot used to determine the CRR and $(N_1)_{60CS}$ for sand for M_w 7.5 earthquakes]

$$\therefore CRR = 0.60 * 0.79 * 1 * 1 = 0.47$$

8. Calculations of Factor of Safety against liquefaction

At depth 17m

$$F.O.S = CRR/CSR$$

$$= 0.47/0.32$$

$$= 1.48 > 1$$

Hence, the soil will not liquefy.

Calculations of CSR, CRR and F.O.S for other depths are done in a similar way and is shown in table 6.10.

The assessment for BH2 shows that the soil layers at this site is not liquefiable in the magnitude 7.5 design earthquake with peak ground acceleration of 0.36g. The plot for factor of safety against liquefaction is shown in Figure 6.2.

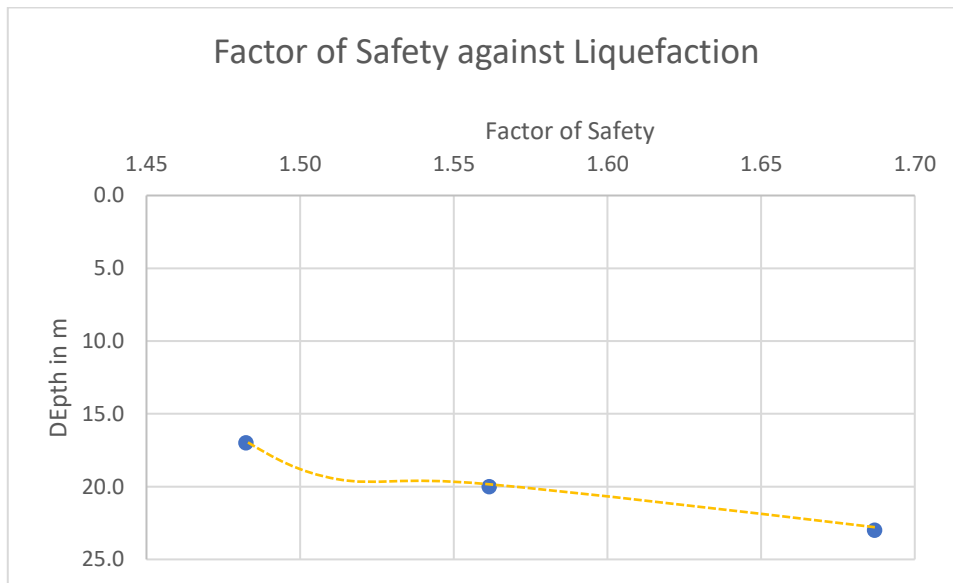


Fig 6.2 Plot for Factor of Safety against Liquefaction for BH2

Table 6.10 Calculation of CSR, CRR and F.O.S for other depths
Borehole no. 2

z(m)	N	FC (%)	σ'_{vo} (kN/m ²)	r _d	CSR	C ₆₀	$N_{60} = \frac{N_{60}}{NC_{60}}$	$C_N = \frac{C_N}{\sqrt{(P_a/\sigma'_{vo})}}$	C _N	(N ₁) ₆₀	α	β	$\frac{(N_1)_{60CS}}{= \alpha + \beta(N_1)_{60}}$	CRR _{7.5}	MSF	K _σ	K _α	CRR	F.O.S	
2.0	3	100	18.44																	
5.0	9	100	46.40																	
8.0	16	100	78.48																	
11.0	24	100	112.32																	
14.0	31	100	147.64																	
17.0	35	15	180.60	0.72	0.32	1.14	39.795	0.74	0.74	29.45	2.5	1.05	33.42	0.60	1	0.789	1	0.47	1.48	
20.0	46	10	216.21	0.64	0.28	1.14	52.302	0.68	0.68	35.57	0.86	1.02	37.14	0.60	1	0.735	1	0.44	1.56	
23.0	55		252.41	0.56	0.25	1.14	62.535	0.63	0.63	39.40	0	1	39.40	0.60	1	0.690	1	0.41	1.69	
26.0	64		289.20																	
29.0	79		327.16																	
32.0	90		366.01																	
35.0	107		405.74																	

6.2.2.1 Calculation of LPI for BH2

LPI is given by-

$$LPI = \int_0^{20} F \cdot w(z) dz$$

Calculations of LPI for all depths for BH2 by Iwasaki et al.(1984) and Sonmez(2003) are shown in Table 6.11

Table 6.11 Calculation of LPI for BH2

z (m)	z _i from mid-layer (m)	F _L	F(z _i) Iwasaki et al.(1984)	F(z _i) Sonmez (2003)	w(z _i)	d(z)	w(z _i)F(z _i)dz [Iwasaki et al.(1984)]	w(z _i)F(z _i)dz [Sonmez (2003)]
2	1	-	-	-	-	-	-	-
5	4	-	-	-	-	-	-	-
8	7	-	-	-	-	-	-	-
11	10	-	-	-	-	-	-	-
14	13	-	-	-	-	-	-	-
17	16	1.48	-	-	-	-	0	0
20	19	1.56	-	-	-	-	0	0
23	22	1.69	-	-	-	-	0	0
26	25	-	-	-	-	-	-	-
29	28	-	-	-	-	-	-	-
32	31	-	-	-	-	-	-	-
35	34	-	-	-	-	-	-	-

∴ LPI = ∑ w(z_i) F(z_i) d(z) = 0 which is very low from Iwasaki hazard level.

6.2.3 Evaluation of Liquefaction Potential for BH3

Soil parameters at various depths are shown in table 6.12.

Table 6.12: Soil parameters at various depths for BH3

Sl No.	Depth, z (m)	Observed N-value	% Fines	Bulk density (KN/m ³)	Submerged density(KN/m ³)
1	1.5	8	100	18.91	9.11
2	3	12	100	19.80	10.00
3	4.5	16		18.23	8.43
4	6	20		18.62	8.82
5	7.5	28		19.89	10.09
6	9	33		20.58	10.78
7	10.5	50		21.95	12.15

1. Calculation of total stress (σ_{vo}) and effective stress(σ'_{vo})

At depth 1.5m, Water table at E.G.L

$$\sigma_{vo} = 18.91 * 1.5 = 28.37 \text{ KN/m}^2$$

$$\sigma'_{vo} = 9.11 * 1.5 = 13.67 \text{ KN/m}^2$$

At depth 3m

$$\sigma_{vo} = 28.37 + 19.80 * 1.5 = 58.07 \text{ KN/m}^2$$

$$\sigma'_{vo} = 9.11 * 3 = 27.33 \text{ KN/m}^2$$

Similarly, total and effective stresses for the other depths are calculated and shown in table 6.13.

Table 6.13 Total and effective stresses at various depths

Depth, z (m)	σ_{vo} (KN/m ²)	σ'_{vo} (KN/m ²)
1.5	28.37	13.67
3	58.07	27.34
4.5	85.41	42.34
6	113.34	54.98
7.5	143.18	68.21
9	174.05	83.35
10.5	206.98	99.52

2. Calculation of $(N_1)_{60}$

At depth 4.5m, $N = 16$

$$(N_1)_{60} = N C_N C_{60}$$

$$C_N = \sqrt{(100/42.34)} = 1.54$$

$$C_{60} = C_{HT} C_{HW} C_{SS} C_{RL} C_{BD} = 1 * 0.984 * 1.1 * 0.85 * 1.05 = 0.966$$

$$\therefore (N_1)_{60} = 16 * 1.54 * 0.966 = 23.80$$

Calculations of $(N_1)_{60}$ for other depths are done in a similar manner.

3. Calculation of $(N_1)_{60CS}$

$$(N_1)_{60CS} = \alpha + \beta(N_1)_{60} = 0 + 1 * 23.80 = 23.80 \text{ [For } FC \leq 5 \text{]}$$

Calculations of $(N_1)_{60CS}$ for other depths are done in a similar manner.

4. Calculations of r_d

$$r_d = 1 - 0.00765z \text{ for } 0 < z \leq 9.15 \text{ m}$$

$$= 1 - 0.00765 * 1.5 = 0.99$$

Calculations of r_d for other depths are done in a similar manner.

The values of $(N_1)_{60}$, $(N_1)_{60CS}$ and r_d are listed in table 6.14

Table 6.14 $(N_1)_{60}$, $(N_1)_{60CS}$ and r_d at various depths

Depth, z(m)	Observed N-value	FC(%)	$(N_1)_{60}$	$(N_1)_{60CS}$	r_d
1.5	8	100	-	-	-
3	12	100	-	-	-
4.5	16		23.80	23.80	0.97
6	20		26.08	26.08	0.95
7.5	28		36.58	36.58	0.94
9	33		39.19	39.19	0.93
10.5	50		56.83	56.83	0.89

5. Calculation of Cyclic Stress Ratio (CSR)

$$\begin{aligned} CSR &= 0.65 * (a_{max}/g) * (\sigma_{vo} / \sigma'_{vo}) * r_d \\ &= 0.65 * 0.36 * (85.41/42.34) * 0.97 = 0.46 \end{aligned}$$

Calculations of CSR for other depths are carried in a similar manner.

6. Calculations of K_σ

$$K_\sigma = 1$$

$$K_\sigma = (\sigma'_{vo}/P_a)^{(f-1)} \text{ [This factor is required only for depth } > 15\text{m]}$$

7. Calculations of Cyclic Resistance Ration (CRR)

$$CRR = CRR_{7.5}(MSF)K_\sigma K_\alpha$$

For $(N_1)_{60CS} = 23.80$, $CRR_{7.5} = 0.28$ [From Plot used to determine the CRR and $(N_1)_{60CS}$ for sand for M_w 7.5 earthquakes]

$$\therefore CRR = 0.28 * 1 * 1 * 1 = 0.28$$

8. Calculations of Factor of Safety against liquefaction

At depth 1.5m

$$F.O.S = CRR/CSR$$

$$= 0.28/0.46$$

$$= 0.61 < 1$$

Hence, the soil will liquefy.

Calculations of CSR, CRR and F.O.S for other depths are done in a similar way and is shown in table 6.15.

The assessment for BH3 shows that the soil layers at this site from 4.5m to 6m depth are liquefiable in the magnitude 7.5 design earthquake with peak ground acceleration of 0.36g. The plot for factor of safety against liquefaction is shown in Figure 6.3.

Table 6.15 Calculation of CSR, CRR and F.O.S for other depths
Borehole no. 3

z(m)	N	FC(%)	σ'_{vo} (kN/m ²)	r_d	CSR	C_{60}	$N_{60} =$ NC_{60}	$C_N =$ $\sqrt{(P_a/\sigma'_{vo})}$	C_N	$(N_1)_{60}$ $=$ $C_N N_{60}$	α	β	$(N_1)_{60CS}$ $= \alpha +$ $\beta ($ $N_1)_{60}$	CRR _{7.5}	MSF	K_σ	K_α	CRR	F.O.S
1.5	8	100	13.67																
3	12	100	27.34																
4.5	16	0	42.34	0.97	0.46	0.97	15.46	1.54	1.54	23.80	0	1	23.80	0.28	1.00	1.00	1.00	0.28	0.61
6	20	0	54.98	0.95	0.46	0.97	19.32	1.35	1.35	26.08	0	1	26.08	0.25	1.00	1.00	1.00	0.25	0.54
7.5	28	0	68.21	0.94	0.46	1.08	30.23	1.21	1.21	36.58	0	1	36.58	0.60	1.00	1.00	1.00	0.60	1.30
9	33	0	83.35	0.93	0.45	1.08	35.63	1.10	1.10	39.19	0	1	39.19	0.60	1.00	1.00	1.00	0.60	1.32
10.5	50	0	99.52	0.89	0.43	1.14	56.83	1.00	1.00	56.83	0	1	56.83	0.60	1.00	1.00	1.00	0.60	1.38

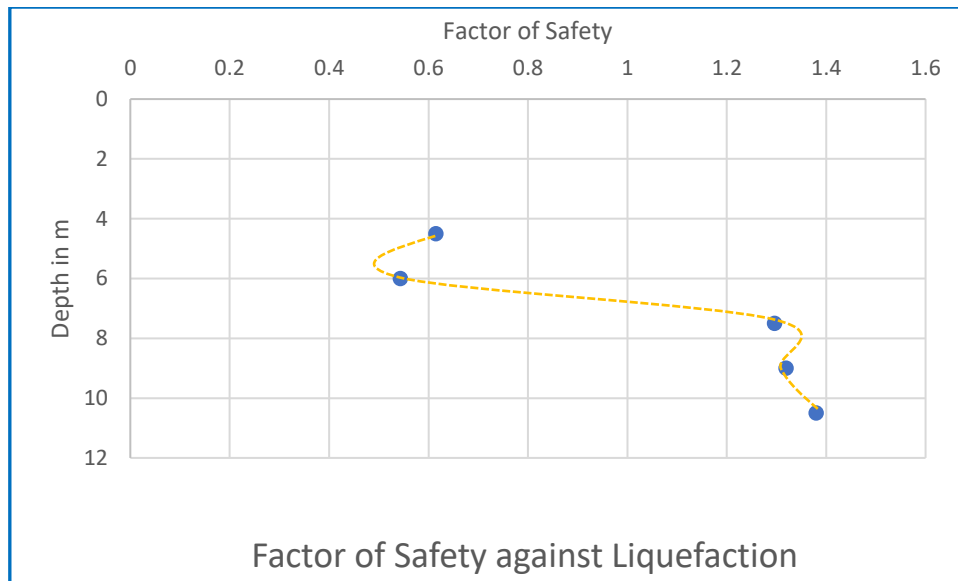


Fig 6.3 Plot for Factor of Safety against Liquefaction for BH3

6.2.3.1 Calculation of LPI for BH3

LPI is given by-

$$LPI = \int_0^{20} F \cdot w(z) dz$$

Calculations of LPI for all depths for BH3 by Iwasaki et al.(1984) and Sonmez(2003) are shown in Table 6.16

Table 6.16 Calculation of LPI for BH3

z(m)	z _i from mid- layer (m)	F _L	F(z _i) Iwasaki et al.(1984)	F(z _i) Sonmez (2003)	w(z _i)	d(z)	w(z _i)F(z _i)dz Iwasaki et al.(1984)	w(z _i)F(z _i)dz Sonmez (2003)
1.5	0.75	-	-	-	-	-	-	-
3	2.25	-	-	-	-	-	-	-
4.5	3.75	0.61	0.39	0.39	8.13	1.5	4.76	4.76
6	5.25	0.54	0.46	0.46	7.38	1.5	5.09	5.09
7.5	6.75	1.30	-	-	-	-	0	0
9	8.25	1.32	-	-	-	-	0	0
10.5	9.75	1.38	-	-	-	-	0	0

$\therefore \text{LPI} = \sum w(z_i) F(z_i) d(z) = 4.76+5.09 = 9.85$ in the range between 5 and 15, which is high from Iwasaki hazard level.

6.2.4 Evaluation of Liquefaction Potential for BH4

Soil parameters at various depths are shown in Table 6.17.

Table 6.17 Soil parameters at various depths for BH4

Sl. No.	Depth, z (m)	Observed N-value	% Fines	Bulk density (KN/m ³)
1	1.5	2		11.28
2	3	5		12.75
3	4.5	11		19.33
4	6	12		22.07
5	7.5	9		22.47
6	9	8		21.48
7	10.5	12		22.08
8	12	16		22.07
9	13.5	16		22.07
10	15	32		22.66
11	16.5	32	4.68	19.52
12	18	35	4.68	20.21
13	19.5	33	4.68	19.97
14	21	Refusal		22.07
15	22	Refusal		22.07
16	24	Refusal		22.07
17	25.5	Refusal		22.07
18	27	Refusal		22.17
19	28.5	Refusal		21.97
20	30	Refusal		22.56

1. Calculation of total stress (σ_{vo}) and effective stress(σ'_{vo})

At depth 1.5m, Water table at 0.7m

$$\sigma_{vo} = 11.28 * 1.5 = 16.92 \text{ KN/m}^2$$

$$\sigma'_{vo} = 16.92 - 9.81(1.5 - 0.7) = 9.07 \text{ KN/m}^2$$

At depth 3m

$$\sigma_{vo} = 16.92 + 12.75 \times 1.5 = 36.05 \text{ KN/m}^2$$

$$\sigma'_{vo} = 36.05 - 9.81(3 - 0.7) = 13.49 \text{ KN/m}^2$$

Similarly, total and effective stresses for the other depths are calculated and shown in Table 6.18.

Table 6.18 Total and effective stresses at various depths

Depth, z(m)	σ_{vo} (KN/m ²)	σ'_{vo} (KN/m ²)
1.5	16.92	9.07
3	36.05	13.48
4.5	65.04	27.76
6	98.15	46.15
7.5	131.85	65.14
9	164.07	82.65
10.5	197.19	101.05
12	230.30	119.44
13.5	263.40	137.83
15	297.39	157.11
16.5	326.67	171.67
18	356.99	187.27
19.5	386.94	202.51
21	420.05	220.90
22	453.15	239.29
24	486.26	257.68
25.5	519.36	276.07
27	552.62	294.61
28.5	585.57	312.85
30	619.41	331.98

2. Calculation of $(N_1)_{60}$

At depth 16.5m, $N = 32$

$$(N_1)_{60} = N C_N C_{60}$$

$$C_N = \sqrt{(100/171.67)} = 0.76$$

$$C_{60} = C_{HT}C_{HW}C_{SS}C_{RL}C_{BD} = 0.75*1*1.1*0.85*1.05 = 0.74$$

$$\therefore (N_1)_{60} = 32*0.76*0.74 = 17.99$$

Calculations of $(N_1)_{60}$ for other depths are done in a similar manner.

3. Calculation of $(N_1)_{60CS}$

At depth 16.5m

$$(N_1)_{60CS} = \alpha + \beta(N_1)_{60} = 0 + 1*18 = 18 \text{ [FC } \leq 5\% \text{]}$$

Calculations of $(N_1)_{60CS}$ for other depths are done in a similar manner.

4. Calculations of r_d

$$r_d = 1 - 0.00765z \text{ for } 0 < z \leq 9.15 \text{ m}$$

$$= 1 - 0.00765*1.5 = 0.99$$

Calculations of r_d for other depths are done in a similar manner.

The values of $(N_1)_{60}$, $(N_1)_{60CS}$ and r_d are listed in Table 6.19.

Table 6.19 $(N_1)_{60}$, $(N_1)_{60CS}$ and r_d at various depths

Depth, z(m)	Observed N-value	FC (%)	$(N_1)_{60}$	$(N_1)_{60CS}$	r_d
1.5	2	-	2.50	-	-
3	5	-	6.29	-	-
4.5	11	-	13.84	-	-
6	12	-	13.05	-	-
7.5	9	-	8.26	-	-
9	8	-	6.51	-	-
10.5	12	-	8.79	-	-
12	16	-	10.89	-	-
13.5	16	-	10.06	-	-
15	32	-	18.94	-	-
16.5	32	4.68	18.00	18.00	0.71
18	35	4.68	18.91	18.91	0.67
19.5	33	4.68	17.09	17.09	0.63
21	Refusal	-	Refusal	-	-
22.5	Refusal	-	Refusal	-	-
24	Refusal	-	Refusal	-	-
25.5	Refusal	-	Refusal	-	-

Depth, z(m)	Observed N-value	FC (%)	(N ₁) ₆₀	(N ₁) _{60CS}	r _d
27	Refusal	-	-	-	-
28.5	Refusal	-	-	-	-
30	Refusal	-	-	-	-

5. Calculation of Cyclic Stress Ratio (CSR)

At depth 16.5m

$$\begin{aligned} \text{CSR} &= 0.65 \cdot (a_{\max}/g) \cdot (\sigma_{vo}/\sigma'_{vo}) \cdot r_d \\ &= 0.65 \cdot 0.36 \cdot (326.67/171.67) \cdot 0.73 = 0.33 \end{aligned}$$

Calculations of CSR for other depths are carried in a similar manner.

6. Calculations of K_σ

$$K_{\sigma} = 1$$

$$\begin{aligned} K_{\sigma} &= (\sigma'_{vo}/P_a)^{(f-1)} \text{ [This factor is required only for depth } > 15\text{m]} \\ &= (171.67/100)^{(0.7-1)} = 0.85 \end{aligned}$$

7. Calculations of Cyclic Resistance Ration (CRR)

$$\text{CRR} = \text{CRR}_{7.5}(\text{MSF})K_{\sigma}K_{\alpha}$$

For (N₁)_{60CS} = 18,

CRR_{7.5} = 0.19 [From Plot used to determine the CRR and (N₁)_{60CS} for sand for M_w 7.5 earthquakes]

$$\therefore \text{CRR} = 0.19 \cdot 1 \cdot 0.85 \cdot 1 = 0.16$$

8. Calculations of Factor of Safety against liquefaction

At depth 16.5m

$$\begin{aligned} \text{F.O.S} &= \text{CRR}/\text{CSR} \\ &= 0.16/0.33 \\ &= 0.50 < 1 \end{aligned}$$

Hence, the soil will liquefy.

Calculations of CSR, CRR and F.O.S for other depths are done in a similar way and is shown in table 6.20.

The assessment for BH4 shows that the soil layers at this site are liquefiable from 16.5m upto 19.5m depth in the magnitude 7.5 design earthquake with peak ground acceleration of 0.36g. The plot for factor of safety against liquefaction is shown in Figure 6.4.

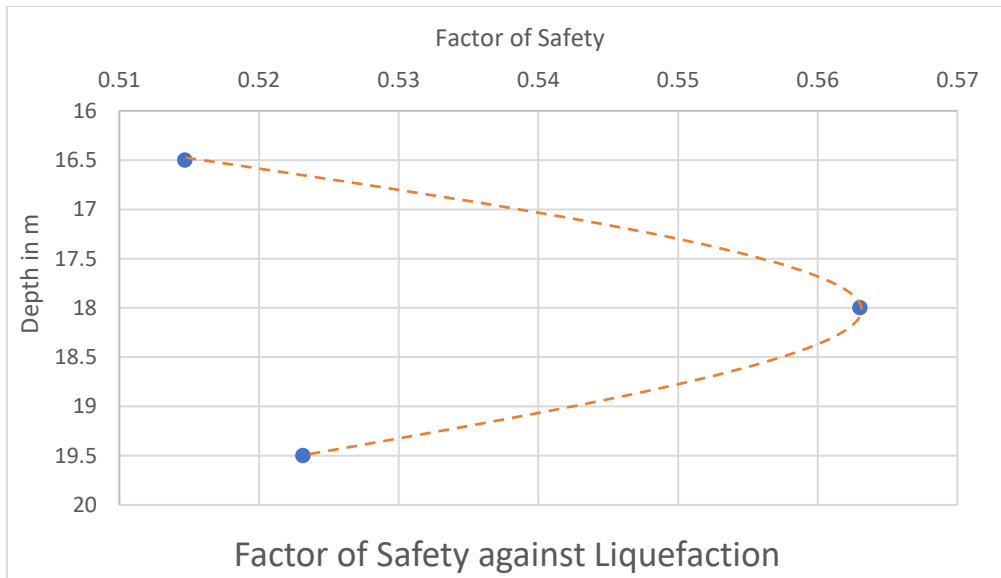


Fig 6.4 Plot for Factor of Safety against Depth for BH4

Table 6.20 Calculation of CSR, CRR and F.O.S for other depths
Borehole no. 4

z(m)	N	FC	σ'_{vo} (kN/m ²)	r _d	CSR	C ₆₀	$\frac{N_{60}}{NC_{60}}$	$C_N = \frac{C_N}{\sqrt{(P_a/\sigma'_{vo})}}$	C _N	$\frac{(N_1)_{60}}{C_N N_{60}}$	α	β	$\frac{(N_1)_{60CS}}{= \alpha + \beta(N_1)_{60}}$	CRR _{7.5}	MSF	K _{σ}	K _{α}	CRR	F.O.S	
1.5	2		9.07																	
3	5		13.48																	
4.5	11		27.76																	
6	12		46.15																	
7.5	9		65.14																	
9	8		82.65																	
10.5	12		101.05																	
12	16		119.44																	
13.5	16		137.83																	
15	32		157.11																	
16.5	32	4.7	171.67	0.71	0.33	0.74	23.68	0.76	0.76	18.00	0	1	18.00	0.19	1.00	0.85	1	0.16	0.5	
18	35	4.7	187.27	0.67	0.31	0.74	25.90	0.73	0.73	18.91	0	1	18.91	0.20	1.00	0.83	1	0.17	0.54	
19.5	33	4.7	202.51	0.63	0.29	0.74	24.42	0.70	0.70	17.09	0	1	17.09	0.18	1.00	0.81	1	0.15	0.5	
21	Refusal		220.90																	
22.5	Refusal		239.29																	
24	Refusal		257.68																	
25.5	Refusal		276.07																	
27	Refusal		294.61																	
28.5	Refusal		312.85																	
30	Refusal		331.98																	

6.2.4.1 Calculation of LPI for BH4

LPI is given by-

$$LPI = \int_0^{20} F \cdot w(z) dz$$

Calculations of LPI for all depths for BH4 by Iwasaki et al.(1984) and Sonmez(2003) are shown in Table 6.21.

Table 6.21 Calculation of LPI for BH4

z(m)	z _i from mid-layer (m)	F _L	F(z _i) Iwasaki et al.(1984)	F(z _i) Sonmez (2003)	w(z _i)	d(z)	w(z _i)F(z _i)d _z Iwasaki et al.(1984)	w(z _i)F(z _i)dz Sonmez (2003)
1.5	0.75	-	-	-	-	-	-	-
3	2.25	-	-	-	-	-	-	-
4.5	3.75	-	-	-	-	-	-	-
6	5.25	-	-	-	-	-	-	-
7.5	6.75	-	-	-	-	-	-	-
9	8.25	-	-	-	-	-	-	-
10.5	9.75	-	-	-	-	-	-	-
12	11.25	-	-	-	-	-	-	-
13.5	12.75	-	-	-	-	-	-	-
15	14.25	-	-	-	-	-	-	-
16.5	15.75	0.51	0.49	0.49	2.13	1.50	1.57	1.57
18	17.25	0.56	0.44	0.44	1.38	1.50	0.91	0.91
19.5	18.75	0.52	0.48	0.48	0.63	1.50	0.45	0.45

$$\therefore LPI = \sum w(z_i) F(z_i) d(z)$$

$$= 1.57+0.91+.45 = 2.93 \text{ falls in the range from 5 to 10, which is low from Iwasaki}$$

hazard level.

6.3 Calculation of Vertical Settlement (Δv) due to liquefaction:

6.3.1 Δv for BH1

The vertical settlement for all the depths is shown in tabular format as Table 6.22.

Table 6.22 Calculation of Vertical Settlement for BH1

Depth, z(m)	F.O.S	% ϵ	Liquefiable level (m)	ΔV (in m)
2	-	-	-	-
5	-	-	-	-
8	-	-	-	-
11	-	-	-	-
14	-	-	-	-
17	1.49	-	-	-
20	1.56	-	-	-
23	1.69	-	-	-
26	-	-	-	-
29	-	-	-	-
32	-	-	-	-
35	-	-	-	-
			Total ΔV	0.00 m

6.3.2 Δv for BH2

The vertical settlement for all the depths is shown in tabular format as Table 6.23.

Table 6.23 Calculation of Vertical Settlement for BH2

Depth, z(m)	F.O.S	% ϵ	Liquefiable level (m)	ΔV (in m)
2	-	-	-	-
5	-	-	-	-
8	-	-	-	-
11	-	-	-	-

14	-	-	-	-
17	1.48	-	-	-
20	1.56	-	-	-
23	1.69	-	-	-
26	-	-	-	-
29	-	-	-	-
32	-	-	-	-
35	-	-	-	-
			Total ΔV	0.00 m

6.3.3 Δv for BH3

At Depth = 4.5m, $(N_1)_{60} = 23.80$ and F.O.S = 0.61

Volumetric strain (% ϵ) = 1.9 (From charts of volumetric strain in % versus factor of safety against cyclic instability, Fig. 6.5)

\therefore Vertical settlement(Δv) due to liquefaction, m = volumetric strain x thickness of liquefiable level
 $= 1.9 \times 1.5/100 = 0.029$ m

At Depth = 6m, $(N_1)_{60} = 26.08$ and F.O.S = 0.54

Volumetric strain (% ϵ) = 1.7 (From charts of volumetric strain in % versus factor of safety against cyclic instability, Fig. 6.5)

\therefore Vertical settlement(Δv) due to liquefaction, m = volumetric strain x thickness of liquefiable level
 $= 1.7 \times 1.5/100 = 0.026$ m

The vertical settlement for all the depths is shown in tabular format as Table 6.24.

Table 6.24 Calculation of Vertical Settlement for BH3

Depth, z(m)	F.O.S	% ϵ	Liquefiable level (m)	ΔV (in m)
1.5	-	-	-	-
3	-	-	-	-
4.5	0.61	1.9	1.5	0.029
6	0.54	1.7	1.5	0.026

7.5	1.30	-	-	-
9	1.32	-	-	-
10.5	1.38	-	-	-
			Total ΔV	0.055 m

6.3.4 Δv for BH4

At Depth = 16.5m, $(N_1)_{60} = 18$ and F.O.S = 0.50

Volumetric strain ($\% \epsilon$) = 2.3 (From charts of volumetric strain in % versus factor of safety against cyclic instability, Fig. 6.5)

\therefore Vertical settlement(Δv) due to liquefaction, m = volumetric strain x thickness of liquefiable level
 $= 2.3 \times 1.5/100 = 0.034$ m

Similarly, the vertical settlement due to liquefaction at other depths are calculated and shown in table 6.25.

Table 6.25 Calculation of Vertical Settlement for BH4

Depth, z(m)	F.O.S	$\% \epsilon$	Liquefiable level (m)	ΔV (in m)
1.5	-	-	-	-
3	-	-	-	-
4.5	-	-	-	-
6	-	-	-	-
7.5	-	-	-	-
9	-	-	-	-
10.5	-	-	-	-
12	-	-	-	-
13.5	-	-	-	-
15	-	-	-	-
16.5	0.5	2.3	1.5	0.034
18	0.54	2.6	1.5	0.039
19.5	0.5	2.5	1.5	0.038
21	-	-	-	-

22.5	-	-	-	-
24	-	-	-	-
25.5	-	-	-	-
27	-	-	-	-
28.5	-	-	-	-
30	-	-	-	-
			Total ΔV	0.111 m

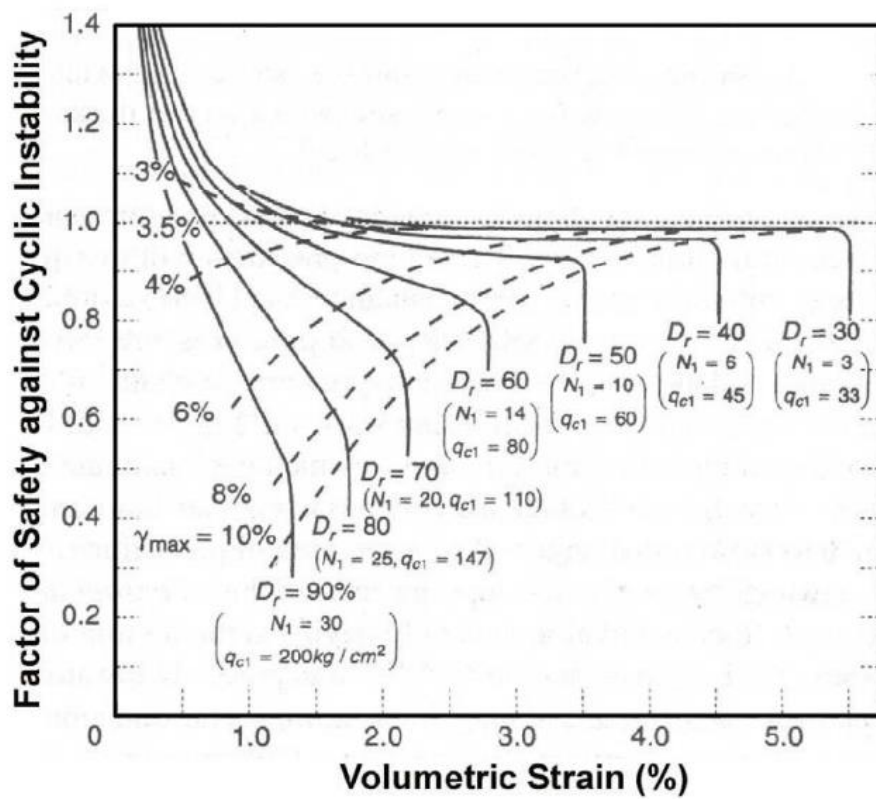


Fig.6.5 Charts of Volumetric Strain in % versus Factor of Safety against Cyclic Instability(Jain, S.K .)

6.4 Evaluation of Liquefaction Potential using measured Shear Wave Velocity, V_s

Water table = 0.5m, Measured shear wave velocity, $V_s = 219.2 \text{ m/s}$

At Depth $z = 1.5\text{m}$,

$$\sigma_{vo} = 16.57 \times 1.5 = 24.86 \text{ kN/m}^2 \text{ and } \sigma'_{vo} = 24.86 - 9.81(1.5-0.5) = 15.05 \text{ kN/m}^2$$

$$r_d = 1 - 0.00765z = 1 - 0.00765 \times 1.5 = 0.99$$

$$\text{CSR} = 0.65 \times 0.36 \times (24.86/15.05) \times 0.99 = 0.38$$

Correction for overburden stress to shear wave velocity V_s for clean sands is given by-

$$V_{s1} = (P_a / \sigma'_{vo})^{0.25} V_s$$

$$= (100/15.05)^{0.25} \times 219.2 = 351.93 \text{ m/s}$$

$CRR_{7.5} = 0.60$ [From fig.5.6 Relation between CRR and V_{s1} for M_w 7.5 Earthquakes]

$$CRR = 0.60 * 1 * 1 * 1 = 0.60$$

$$F.O.S = CRR/CSR = 0.60/0.38 = 1.57$$

Calculations of factor of safety using V_s data for other depths are done in a similar manner and is shown in table 6.26.

The assessment with V_s data shows that the soil layers at this site are not liquefiable for the magnitude 7.5 design earthquake with peak ground acceleration of 0.36g. The plot for factor of safety against liquefaction is shown in Figure 6.6.

Table 6.26 Calculation of CSR, CRR and F.O.S for all depths using V_s data

z (m)	Density (kN/m ³)	σ_{vo} (kN/m ²)	σ'_{vo} (kN/m ²)	r_d	CSR	V_s (m/s)	V_{s1} (m/s)	$CRR_{7.5}$	CRR	F.O.S
1.5	16.57	24.86	15.05	0.99	0.38	219.2	306.88	0.60	0.60	1.57
3	17.26	50.75	26.22	0.98	0.44	226.3	316.25	0.60	0.60	1.36
4.5	19.123	79.43	40.19	0.97	0.45	232.4	291.88	0.60	0.60	1.34
6	19.61	108.84	54.89	0.95	0.44	238.7	277.32	0.60	0.60	1.36
7.5	20.5	139.59	70.92	0.94	0.43	247.5	269.70	0.60	0.60	1.38
9	20.69	170.63	87.24	0.93	0.43	255.6	264.47	0.60	0.60	1.41
10.5	21.08	202.25	104.15	0.89	0.41	259.3	256.68	0.60	0.60	1.48
12	21.38	234.32	121.50	0.85	0.39	268.3	255.55	0.60	0.60	1.56
13	21.58	266.69	144.06	0.83	0.36	278.2	253.93	0.60	0.60	1.68
15	21.67	299.19	156.95	0.77	0.35	286.8	256.24	0.60	0.60	1.74
16.5	20.79	330.38	173.42	0.73	0.33	296.1	258.03	0.60	-	-
18	21.08	362.00	190.32	0.69	0.31	299.3	254.82	0.60	-	-
19.5	21.67	394.50	208.11	0.65	0.29	303.9	253.02	0.60	-	-
21	21.77	427.16	226.05	0.61	0.27	309.6	252.49	0.60	-	-
22.5	21.87	459.96	244.14	0.57	0.25	311.2	248.96	0.60	-	-
24	22.06	493.05	262.52	0.53	0.23	336.9	264.67	0.60	-	-
25.5	22.26	526.44	281.19	0.51	0.22	347.4	268.27	0.60	-	-
27	22.36	559.98	300.02	0.50	0.22	354.7	269.51	0.60	-	-
28.5	22.46	593.67	318.99	0.49	0.21	359.1	268.70	0.60	-	-
30	22.65	627.65	338.25	0.48	0.21	361.4	266.49	0.60	-	-

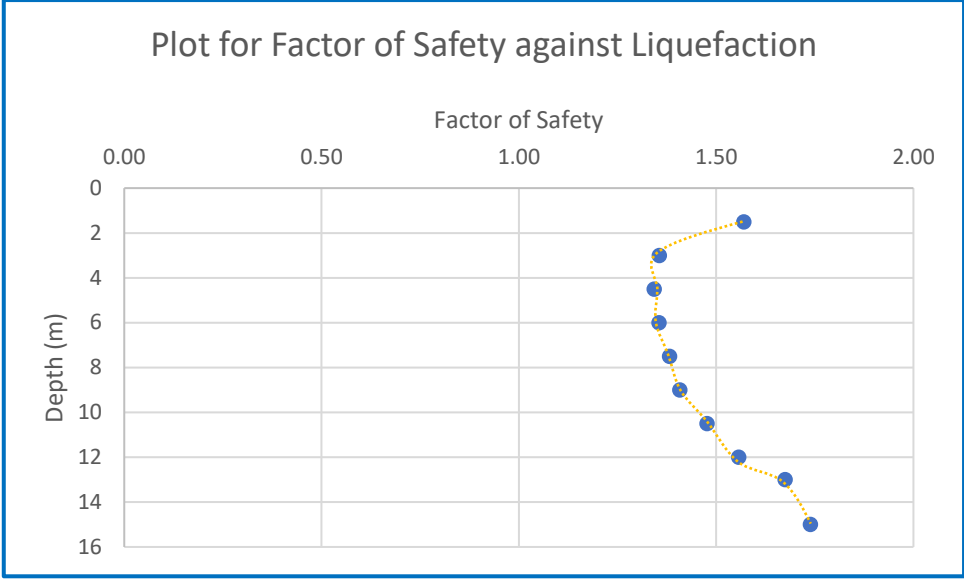


Fig.6.6 Plot for Factor of Safety against Depth using Vs data

Chapter 7

Evaluation of Liquefaction Potential with Surcharge

7.1 Introduction

A circular water tank imposing a surcharge at ground surface is considered at the site for the liquefaction analysis of soil. Structural loads approximated as 180kPa imposed by the water tank having circular area of 37 m diameter is taken for the analysis (Jain et al. 2019). The calculations for this assessment considering a surcharge are procedurally similar to that of calculations for sites without surcharge from chapter 6 but for this case, structural loads needs to be considered at ground surface. The vertical stress and horizontal shear stresses induced by the structure to be taken for this assessment. Hence, there is a need to modify the typical procedure of evaluating the liquefaction potential by incorporating the stresses induced by a structure(Foster and Ahlvin.1954). In this study, the cyclic stress ratio (CSR) has been determined for free field and by taking the vertical stress and shear stress into account. The equation of cyclic stress ratio, CSR in absence of a structure is given by the following equation-

$$CSR = 0.65*(a_{max}/g)*(\sigma_{vo}/ \sigma'_{vo})*r_d.$$

This expression of CSR was modified as follows-

$$CSR = \{0.65(a_{max}/g)r_d\sigma_{vo} + \Delta\tau_{zh}\} / (\sigma'_{vo} + \Delta\sigma_z)$$

where $\Delta\tau_{zh}$ is the horizontal shear stress increment in presence of structure

and $\Delta\sigma_z$ is the vertical stress increment in presence of structure

7.2 Calculation of Vertical Stress Increment, $\Delta\sigma_z$ and Horizontal Shear Stress increment, $\Delta\tau_{zh}$ due to a circular loading with SPT data:

7.2.1 Vertical Stress Increment and Horizontal Shear Stress increment for BH1

At Depth, $z = 17\text{m}$

$$r_d = 0.72, \sigma_{vo} = 347.78, \sigma'_{vo} = 185.92, q = 180\text{kPa}, a = 37/2 = 18.5\text{m}$$

Now, $z/a = 17/18.5 = 0.92$ and $r/a = 1$ (assumed) where z is the depth, a is the radius of the circular tank and r is the radial distance.

From the charts for Shear Stresses due to circular loading of Foster and Ahlvin (1954), we get (Fig. 7.1)

$$\Delta\tau_{zh}/q \times 100(\%) = 20\%$$

$$\Delta\tau_{rz}/180 \times 100=20$$

$$\therefore \Delta\tau_{rz} = 36.00 \text{ kPa}$$

From the charts for Vertical Stresses due to circular loading of Foster and Ahlvin(1954), we get (Fig. 7.2)

$$\Delta\sigma_z/q \times 100(\%) = 35\%$$

$$\Delta\sigma_z/180 \times 100(\%) = 35\%$$

$$\therefore \Delta\sigma_z = 63.00 \text{ kPa}$$

$$\text{Now, CSR} = \{0.65(a_{\max}/g)r_d\sigma_{vo} + \Delta\tau_{zh}\} / (\sigma'_{vo} + \Delta\sigma_z)$$

$$= \{0.65 \cdot 0.36 \cdot 0.72 \cdot 347.78 + 36\} / (185.92 + 63)$$

$$= 0.38$$

$$\text{F.O.S} = \text{CRR} / \text{CSR}$$

$$= 0.47 / 0.38 = 1.24 \text{ (CRR same as calculated without considering structure in chapter 6)}$$

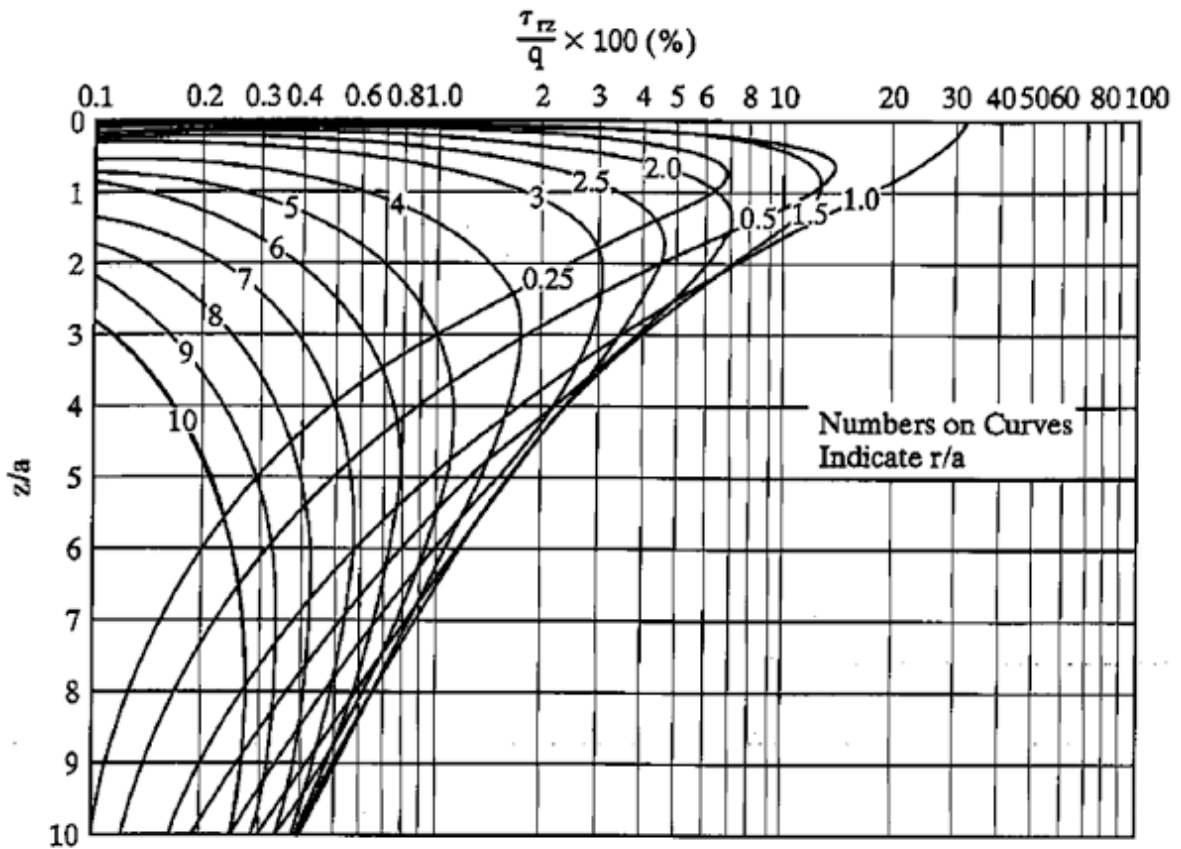


Fig. 7.1 Charts for Shear Stresses due to circular loading of Foster and Ahlvin, 1954

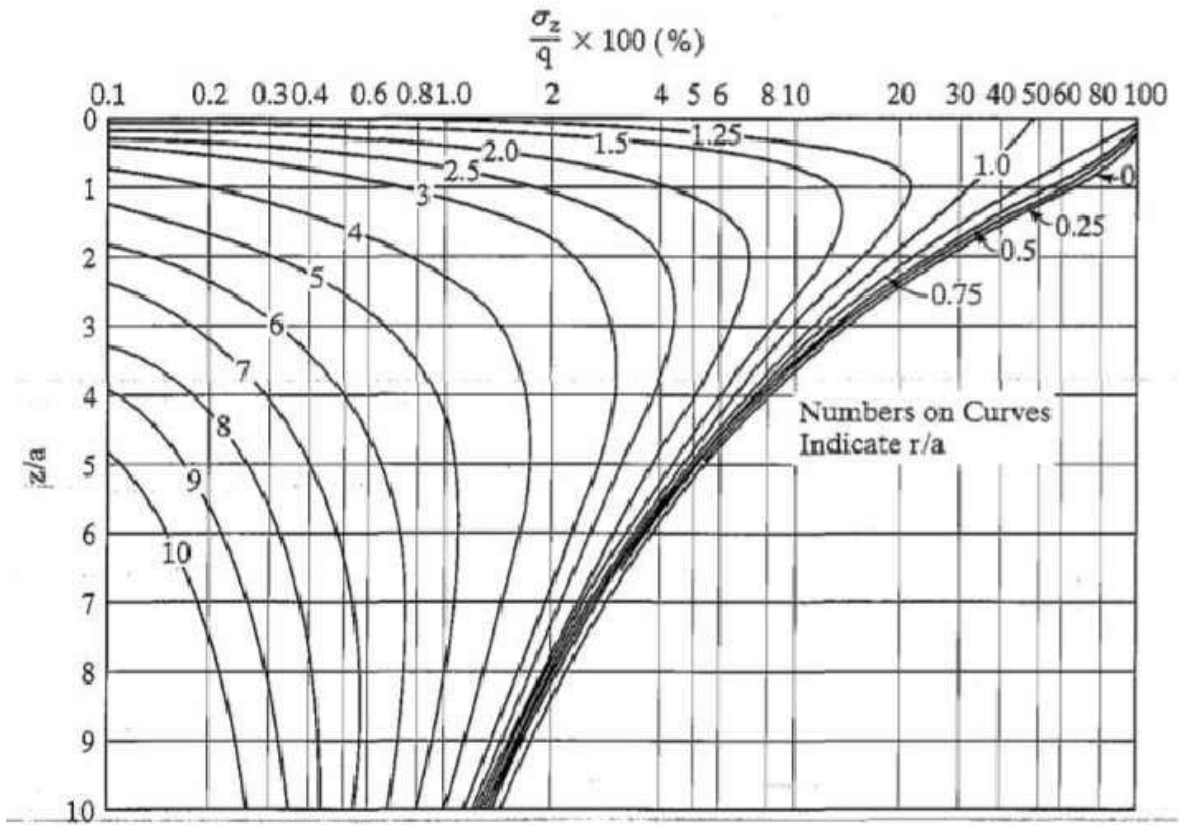


Fig. 7.2 Charts for Vertical Stresses due to circular loading of Foster and Ahlvin, 1954

At Depth, $z = 20\text{m}$

$r_d = 0.64, \sigma_{vo} = 412.82, \sigma'_{vo} = 221.53, q = 180\text{kPa}, a = 37/2 = 18.5\text{m}$

Now, $z/a = 20/18.5 = 1.08$ and $r/a = 1$ (assumed) where z is the depth, a is the radius of the circular tank and r is the radial distance.

From the charts for Shear Stresses due to circular loading of Foster and Ahlvin (1954), we get

$\Delta\tau_{zh}/q \times 100(\%) = 17\%$

$\Delta\tau_{rz}/180 \times 100 = 17$

$\therefore \Delta\tau_{rz} = 30.60 \text{ kPa}$

From the charts for Vertical Stresses due to circular loading of Foster and Ahlvin (1954), we get

$\Delta\sigma_z/q \times 100(\%) = 31\%$

$\Delta\sigma_z/180 \times 100(\%) = 31\%$

$\therefore \Delta\sigma_z = 55.80 \text{ kPa}$

Now, $CSR = \{0.65(a_{max}/g)r_d\sigma_{vo} + \Delta\tau_{zh}\} / (\sigma'_{vo} + \Delta\sigma_z)$

$$= \{0.65*0.36*0.64*412.82+30.60\}/(221.53+55.80)$$

$$= 0.333$$

$$\text{F.O.S} = \text{CRR}/\text{CSR}$$

$$= 0.44/0.333$$

$$= 1.32 \text{ (CRR same as calculated without considering structure in chapter 6)}$$

At Depth, z = 23m

$$r_d = 0.56, \sigma_{vo} = 479.03, \sigma'_{vo} = 258.31, q = 180\text{kPa}, a = 37/2 = 18.5\text{m}$$

Now, $z/a = 23/18.5 = 1.24$ and $r/a = 1$ (assumed) where z is the depth, a is the radius of the circular tank and r is the radial distance.

From the charts for Shear Stresses due to circular loading of Foster and Ahlvin (1954), we get

$$\Delta\tau_{zh}/q \times 100(\%) = 15\%$$

$$\Delta\tau_{rz}/180 \times 100 = 15$$

$$\therefore \Delta\tau_{rz} = 27 \text{ kPa}$$

From the charts for Vertical Stresses due to circular loading of Foster and Ahlvin(1954), we get

$$\Delta\sigma_z/q \times 100(\%) = 29\%$$

$$\Delta\sigma_z/180 \times 100(\%) = 29\%$$

$$\therefore \Delta\sigma_z = 52.20 \text{ kPa}$$

$$\text{Now, CSR} = \{0.65(a_{\max}/g)r_d\sigma_{vo} + \Delta\tau_{zh}\} / (\sigma'_{vo} + \Delta\sigma_z)$$

$$= \{0.65*0.36*0.56*479.03+27\}/(258.31+52.20)$$

$$= 0.29$$

$$\text{F.O.S} = \text{CRR}/\text{CSR}$$

$$= 0.41/0.29$$

$$= 1.41 \text{ (CRR same as calculated without considering structure in chapter 6)}$$

Table 7.1 Calculations for $\Delta\tau_{rz}$, $\Delta\sigma_z$, CSR and F.O.S for BH1

Depth, z (m)	r_d	σ_{vo} (kN/m ²)	σ'_{vo} (kN/m ²)	$\Delta\tau_{rz}$ (kN/m ²)	$\Delta\sigma_z$ (kN/m ²)	CSR	CRR	F.O.S
2.0	-	-	-	-	-	-	-	-

Depth, z (m)	r_d	σ_{vo} (kN/m ²)	σ'_{vo} (kN/m ²)	$\Delta\tau_{rz}$ (kN/m ²)	$\Delta\sigma_z$ (kN/m ²)	CSR	CRR	F.O.S
5.0	-	-	-	-	-	-	-	-
8.0	-	-	-	-	-	-	-	-
11.0	-	-	-	-	-	-	-	-
14.0	-	-	-	-	-	-	-	-
17.0	0.72	347.78	185.92	36.00	63.00	0.38	0.47	1.24
20.0	0.64	412.82	221.53	30.60	55.80	0.333	0.44	1.32
23.0	0.56	479.03	258.31	27.00	52.20	0.29	0.41	1.41
26.0	-	-	-	-	-	-	-	-
29.0	-	-	-	-	-	-	-	-
32.0	-	-	-	-	-	-	-	-
35.0	-	-	-	-	-	-	-	-

Similarly the calculations of $\Delta\tau_{rz}$, $\Delta\sigma_z$, CSR and F.O.S for BH2, BH3, BH4 are done and shown in tables 7.2, 7.3 and 7.4 respectively.

Table 7.2 Calculations for $\Delta\tau_{rz}$, $\Delta\sigma_z$, CSR and F.O.S for BH2

Depth, z(m)	r_d	σ_{vo} (kN/m ²)	σ'_{vo} (kN/m ²)	$\Delta\tau_{rz}$ (kN/m ²)	$\Delta\sigma_z$ (kN/m ²)	CSR	CRR	F.O.S
2.0	-	-	-	-	-	-	-	-
5.0	-	-	-	-	-	-	-	-
8.0	-	-	-	-	-	-	-	-
11.0	-	-	-	-	-	-	-	-
14.0	-	-	-	-	-	-	-	-
17.0	0.72	342.47	180.60	36.00	63.00	0.36	0.47	1.31
20.0	0.64	407.51	216.21	30.60	55.80	0.32	0.44	1.40

Depth, z(m)	r_d	σ_{vo} (kN/m ²)	σ'_{vo} (kN/m ²)	$\Delta\tau_{rz}$ (kN/m ²)	$\Delta\sigma_z$ (kN/m ²)	CSR	CRR	F.O.S
23.0	0.56	473.14	252.41	27.00	52.20	0.27	0.41	1.51
26.0	-	-	-	-	-	-	-	-
29.0	-	-	-	-	-	-	-	-
32.0	-	-	-	-	-	-	-	-
35.0	-	-	-	-	-	-	-	-

Table 7.3 Calculations for $\Delta\tau_{rz}$, $\Delta\sigma_z$, CSR and F.O.S for BH3

Depth, z(m)	r_d	σ_{vo} (kN/m ²)	σ'_{vo} (kN/m ²)	$\Delta\tau_{rz}$ (kN/m ²)	$\Delta\sigma_z$ (kN/m ²)	CSR	CRR	F.O.S
1.5	-	-	-	-	-	-	-	-
3	-	-	-	-	-	-	-	-
4.5	0.97	85.41	42.34	55.80	81.00	0.61	0.28	0.46
6	0.95	113.34	54.98	54.00	77.40	0.60	0.25	0.42
7.5	0.94	143.18	68.21	50.40	75.60	0.57	0.60	1.05
9	0.93	174.05	83.35	48.60	73.80	0.55	0.60	1.09
10.5	0.89	206.98	99.52	46.80	72.00	0.52	0.60	1.14

Table 7.4 Calculations for $\Delta\tau_{rz}$, $\Delta\sigma_z$, CSR and F.O.S for BH4

Depth, z(m)	r_d	σ_{vo} (kN/m ²)	σ'_{vo} (kN/m ²)	$\Delta\tau_{rz}$ (kN/m ²)	$\Delta\sigma_z$ (kN/m ²)	CSR	CRR	F.O.S
1.5	-	-	-	-	-	-	-	-
3	-	-	-	-	-	-	-	-
4.5	-	-	-	-	-	-	-	-
6	-	-	-	-	-	-	-	-
7.5	-	-	-	-	-	-	-	-
9	-	-	-	-	-	-	-	-
10.5	-	-	-	-	-	-	-	-
12	-	-	-	-	-	-	-	-
13.5	-	-	-	-	-	-	-	-
15	-	-	-	-	-	-	-	-
16.5	0.71	326.67	171.672	38.7	61.2	0.40	0.16	0.41
18	0.67	356.985	187.272	36	57.6	0.37	0.17	0.45
19.5	0.63	386.94	202.512	30.6	55.8	0.34	0.15	0.43
21	-	-	-	-	-	-	-	-
22.5	-	-	-	-	-	-	-	-
24	-	-	-	-	-	-	-	-
25.5	-	-	-	-	-	-	-	-
27	-	-	-	-	-	-	-	-
28.5	-	-	-	-	-	-	-	-
30	-	-	-	-	-	-	-	-

7.3 Calculation of Vertical Stress Increment, $\Delta\sigma_z$ and Horizontal Shear Stress increment, $\Delta\tau_{zh}$ due to a circular loading with measured Vs data:

At Depth, $z = 1.5\text{m}$

$$r_d = 0.99, \sigma_{vo} = 24.86, \sigma'_{vo} = 15.05, q = 180\text{kPa}, a = 37/2 = 18.5\text{m}$$

Now, $z/a = 1.5/18.5 = 0.08$ and $r/a = 1$ (assumed) where z is the depth, a is the radius of the circular tank and r is the radial distance.

From the charts for Shear Stresses due to circular loading of Foster and Ahlvin (1954), we get

$$\Delta\tau_{zh}/q \times 100(\%) = 32.5\%$$

$$\Delta\tau_{rz}/180 \times 100 = 32.5$$

$$\therefore \Delta\tau_{rz} = 58.50 \text{ kPa}$$

From the charts for Vertical Stresses due to circular loading of Foster and Ahlvin (1954), we get

Now, $z/a = 1.5/18.5 = 0.08$ and $r/a = 0/18.5 = 0$ (vertical loading at center)

$$\Delta\sigma_z/q \times 100(\%) = 100\%$$

$$\Delta\sigma_z/180 \times 100(\%) = 100\%$$

$$\therefore \Delta\sigma_z = 180 \text{ kPa}$$

$$\begin{aligned} \text{Now, CSR} &= \{0.65(a_{\max}/g)r_d\sigma_{vo} + \Delta\tau_{zh}\} / (\sigma'_{vo} + \Delta\sigma_z) \\ &= \{0.65*0.36*0.99*24.86+58.50\}/(15.05+180) \\ &= 0.33 \end{aligned}$$

$$\text{F.O.S} = \text{CRR}/\text{CSR}$$

$$= 0.60/0.33$$

$$= 1.82 \text{ (CRR same as calculated without considering structure in chapter 6)}$$

Similarly, calculations for $\Delta\tau_{rz}$, $\Delta\sigma_z$, CSR and F.O.S for all depths using Vs data are done and shown in table 7.5.

Table 7.5 Calculations for $\Delta\tau_{rz}$, $\Delta\sigma_z$, CSR and F.O.S for all depths using Vs data

Depth, z(m)	r_d	σ_{vo} (kN/m ²)	σ'_{vo} (kN/m ²)	$\Delta\tau_{rz}$ (kN/m ²)	$\Delta\sigma_z$ (kN/m ²)	CSR	CRR	F.O.S
1.5	0.99	24.86	15.05	58.50	180.00	0.33	0.60	1.82
3	0.98	50.75	26.22	56.70	88.20	0.60	0.60	1.01

Depth, z(m)	r_d	σ_{vo} (kN/m ²)	σ'_{vo} (kN/m ²)	$\Delta\tau_{rz}$ (kN/m ²)	$\Delta\sigma_z$ (kN/m ²)	CSR	CRR	F.O.S
4.5	0.97	79.43	40.19	55.80	81.00	0.61	0.60	0.99
6	0.95	108.84	54.89	54.00	77.40	0.59	0.60	1.01
7.5	0.94	139.59	70.92	50.40	75.60	0.55	0.60	1.08
9	0.93	170.63	87.24	48.60	73.80	0.53	0.60	1.13
10.5	0.89	202.25	104.15	46.80	72.00	0.51	0.60	1.19
12	0.85	234.32	121.50	44.10	71.10	0.47	0.60	1.27
13.5	0.83	266.69	144.06	41.40	66.60	0.44	0.60	1.36
15	0.77	299.19	156.95	39.60	63.00	0.43	0.60	1.41
16.5	0.73	330.38	173.42	38.70	61.20	0.41	-	-
18	0.69	362.00	190.32	36.00	57.60	0.38	-	-
19.5	0.65	394.50	208.11	30.60	55.80	0.34	-	-
21	0.61	427.16	226.05	29.70	54.00	0.32	-	-
22.5	0.57	459.96	244.14	27.00	52.20	0.30	-	-
24	0.53	493.05	262.52	25.20	50.40	0.27	-	-
25.5	0.51	526.44	281.19	23.40	48.60	0.26	-	-
27	0.50	559.98	300.02	21.60	47.70	0.25	-	-
28.5	0.49	593.67	318.99	20.70	45.00	0.24	-	-
30	0.48	627.65	338.25	19.80	43.20	0.24	-	-

Chapter-8

Results and Discussions

8.1 Introduction

The evaluation of liquefaction potential for the boreholes bearing nos. BH1, BH2, BH3 and BH4 were carried out with N-value from Standard Penetration Test and measured Shear wave velocity, V_s . The evaluation process was carried out in absence of structure at the site. If the site is found liquefiable where factor of safety < 1 , then the vertical settlement or deformation is determined as per charts of volumetric strain (%) versus factor of safety against cyclic instability (Kenji Ishihara and Mitsutoshi Yoshimine, 1992). Liquefaction Potential Index, LPI -a parameter to measure the hazard level is then computed by means of the two approaches such as Iwasaki et al. (1984) and Sonmez (2003) respectively. This evaluation was carried as per the conventional approach termed as the “Simplified procedure” by considering the soil as if it is in the free field, away from the structure, without considering any structure at the site. It has been found from the studies available in the literature that the excess pore pressure distribution near a structure can significantly differ from that in the free field. It indicates that the presence of structure at ground surface has significant effect on liquefaction potential in terms of vertical stress and horizontal shear stresses induced by a structure. To observe this effect, liquefaction analysis was also carried out for the same site by considering a structure at ground surface. The vertical stress and horizontal shear stress induced by the structure were considered in the evaluation process as per Foster and Ahlvin (1954). This study was done to compare the results of liquefaction potential for sites without and with structures. The detailed calculations without and with the structure with respect to the boreholes are shown in chapters 6 and 7. A “Spreadsheet” in Microsoft excel was also designed for the analysis of liquefaction potential and is shown below in the Figures 8.1 and 8.2.

EVALUATION OF LIQUEFACTION POTENTIAL OF SOIL USING SPT DATA

Method used: Simplified Procedure
 Test conducted: Standard Penetration Test
 BH no. 1

Soil parameters

z(m)	2	5	8	11	14	17	20	23
Bulk density (kN/m ³)	17.76	20.5	20.01	20.8	21.39	21.39	21.68	22.07
N	5	17	14	21	29	43	61	65
W.T (m)	0.5	a _{max} /g		0.36				

Calculation of Cyclic Stress Ratio (CSR)

Total stress	35.52	97.02	157.05	219.45	283.62	347.79	412.83	479.04
Effective stress	20.81	52.88	83.48	116.445	151.185	185.925	221.535	258.315
r _d						0.72	0.64	0.56
CSR						0.32	0.28	0.24

Calculation of Cyclic Stress Ratio, CSR(mod)

a	18.5 m							
z/a						0.92	1.08	1.24
Note: Calculation of stresses								
Horizontal shear stress increment						36.00	30.60	27.00
Vertical stress increment						63.00	55.80	52.20
CSR(modified)						0.38	0.33	0.29

Correction factors

C _{HT}	1							
C _{HW}	0.984							
C _{SS}	1.1							
C _{BD}	1.05							
C _{RL}	0.75 if z upto 3m 0.85 if z upto next 6m 0.95 if z upto next 9m 1 z from 9m onwards							
C _{RL} (Calc)						1	1	1
C ₆₀						1.14	1.14	1.14

Overburden correction factors

P _a	100 kPa							
C _{N<1.7}	2.19	1.38	1.09	0.93	0.81	0.73	0.67	0.62

Note: If CN ≤ 1.7 then take the calculated value else if CN > 1.7 then take the value as 1.7

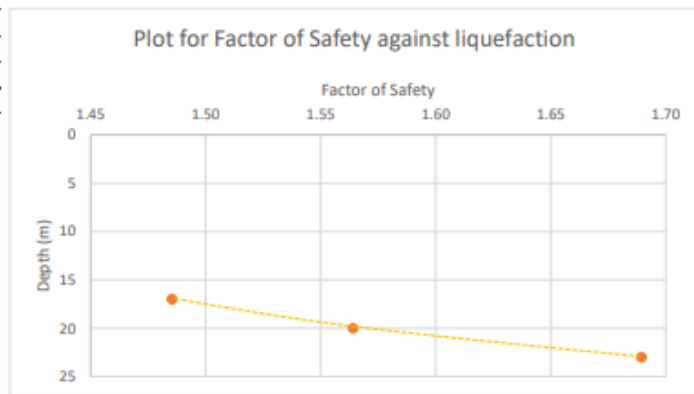
C _N	1.7	1.38	1.09	0.93	0.81	0.73	0.67	0.62
----------------	-----	------	------	------	------	------	------	------

Effects of fines content FC

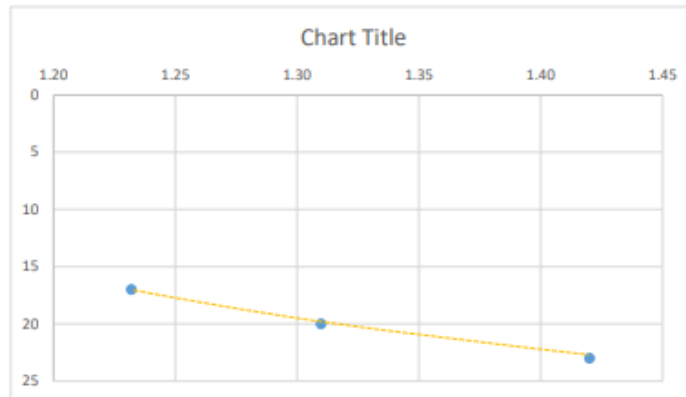
(N ₁) ₆₀	-	-	-	-	-	35.84	46.58	45.96
---------------------------------	---	---	---	---	---	-------	-------	-------

FC	100	100	100	100	100	0	0	0
Note: Values of	α	β						
if $FC \leq 5$	0	1						
if $5 < FC < 35$	$e^{[1.76-(190/FC^2)]}$	$0.99+FC^{1.5}/1000$						
if $FC \geq 35$	0.5	1.2						
α (Final)	-	-	-	-	-	0.00	0.00	0.00
β (Final)	-	-	-	-	-	1.00	1	1
$(N_1)_{60CS}$	-	-	-	-	-	35.84	46.58	45.96
Calculation of Cyclic Resistance Ratio (CRR)								
K_{σ}	1	For Depth upto 15 metre			If $K_{\sigma} > 15$ then		K_{σ}	
K_a	1							
$CRR_{7.5}$						0.60	0.6	0.6
MSF	1							
CRR						0.47	0.44	0.41
F.O.S without Structure	-	-	-	-	-	1.49	1.56	1.69
F.O.S with Structure	-	-	-	-	-	1.23	1.31	1.42

FOS	Depth(m)
1.49	17
1.56	20
1.69	23



FOS	Depth(m)
1.23	17
1.31	20
1.42	23



Calculation of Horizontal shear stress increment and Vertical stress increment

q	180 kPa			
z(m)	$(\Delta\tau_{vh}/q) \times 100\%$	$(\Delta\sigma_z/q) \times 100\%$	$\Delta\tau_{vh}(\text{kPa})$	$\Delta\sigma_z (\text{kPa})$
2.0				
5.0				
8.0				
11.0				
14.0				
17.0	20.0	35.0	36	63
20.0	17.0	31.0	30.6	55.8
23.0	15.0	29.0	27	52.2
26.0				
29.0				
32.0				
35.0				

Note: Calculation of horizontal shear stress and vertical stress as per charts of Foster and Ahlvin 1954

Calculation of correction factor, K_σ

N value	0 to 4	4 to 10	10 to 30	30 to 50	>50
Compactness	very loose	loose	medium	dense	very dense
Rel.density $D_r(\%)$	0 to 15	15 to 35	35 to 65	65 to 85	85 to 100

Calculation for K_σ

$$\text{For } z > 15\text{m} \quad K_\sigma = (\sigma'_{vo}/P_a)^{(f-1)}$$

For $D_r = 40\%-60\%$, $f=0.8 \sim 0.7$

For $D_r = 65\%-80\%$, $f=0.7 \sim 0.6$

z(m)	f	σ'_{vo}	K_σ
17	0.6	185.93	0.78
20	0.6	221.54	0.73
23	0.6	258.32	0.68

Fig. 8.1 Spreadsheet for the Analysis of Liquefaction Potential with SPT data

EVALUATION OF LIQUEFACTION POTENTIAL OF SOIL USING MEASURED V_s DATA

Method used: Simplified Procedure
 Test conducted: Seismic cross hole test

Soil parameters										
z(m)	1.5	3	4.5	6	7.5	9	10.5	12	13.5	15
Bulk density (kN/m^3)	16.57	17.26	19.12	19.61	20.5	20.69	21.08	21.38	21.58	21.67
W.T (m)	0.5	a_{max}/g		0.36						
Calculation of Cyclic Stress Ratio (CSR)										
Total stress	24.86	50.75	79.43	108.84	139.59	170.63	202.25	234.32	266.69	299.19
Effective stress	15.05	26.22	40.19	54.885	70.92	87.24	104.15	121.5	139.16	156.95
τ_d	0.99	0.98	0.97	0.95	0.94	0.93	0.89	0.85	0.81	0.77
CSR	0.38	0.44	0.45	0.44	0.43	0.43	0.41	0.39	0.36	0.35
Calculation of Cyclic Stress Ratio, CSR(mod)										
a	18.50 m									
z/a	0.08	0.16	0.74	0.32	0.41	0.49	0.57	0.65	0.73	0.81
<i>Note: Calculation of stresses</i> STRESS INCREMENT										
Horizontal shear stress increment	58.50	56.70	55.80	54.00	50.40	48.60	46.80	44.10	41.40	39.60
Vertical stress increment	180.00	88.20	81.00	77.40	75.60	73.80	72.00	71.10	66.60	63.00
CSR(modified)	0.33	0.60	0.61	0.59	0.55	0.53	0.51	0.47	0.45	0.43
Overburden correction factors										
V_s	219.2	226.3	232.4	238.7	247.5	255.6	259.3	268.3	278.2	286.8
P_a	100 kPa									
$C_N < 1.4$	1.61	1.40	1.26	1.16	1.09	1.03	0.99	0.95	0.92	0.89
<i>Note: If $C_N \leq 1.4$ then take the calculated value else if $C_N > 1.4$ then take the value as 1.4</i>										
C_N	1.4	1.40	1.26	1.16	1.09	1.03	1.0	0.95	0.92	0.89
Calculation of Cyclic Resistance Ratio (CRR)										
V_{s1}	306.9	316.2	291.9	277.3	269.7	264.5	256.7	255.6	256.1	256.2
K_c	1 For Depth upto 15 metre									
K_a	1									
CRR _{1.5}	0.60	0.60	0.60	0.60	0.60	0.60	0.60	0.60	0.60	0.60
<i>Note: If $V_{s1} < 210\text{m/s}$ then refer fig.10 for calculation of CRR_{1.5}</i> FIG.10										
MSF	1									
CRR	0.60	0.60	0.60	0.60	0.60	0.6	0.6	0.6	0.6	0.6
Factor of Safety, F.O.S										
(Without structure)	1.57	1.36	1.34	1.36	1.38	1.41	1.48	1.56	1.64	1.74
Factor of Safety, F.O.S										
(With structure)	1.82	1.01	0.99	1.01	1.08	1.13	1.19	1.27	1.34	1.41

FOS	Depth(m)
1.57	1.5
1.36	3
1.34	4.5
1.36	6
1.38	7.5
1.41	9
1.48	10.5
1.56	12
1.64	13.5
1.74	15

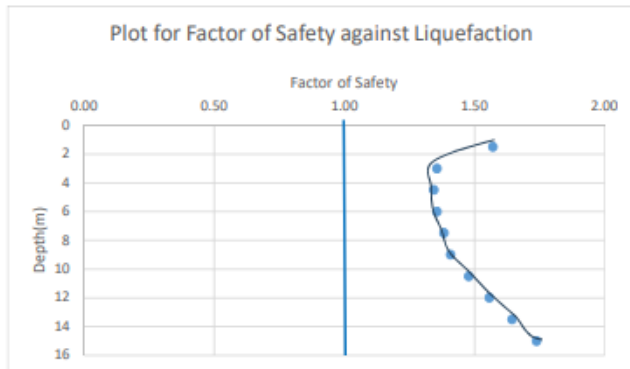


Fig. Plot for Factor of Safety against Liquefaction (without structure)

FOS	Depth(m)
1.82	1.5
1.01	3
0.99	4.5
1.01	6
1.08	7.5
1.13	9
1.19	10.5
1.27	12
1.34	13.5
1.41	15

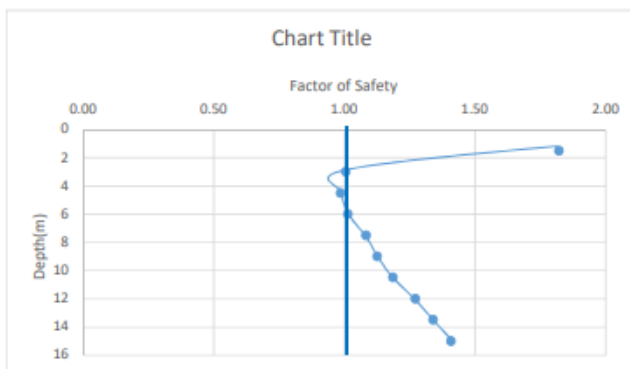


Fig. Plot for Factor of Safety against Liquefaction (with structure)

Calculation of horizontal shear stress increment and vertical stress increment

q	180 kPa			
Depth	$(\Delta\tau_{vh}/q) \times 100\%$	$(\Delta\sigma_z/q) \times 100\%$	$\Delta\tau_{vh}$ (kPa)	$\Delta\sigma_z$ (kPa)
1.5	32.5	100.0	58.50	180.00
3	31.5	49	56.70	88.20
4.5	31.0	45.0	55.80	81.00
6	30.0	43.0	54.00	77.40
7.5	28.0	42.0	50.40	75.60
9	27.0	41.0	48.60	73.80
10.5	26	40	46.80	72.00
12	24.5	39.5	44.10	71.10
13.5	23.0	37.0	41.40	66.60
15	22.0	35.0	39.60	63.00

Note: Calculation of horizontal shear stress and vertical stress as per charts of Foster and Ahlvin 1954

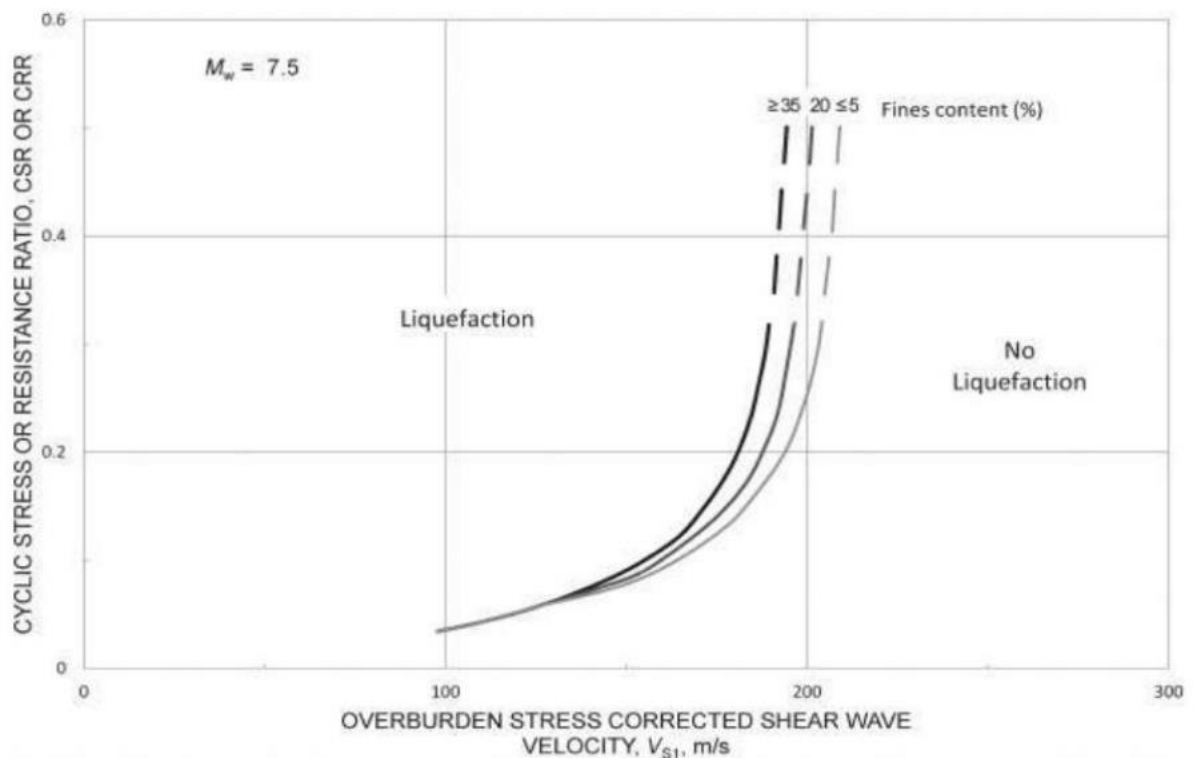


FIG. 10 RELATION BETWEEN CRR AND V_{s1} FOR M_w 7.5 EARTHQUAKES

Fig. 8.2 Spreadsheet for the Analysis of Liquefaction Potential with V_s data

Similarly, this spreadsheet can be used for the analysis of liquefaction potential for the other boreholes.

8.2 Results

8.2.1 The results obtained from the assessment of liquefaction potential of soil with SPT data are as follows:-

1. The assessment of liquefaction potential for site without any structure with respect to boreholes bearing no. BH1, BH2 shows that there is no presence of liquefiable soil layer, whereas in BH3, there is a liquefiable layer from 4.5m to 6m and in BH4, there are liquefiable layers from 16.5m to 19.5m.
2. The vertical settlements or deformations due to liquefaction for BH1 and BH2 are found to be 0(zero) due to presence of non-liquefiable layer, whereas for BH3 and BH4 are found to be 0.055m and 0.111m respectively.
3. Liquefaction potential index (LPI) found with respect to boreholes BH1 and BH2 are 0(zero) which means hazard level is very low, whereas for BH3 and BH4 are found to be 9.85 and 2.93 respectively. LPI 9.85 and 2.93 means that that the hazard levels are high and low respectively for the site.
4. The assessment shows that soil in absence or presence of structure at ground surface will have the same cyclic resistance ratio (CRR).
5. The cyclic stress ratio (CSR) induced by earthquake with respect to soil without structure will vary with the same soil when a structure is present on ground surface. Consequently, the factor of safety also changes due to the induced vertical and shear stresses of structure.

8.2.2 The results obtained from the assessment of liquefaction potential of soil with measured Vs data are as follows:-

1. The assessment of liquefaction potential for site without any structure against the borehole shows that the soil is not liquefiable.
2. There will be no vertical settlement or deformation due to presence of non-liquefiable soil layer.
3. Computation of LPI is not required as no liquefaction occurred.
4. The assessment shows that soil in absence or presence of structure at ground surface will have the same cyclic resistance ratio (CRR).

5. The cyclic stress ratio (CSR) induced by earthquake with respect to soil without structure will vary with the same soil when a structure is present on ground surface. Consequently, the factor of safety also changes due to the induced vertical and shear stresses of structure. It is seen from the results of liquefaction analysis that the F.O.S decreases with the same soil when a structure is placed on the ground surface.

8.3 Discussions

Detailed liquefaction hazard assessment at few points of North Guwahati area, Guwahati has been conducted in this project with SPT N-value and measured Shear wave velocity, V_s . Since Guwahati falls under high seismic zone-V, it is essential to carry liquefaction potential of soil. Due to occurrence of earthquake periodically in this region, there is a high risk of soil being susceptible to liquefaction. The peak ground acceleration (PGA) -an important parameter for assessing soil liquefaction observed for this region is 0.36 which is very high. It is already mentioned about the presence of structure at ground surface which has significant effect on the liquefaction potential of soil. Therefore it is important to carry liquefaction analysis by considering structure at site. Based on the presented results of the study, soil will not be susceptible to liquefaction with corrected shear wave velocity $V_{S1} \geq 248$ m/s. Based on correlations of penetration and V_s , CRR yields a value of about 0.6 for V_{S1} equal to 210 m/s which is equivalent to a corrected SPT blow count of 30 in clean sand (Seed et al.1985.). However, when a structure is considered at the site then the same soil may be susceptible to liquefaction as found from this assessment. It clearly indicates that the presence of structure at site has significant effect on the liquefaction potential of soil.

Chapter-9

Advantages and Disadvantages of SPT and Shear Wave Velocity

9.1 Introduction

The Simplified procedure introduced by Seed & Idriss in the year 1971 is used worldwide for evaluation of liquefaction resistance of soils by using data from Standard Penetration Test (SPT). Other field tests such as Cone Penetration Test (CPT), Becker Penetration Test (BPT) and small strain Shear Wave Velocity (V_s) can be adopted for using this procedure. SPTs and CPTs are preferred in general for evaluation of liquefaction resistance due to more extensive database and experiences from past but the other tests may be conducted in situations where sites underlain by gravelly sediments or where entry of large equipment is bounded (Youd et al.2001).

9.2 The advantages and disadvantages of SPT and V_s tests are enumerated below in Table 9.1

Table 9.1 Advantages and disadvantages of SPT and V_s methods

Characteristic	Test methods	
	SPT	V_s
Past measurements at liquefaction sites	Abundant	Limited
Type of stress-strain behaviour influencing test	Large strain, partially drained	Small strain, no excess pore water pressure
Quality control and repeatability	Poor to good	Good
Detection of variability of soil deposits	Good for closely spaced tests	Fair
Soil types in which test is recommended	Non-gravel	All
Soil sample retrieved	Yes	No
Test measures index or engineering property	Index	Engineering

Chapter-10

Conclusion and Future Scope

10.1 Conclusion

In this project work, the various factors influencing soil liquefaction have been studied. Initial identification of soil liquefaction with the help of grain size distribution has been further studied. Thereafter, the detailed investigation of sub-soil has been done by conducting Standard Penetration Test and Shear wave velocity for the evaluation of liquefaction potential of soil. The evaluation process was carried out for the site without and with a structure as per the conventional approach “Simplified Procedure” introduced by Seed and Idriss, 1974. The factor of safety determined from this procedure was adopted for the computation of liquefaction potential index, LPI-a parameter to assess soil liquefaction. The two approaches such as Iwasaki et al (1984) and Sonmez (2003) were used for the computation of LPI. Deformations or vertical settlement that occurred due to liquefaction of soil were calculated as per the Charts for Volumetric Strain in % versus Factor of Safety against Cyclic Instability. For site with structure, the vertical stress and horizontal shear stresses induced by the structure were determined as per the approach of “Foster and Ahlvin, 1954”. It is evident from the analysis with SPT data that sand with $(N_1)_{60}$ value smaller than 30 are susceptible to soil liquefaction whereas sand with $(N_1)_{60}$ value greater than 30, one can presume it is not liquefiable from the established thresholds for liquefaction, as mentioned in Seed and Idriss (1971). The following conclusions derived from the present project work.

1. The boreholes of the study area with SPT data for BH1 and BH2 are found to be non-liquefiable, whereas BH3 and BH4 are found to be liquefiable at some depths.
2. The borehole of the study area with measured V_S data are found to be non-liquefiable.
3. In the analysis with V_S data, it is observed that the soil will not liquefy with V_{S1} equal to 210 m/s, as found from the correlation of penetration - V_{S1} where CRR yields an approximate value of 0.60 at V_{S1} 210 m/s, which is equivalent to a corrected SPT blow count of 30 in clean sand.

4. The analysis with measured V_s data indicates that the site without a structure not susceptible to liquefaction liquefied at 4.5m depth for the same site when a structure is considered.

5. The analysis indicates that the soil strata at greater depths are less susceptible to liquefaction for both SPT and measured V_s .

6. It is also observed that factor of safety for site in absence of structure decreases with the same site when a structure is placed on the ground surface, which indicates that the presence of structure at site surface has significant effect on the liquefaction potential of soil. Thus, it is important to study liquefaction potential of soil, prior to construction of any important structure.

10.2 Future Scope

Though a study on deterministic methods, such as SPT and V_s , to evaluate soil liquefaction potential has been carried out, and various factors influencing soil liquefaction have been examined, it represents just a segment of a comprehensive research endeavour. Further exploration is necessary pertaining to geological and environmental conditions that influence soil liquefaction. Following are the future scopes of the work.

1. The Microsoft “Spreadsheet” designed for the assessment of liquefaction potential can be applied for other earthquake magnitudes apart from 7.5 M_w as well as for other peak ground accelerations (PGA) and soil parameters.

2. The results obtained from this assessment can be further utilized in the study of other methodologies which is similar to Liquefaction potential index, LPI to measure the hazard level.

3. In this study, the effects on fines content (F.C) have been considered for the assessment of liquefaction potential but age correction factors are not considered. Hence, this study can be further utilized for the study of aging effects on cyclic resistance ratio.

References

- Andrus, R. D. , and Stokoe, K. H. (2000). “Liquefaction resistance of soils from Shear-Wave velocity.” *J. Geotech. Geoenviron. Eng.* 2000.126:1015-1025.
- Andrus, R. D. , Stokoe, K. H. , and Juang, C. H. (2004). *Guide for Shear-Wave-Based Liquefaction Potential Evaluation*. DOI: 10.1193/1.1715106.
- Banerjee, A. (2017). “Response of unsaturated soils under monotonic and dynamic loading over moderate suction states.” Doctoral Dissertation, Dept. of Civil Engineering, Univ. of Texas at Arlington.
- Banerjee, A., Puppala, A. J., and Hoyos, L. R. (2022). “Liquefaction Assessment in Unsaturated Soils.” *Journal of Geotechnical and Geoenvironmental Engineering*, 148(9). [https://doi.org/10.1061/\(asce\)gt.1943-5606.0002851](https://doi.org/10.1061/(asce)gt.1943-5606.0002851).
- Bayat, E.E., Yegian, M.K., Alshawabkeh, A., and Gokyer, S. (2012). “Liquefaction response of partially saturated sands. I. E. results.” *J. Geotech. Geoenviron. Eng.* 139 (6): 863–871. [https://doi.org/10.1061/\(ASCE\)GT.1943-5606.0000815](https://doi.org/10.1061/(ASCE)GT.1943-5606.0000815).
- Begom, Sabjuna Ferdousi Barbhuiya., Dey, S., Pao, B., Jaman, Z., Kharka, B., and Nath, N., (2020). “Determination of liquefaction potential of Guwahati city.” [Unpublished master’s thesis].
- Ben-Zeev, S., Goren, L., Toussaint, R and Aharonov, E. (2023). “Drainage explains soil liquefaction beyond the earthquake near-field.” *Nature Communications*, 14(1). <https://doi.org/10.1038/s41467-023-41405-4>.
- Bwambale, B. (2018). “Reducing Uncertainty in the Assessment of Aging Effects on Soil Liquefaction Recommended Citation.” In *All Dissertations Dissertations* (Vol. 8). https://tigerprints.clemson.edu/all_dissertations.
- Chanda, S., Kumar, N., and Kushwaha, D. (2023). “Liquefaction Potential Index (LPI): A Parameter to Assess Liquefaction Hazard.” In *Advances in Natural and Technological Hazards Research* (Vol. 53, pp. 103–112). Springer Science and Business Media B.V. https://doi.org/10.1007/978-981-99-3955-8_7.
- Chillarige, A. V., Morgenstern, N. R., Robertson, P. K., and Christian, H. A. (1997). “Seabed instability due to flow liquefaction in the Fraser River delta.” *Can. Geotech. J.*, 34(4), 520–533.
- Clement, C., Toussaint, R., Stojanova, M., and Aharonov, E. (2017). “The art of sinking intruder during earthquakes.” Under-Review.
- Das, T. , Sharma, M. , and Choudhury, D. (2023). *Bearing Capacity and Liquefaction Assessment of Shallow Foundations Resting on Vibro-Stone Column Densified Soil in Vallur Oil Terminal, India*. *Indian Geotech J* (December 2023) 53(6):1392–1413 <https://doi.org/10.1007/S40098-023-00758-9>.
- Debnath, R., Saha, R., and Haldar, S. (2021). “Assessment of small strain dynamic soil properties of railway site Agartala, India, by bender element tests.” <https://doi.org/10.1007/S12517-022-10749-4>.

Bayat, E.E., Yegian, M.K., Alshawabkeh, A., and Gokyer, S. (2012). “Liquefaction response of partially saturated sands. I. E. results.” *J. Geotech. Geoenviron. Eng.* 139 (6): 863–871. [https://doi.org/10.1061/\(ASCE\)GT.1943-5606.0000815](https://doi.org/10.1061/(ASCE)GT.1943-5606.0000815).

EN 1998-5: Eurocode 8: “Design of structures for earthquake resistance” – Part 5: Foundations, retaining structures and geotechnical aspects. (2004).

Foster, C. R., and A. R. G. (1954.). “Stresses and Deflections Induced by a Uniform Circular Load.”

Grozic, J. L. H., Robertson, P. K., and Morgenstern, B. R. (2000). “Cyclic liquefaction of loose gassy sand.” *Can. Geotech. J.*, 37(4), 843–856.

Hsu, J. R. C., Jeng, D. S., and Lee, C. P. (1995). “Oscillatory soil response and liquefaction in an unsaturated layered seabed.” *Int. J. Numer. Anal. Methods Geomech.*, 19(12), 825–849.

Indian Standard IS- 1893(Part 1) :2016. “Criteria for earthquake resistant design of structures – Part 1 General provisions and buildings (Sixth Revision)”

Indian Standard IS-2131:1981 Reaffirmed 2002. “Method for Standard Penetration Test for soils (First Revision).”

Indian Standard IS- 13372 (Part 2) : 1992. “Code of Practice for Seismic Testing of Rock Mass Part 2 Between the Borehole.”

Ishihara, K., and Yoshimine, M. (1992). “Evaluation of Settlements in Sand Deposits Following Liquefaction During Earthquakes.” <https://doi.org/10.3208/Sandf1972.32.173>.

Iwasaki T. (1986). “Soil liquefaction studies in Japan. State of the Art. *Soil Dyn Earthquake Eng* 5(1):2–68.”

Iwasaki, T., Arakawa, Tadashi., and Tokida, K. (1984). “Simplified procedures for assessing soil liquefaction during earthquakes.” [https://doi.org/10.1016/0261-7277\(84\)90027-5](https://doi.org/10.1016/0261-7277(84)90027-5).

Jain, S. K. , Jaiswal, O. R. , Ingle R. K. , and R. Debasis. (2019). “Explanatory Examples on Indian Seismic Code IS 1893 (Part I).”

Jain, S.K Sudhir Jain(2019). “Explanatory Examples on Indian Seismic Code IS 1893 (Part I).”

Kramer, S. L. (1996). “Geotechnical earthquake engineering, Prentice Hall, Upper Saddle River, NJ.”

Latha, G. M., and Lakkimsetti, B. (2022). “Morphological Perspectives to Quantify and Mitigate Liquefaction in Sands.” *Indian Geotechnical Journal*, 52(5), 1244–1252. <https://doi.org/10.1007/s40098-022-00649-5>.

Lentini, V., and Castelli, F. (2018). Liquefaction Resistance of Sandy Soils from Undrained Cyclic Triaxial Tests. <https://doi.org/10.1007/S10706-018-0603>.

Liao, S.S.C., and Whitman, R.V. (1986). [https://doi.org/10.1061/\(ASCE\)0733-9410\(1986\)112:3\(373\)](https://doi.org/10.1061/(ASCE)0733-9410(1986)112:3(373)).

- Mele, L., Tian, J. T., Lirer, S., Flora, A., and Koseki, J. (2019). "Liquefaction resistance of unsaturated sands: Experimental evidence and theoretical interpretation." *Géotechnique* 69 (6): 541–553. <https://doi.org/10.1680/Jgeot.18.P.042>.
- Mele, L., Lirer, S., and Flora, A. (2022). "Liquefaction triggering of non-saturated sandy soils." *Geotechnique Letters*, 13(1). <https://doi.org/10.1680/jgele.22.00076>.
- Okamura, M., and Noguchi, K. (2009). "Liquefaction resistances of unsaturated non-plastic silt." *Soils Found.* 49 (2): 221–229. <https://doi.org/10.3208/Sandf.49.221>.
- Pokhrel, R.M., Glider, C. E. L., Vardanega, P. J., Luca, F. D., Risi, R. D., Werner, M J., Sextos, A (2021). "Liquefaction potential for the Kathmandu Valley, Nepal: a sensitivity study. *Bulletin of Earthquake Engineering* (2022)" 20:25–51 <https://doi.org/10.1007/S10518-021-01198-7>.
- Rauch, A. F (1997). "Analysis of soil borings for liquefaction resistance. In *Engineering, Environmental Science*."
- Saran, S (1999.). "Soil dynamics and machine foundations." Galgotia Publications pvt.ltd.
- Satyam, N. , and Rao, K. S. (2014). Liquefaction Hazard Assessment Using SPT and VS for Two Cities in India. *Indian Geotech J* DOI 10.1007/S40098-014-0098-2.
- Seed, H. B., Tokimatsu, K., Harder, L. F., and Chung, R. M. (1985). "The influence of SPT procedures in soil liquefaction resistance evaluations." *J. Geotech. Engrg., ASCE*, 111(12), 1425–1445.
- Sonmez, H (2003). "Modification of the liquefaction potential index and liquefaction susceptibility mapping for a liquefaction." *Prone Area (Inegol, Turkey), Environ. Geol.*, 44, 862–871, [Doi:10.1007/S00254-003-0831-0](https://doi.org/10.1007/S00254-003-0831-0), 200.
- Stark, T.D., and Olson, S.M (1995). "Liquefaction Resistance Using CPT and Field Case Histories." *J. Geotech. Engrg., ASCE*, 121(12), 856–869.
- Unno, T., Kazama, M., Uzuoka, R., and Sento, N. (2008). "Liquefaction of unsaturated sand considering the pore air pressure and volume compressibility of the soil particle skeleton." <https://doi.org/10.3208/sandf.48.87>.
- Youd, T.L., and Idriss, I.M. (2001). "Liquefaction Resistance of Soils: Summary Report from the 1996 NCEER and 1998 NCEER/NSF Workshops on Evaluation of Liquefaction Resistance of Soils." *Journal of Geotechnical and Geoenvironmental Engineering*, 127(10), 817–83
- Zeev, S. Ben, Goren, L., Perez, S., Toussaint, R., Clément, C., and Aharonov, E. (2017). "The Combined Effect of Buoyancy and Excess Pore Pressure in Facilitating Soil Liquefaction." *Poromechanics 2017 - Proceedings of the 6th Biot Conference on Poromechanics*, 107–116. <https://doi.org/10.1061/9780784480779.013>